



UNIVERSITÀ DEGLI STUDI DI SALERNO



UNIVERSITÀ DEGLI STUDI DI SALERNO  
Dipartimento di Farmacia

PhD Program  
in **Drug Discovery and Development**  
XXXI Cycle — Academic Year 2018/2019

***PhD Thesis in***

***Development of technological  
approaches based on supercritical  
fluids for the production of polymeric  
micro-nano particulate systems for  
wound healing***

Candidate

*Rosalía Rodríguez Dorado*

Supervisor

Prof. *Pasquale Del Gaudio*

PhD Program Coordinator: Prof. Dr. *Gianluca Sbardella*



## CONTENTS

ABSTRACT .....	I
1. INTRODUCTION .....	1
1.1. Wounds and healing process .....	3
1.1.1. <i>Factors influencing wound healing</i> .....	5
1.1.2. <i>Types of wounds</i> .....	6
1.1.3. <i>Chronic wounds</i> .....	7
1.1.4. <i>Incidence of chronic wounds in the world</i> .....	9
1.2. Wound dressings .....	10
1.2.1. <i>Traditional wound healing devices</i> .....	10
1.2.2. <i>Modern wound dressings</i> .....	12
1.3. Polymers for dressing applications.....	15
1.4. “ <i>In-situ</i> ” gelling formulations.....	21
1.5. Aerogels.....	22
1.5.1. <i>Aerogels classification</i> .....	24
1.5.2. <i>Aerogels for pharmaceutical application</i> .....	25
1.6. Supercritical fluids technologies .....	26
1.6.1. <i>Supercritical Assisted Atomization (SAA)</i> .....	28
1.6.2. <i>Supercritical Antisolvent Extraction (SAE)</i> .....	29
1.7. Prilling technology .....	30
1.8. Aims of the project .....	33
2. MATERIALS AND METHODS .....	37
2.1. Chemicals .....	39
2.2. Methods .....	41
2.2.1. <i>Encapsulation technique: laminar jet break-up or prilling</i> .....	41
2.2.2. <i>Supercritical Fluids-based technologies</i> .....	42
2.2.2.1. <i>Supercritical Assisted Atomization (SAA)</i> .....	42

2.2.2.2. Supercritical Antisolvent Extraction (SAE) or “supercritical drying” .....	43
2.2.3. <i>Artificial Intelligence (AI) tools</i> .....	45
2.2.4. <i>Analytical technologies</i> .....	46
2.2.4.1 Scanning Electron Microscopy.....	46
2.2.4.2 Nitrogen Adsorption Porosimetry .....	47
2.2.4.3 Differential Scanning Calorimetry (DSC).....	48
2.2.4.4 FTIR-ATR spectroscopy .....	49
2.2.4.5 Fluorescent Microscopy .....	49
2.2.4.6 Density measurements.....	50
2.2.4.7 Beads hardness assays .....	52
2.2.4.8. Dynamic Light Scattering (DLS) .....	53
2.2.5. <i>Experimental procedures</i> .....	53
2.2.5.1 Dry powders preparation .....	53
2.2.5.2 Aerogels preparation .....	55
2.2.5.3 Swelling and fluid uptake studies.....	58
2.2.5.4 Permeation in vitro assays .....	60
2.2.5.5 Drug content and encapsulation efficiency .....	61
2.2.5.6 Stability tests under storage.....	62
3. RESULTS AND DISCUSSION.....	65
SECTION A .....	67
3.1. “ <i>IN-SITU</i> ” GELLING POWDER FORMULATIONS FOR WOUND HEALING .....	67
SECTION B.....	87
3.2. AEROGELS FORMULATIONS FOR WOUND HEALING .....	87
3.2.1. Alginate aerogel beads .....	89
3.2.2. Core-shell microparticles obtained by inverse gelation optimized by artificial intelligent tools for aerogels production .....	103

3.2.3. Supercritical drying of core-shell microparticles for the manufacturing of ketoprofen lysinate loaded aerogels.....	123
4. CONCLUSIONS .....	135
References .....	139
SUPPLEMENTARY MATERIAL .....	153
APPENDIX I.....	159
LIST OF PUBLICATIONS.....	161
Papers .....	161
Presentation at conferences .....	161



## ABSTRACT

The PhD project titled “Development of technological approaches based on supercritical fluids for the production of polymeric micro-nano particulate systems for wound healing” aimed to develop novel formulations for topical administration to wounds using innovative, inexpensive and environmentally-friendly technologies based on the use of supercritical-CO<sub>2</sub> (sc-CO<sub>2</sub>): supercritical assisted atomization (SAA) and supercritical assisted extraction (SAE) in tandem with prilling. The specific goal of the project was the designing and development of “*in-situ*” gelling formulations in form of powders or aerogels using polysaccharide-based polymers as carriers for the encapsulated drugs, due to their biocompatibility, biodegradability, low cost and healing improving properties. Optimization of the process parameters were implemented to obtain either submicrometric particulate particles or aerogel beads with desired properties. Size distribution, textural properties, fluid uptake capability and controlled drug release profiles of the optimized formulations have been studied to evaluate the quality of the different wound healing devices.

During the first year, supercritical assisted atomization (SAA) was investigated. SAA was applied for the production of “*in-situ*” gelling dry powders loaded with doxycycline used as antimicrobial drug due to its inhibiting activity against matrix metalloprotease-2 (MMP-2) and metalloprotease-9 (MMP-9) that could enhance the healing process. High mannuronic content alginate, low methoxyl grade amidated pectin and low molecular weight chitosan, in different combinations, were used as excipients. Process optimization lead to high process yields (up to 89.0%) and the obtained powders showed good technological characteristics since were able to completely gel in three minutes when in contact with simulated

wound fluid. Moreover, powders were able to prolong the release of the doxycycline until up to 21 hours after a fast release during the first two hours (“burst effect”).

The second year was focused on the development and characterization of aerogel formulations, in form of beads or capsules, obtained by prilling technique in tandem with the supercritical antisolvent extraction (SAE). High mannuronic content alginate was used as carrier for these formulations. Alginate gel beads were produced by prilling using either aqueous or ethanolic calcium chloride solutions as gelling bath thus producing hydrogels or alcogels in a very narrow size distribution (about 2.4 mm  $\pm$  6.0%). Subsequently they were submitted to different supercritical-CO<sub>2</sub> drying processes for the production of aerogel in form of spherical beads. The resulted aerogels showed very high porosities (98.4-99.8%) and surface areas (271.0-537.3%) for the different sc-CO<sub>2</sub> drying processes. Moreover, influence of alginate molecular weight on aerogel properties was studied, resulting to influence the grade of shrinking and the porosity of the aerogels. In addition, the hydrogels and alcogels were also submitted to freeze-drying and oven drying with the purpose to make a comparison in terms of textural properties. Differently, the production of aerogels capsules with controllable shell thickness was designed with the purpose to increase the exudates absorption when beads gel in contact with wounds. For this purpose, core-shell gel microparticles were produced by prilling in co-axial configuration through the development of a new inverse gelation methodology optimized by Artificial Intelligent (AI) tools (Artificial Neural Networks, ANNs, and Neurofuzzy-Logic in combination with genetic algorithms). The obtained core-shell microparticles were formed by a hydrophilic alginate phase as the outer layer and a hydrophobic phase (water-in-oil emulsion) as the inner one of the particles; such core was subsequently removed by supercritical-CO<sub>2</sub> drying producing alginate aerogels with an inner void cavity.

The third year was focused on the development and characterization of drug-loaded aerogel capsules through supercritical antisolvent extraction (SAE) in tandem with prilling. Drug loaded microparticles were produced by the novel inverse gelation previously cited through prilling in co-axial configuration using ketoprofen lysinate, as model drug, and alginate as polymeric excipient. Aerogel capsules with a thin alginate shell layer and a hollow inner cavity, in which the ketoprofen was present, were produced after the supercritical drying of core-shell microparticles. Aerogel capsules showed good textural properties in terms of porosity (up to 93.1%) and surface area being promising formulations for high fluid uptake (about 500% the weight of the aerogel) from the wounds within seconds.

The supercritical drying processes and the characterization of the textural properties of aerogels were carried out during a 7 months period in the University of Santiago de Compostela (Spain).

Hence, such novel technologies, using polymers above mentioned, are promising technologies for the development of a new non-expensive generation of dressing formulations with small particle size (*“in-situ”* gelling powders) or large particles in order to be easily handled (aerogels) both with high surface areas that make them able to absorb high amount of exudate from wounds maintaining at the same time the moisture environment at the wound bed acting as non-traumatic dressings.







# **1. INTRODUCTION**



### **1.1. Wounds and healing process**

A wound is defined as an injury caused by a cut, blow, or other impact that typically involves laceration or breaking of a membrane (such as the skin) and usually damage to underlying tissues. The skin is the largest organ of the humans composed of the epidermis and dermis, including the subcutaneous fat or dermal adipocyte layer, which protects the underlying organs of the body from the external factors. For this reason, the skin is always involved when other tissues are injured and must take part of the wound healing process in order to allow the survival of the organisms (*Takeo et al., 2015*). The normal healing of wounds consists on a biological process that involves complex biochemical and cellular responses and it is defined by four overlapping phases (*Boateng. et al., 2008*):

- 1) The haemostasis phase is the first process that occurs immediately after tissue injuries and is characterized by bleeding, produced as a result of the disruption of blood vessels, and the development of a fibrin clot that serves as a reservoir of growth factors implicated in wound repair as well as to promote the exudates coagulation making the bleeding to stop (*Boateng et al., 2008*).
- 2) The inflammatory phase is referred to the innate initial reaction of the body just after the injury takes place that last about 3 days leading to tissue repair and restoration of function or even last for up to 2 weeks in some case. This phase is characterized by the influx of leukocytes into the area of the injury. During the early inflammatory state neutrophils and monocytes, the predominant cells at the site of the injury, emigrate from capillaries into the wound tissue in only a few days. Instead, later in inflammation stage, the macrophages are the predominant cells being responsible of phagocytize, digest and kill pathogenic organisms, scavenge tissue debris and destroy any remaining neutrophil. They can be considered as factories for growth factor production and play a pivotal

role in the transition between inflammation and repair. The growth factors involved in the initiation and control of inflammation in wound repair processes are: the platelet-derived growth factor (PDGF), important in the early inflammatory phase of wound healing; the transformed growth factors TGF- $\alpha$ , that plays an important role in keratinocyte migration and reepithelialisation; and the transformed growth factors TGF- $\beta_1$ , TGF- $\beta_2$ , and TGF- $\beta_3$ , which strongly promote the migration of fibroblasts and endothelial cells as well as the deposition of extracellular matrices by fibroblasts during granulation tissue formation. Whereas increasing TGF- $\beta_1$  promotes scar formation, TGF- $\beta_3$  exhibits an antiscarring effect (*Li et al., 2007*).

- 3) During the migration or proliferative phase, a permeability barrier is created (reepithelization), the appropriate blood supply is established (angiogenesis) and the injured dermal tissue is reinforced (fibroplasia). Firstly, the keratinocyte migration to the injured area takes place to replace damaged and lost tissue. In this step the extracellular matrix, integrin receptors, matrix metalloproteinases, as MMP-2 and MMP-9, and growth factors are involved. Then, keratinocytes proliferate growing over the wound from the margins under the dried scab accompanied by epithelial thickening. Granulation tissue is formed giving strength and form to the skin during the proliferative phase that last between 2-3 days. The maximum of blood vessels and granulation tissue is reached by the fifth day and the epithelial thickening continues for up to 2 weeks with the fibroblast proliferation and the collagen synthesis (*Boateng et al., 2008; Li et al., 2007*).
- 4) Afterwards, during the maturation or remodelling phase, the cellular connective tissue is formed and the new epithelium is strengthened thus determining the nature of the final scar. The cellular granular tissue

changes to an acellular mass from several months up to about two years (Boateng *et al.*, 2008).

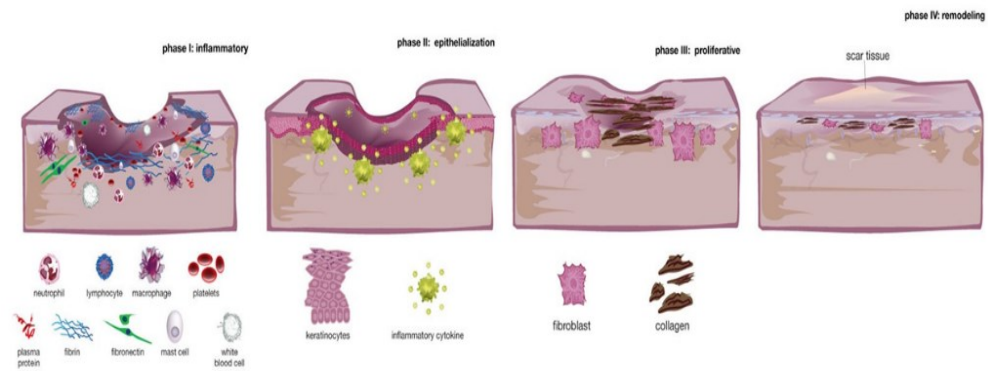


**Figure 1. Schematic representation of the healing process**

### 1.1.1. Factors influencing wound healing

There are multiple factors influencing the time of wound repairing as the wound size, depth and location as well as different systemic and local factors (table 1) (Guo & Di Pietro, 2010). However, one of the most important components present in the entire wound healing stages that influence the time of healing is the exudate: the liquid composed by blood from which the red cells and platelets were removed that is formed from chronic wounds, fistulae or other more acute injuries when haemostasis has been achieved (Cutting, 2003). The presence of exudate maintains the moist in the wound bed and supplying it with nutrients, helping to control the presence of bacteria and reducing the possibility of infection at the wound surface. However, in some cases, as occurs in chronic wounds, there is an excess of exudates that can impair the healing process: it can cause oedema, venous or lymphatic insufficiency as well as a reduction in the mobility and autolytic debridement (liquefying hard and eschar-like necrotic tissue) (Widgerow *et al.*, 2015). Accordingly, the design of wound dressings able to remove the excess of

exudate and at the same time being able to keep the moisture environment at the wound bed is an important target to achieve.

**Table 1. Systemic and local factors influencing the duration of wound repair.**

Systemic factors	Local factors
<ul style="list-style-type: none"> <li>- Ageing of population</li> <li>- Malnutrition and obesity</li> <li>- Bad habits (smoking and alcohol consumption)</li> <li>- Medications (corticosteroids)</li> <li>- Chronic medical conditions (cardiac failure, connective tissue disease, hypoxia, vascular disease, diabetes, cancer and immunosuppression)</li> </ul>	<ul style="list-style-type: none"> <li>- Venous and arterial vascular disease or pressure</li> <li>- Infection</li> <li>- Neuropathy</li> <li>- Necrotic tissue in the wound bed</li> <li>- Wound tension</li> <li>- Unfavourable local environment (too dry or too wet wound, contact dermatitis, inappropriate topical products or dressings)</li> <li>- Inappropriate treatment</li> <li>- Malignant wound</li> <li>- Repetitive trauma</li> <li>- Radiation</li> </ul>

*1.1.2. Types of wounds*

A wound is a “*disruption of normal anatomic structure and function*” by the Wound Healing Society and can be described as a defect or break in the skin, due to a physical or thermal damage or to the presence of an underlying medical or physiological condition (*Suvarna & Munira, 2013*). In a more

specific way, it is possible to differentiate between two types of wounds depending on the nature and time of the repairing process:

- Acute wounds: consists on tissue injuries mechanically produced by external factors like abrasions and tears (caused by friction of the skin with hard surfaces), including burns and chemical injuries, and also penetrating wounds (caused by knives and gun shots) and surgical wounds, that heal completely in the expected time frame (8-12 weeks) following the normal healing process and producing a minimal scarring.
- Chronic wounds: are the tissue injuries that heal slowly (beyond 12 weeks) and often reoccur due to persistent infections, to a diseases such as diabetes and other patient related factors or to a poor primary treatment due to the lack of funding to access to proper therapies, medical technologies and trained wound-care professionals. Decubitus ulcers (bedsores or pressure sores) and leg ulcers (venous, ischaemic or of traumatic origin) are the most commonly chronic wounds. (*Boateng et al., 2008*)

### *1.1.3. Chronic wounds*

The formation of a chronic wound is due to a failure or disruption of the orderly sequence of events in more than one of the previously defined healing stages (*Lazarus et al., 1994*). One of the main problems of chronic wounds is the presence of excessive amounts of exudates that result in maceration of healthy skin tissue around the wound inhibiting the healing. Furthermore, the presence of bacterial infection caused by *Staphylococcus aureus* or *Pseudomonas aeruginosa*, two of the most commons among other pathological bacteria, can complicate the healing process leading to cellulitis, bacteraemia and septicaemia, infective venous eczema, gangrene, haemorrhage and lower-extremity amputations (*Fazli et al., 2009*). The bad smell and staining caused by exudate, the presence of pain and the loss of

function and mobility, even in small wounds, have a negative impact on the patient quality of life leading to depression, distress and anxiety, embarrassment and in some cases social isolation. Moreover, financial burden for the patients and their families, a prolonged hospital stay and chronic morbidity or even death (*Guo & Di Pietro, 2010; Järbrink et al., 2017*).

Chronic wound can be divided into four different categories due to the causes that produce the wound:

- Venous leg ulcers: are caused by chronic venous insufficiency, occur in the gaiter area and are shallow with irregular shape and the presence of red granulation or yellow fibrinous tissue. Those ulcers are associated with oedema, hemosiderin pigment, venous eczema and lipodermatosclerosis.
- Arterial ulcers: are painful and distal wounds that often are dry or necrotic with poor granulation tissue. This kind of leg ulcer is common in smokers and patients with diabetes mellitus, hyperlipidemia and hypertension.
- Diabetic foot ulcers: are caused by peripheral neuropathy and angiopathic changes being most common in the soles of the feet due to a repetitive pressure.
- Pressure ulcers: are recognized by localized areas of tissue necrosis found over bony prominences that are due to an unrelieved pressure leading to localized tissue injury (*Morton et al., 2016*).



**Figure 2. From left to right: examples of venous leg ulcer, arterial leg ulcer, diabetic foot ulcer and pressure sore.**

#### *1.1.4. Incidence of chronic wounds in the world*

Chronic wounds are considered as a silent epidemic that affect a large fraction of the world population. Different epidemiologic studies have demonstrated that during their lifetime, 1-2% of population in developed countries will experience a chronic wound. Only in U.S, chronic wounds affect 6.5 million people while the number rises to 20 million worldwide. The burden of chronic wounds is continuously growing due to the aging population, the increase of health care costs and the heavily rise in the incidence of diabetes and obesity worldwide (*Sen et al., 2009*) being around \$39 billion per year in U.S, while the economic burden related to the use of wound dressings will reach more than \$24 billion in 2021 (*Frykberg et al., 2015; Han & Ceilley, 2017*). Moreover, it is estimated that up to 25% of people suffering diabetes is going to develop a diabetic foot ulcer during their life, being the cost of a single episode nearly \$50.000 and the costs related to amputations nearly \$3 billion per year, whereas in the case of venous ulcers, the annual cost is estimated to \$2.5–3.5 billion. Beyond of the treatment costs, there is the mortality rate due to these diseases: 60.000 people in U.S die per year due to bedsores-related problems and the 5-years mortality rate after limb amputation is estimated in 50% (*Sen et al., 2009*).

### Global Wound Healing Device Market, by Segments, 2015

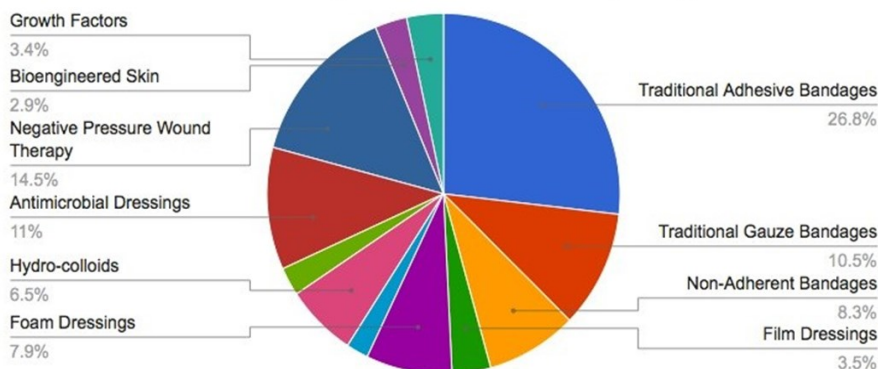


**Figure 3. Economic burden of wound dressings divided by segments.**

#### 1.2. Wound dressings

The development of wound dressings is still in continuous progress since it is difficult to develop a dressing able to satisfy all the requirements for the proper healing of a wound. Thus, ideal wound dressings should have a proper adherence to the wound site fitting completely the wound bed while being easy to apply and remove without provoke any pain to the patient; they must provide a good absorbance of exudates as well as transpiration in order to remove great amounts of exudate without drying the wound; they must be able to tailor the delivery of active pharmaceutical ingredients (APIs) and being inexpensive. Dressings can be classified depending on their function on the wound, the type of material used to their production and the physical form of the dressing. They can also be classified in a more general definition as traditional, modern and advanced dressings, skin replacement products and wound healing devices (*Boateng et al., 2008*).

##### 1.2.1. Traditional wound healing devices.

The traditional wound healing agents are those commonly used in the past including topical pharmaceutical formulations and traditional dressings

which nowadays are less employed and are being substituted by the modern wound dressings. Among the topical pharmaceutical formulations there are semi-solid preparations (as silver sulphadiazine cream and silver nitrate ointment) and solutions, as povidoneiodine, containing antimicrobial agents for reducing the bacterial load in the wound. However, these dosage forms have short residence times in the wound site especially when a high amount of exudate is presented. By the other hand, traditional dressings includes: cotton wool, as the *Gamgee tissue*, applied over a primary wound dressing and used to absorb exudate; natural or synthetic bandages, as the *Cotton Conforming Bandage 1988*, used for the retention of light dressings, *Compression Bandages* for the treatment of venous insufficiency as well as *Short Stretch Compression Bandage* used for venous leg ulcers and lymphoedema or *Polyamide and Cellulose Contour Bandage Knitted BP 1988* used for dressing retention; and gauzes like sterile gauze pads for packing open wounds that absorb fluid and exudates. This traditional dressings can be used as primary or secondary dressings, or forming part of a composite of several dressings but they are dry and do not provide a moist wound environment. Furthermore, in the case of gauzes, they need to be changed regularly to prevent maceration of the healthy tissue, they lose its bacterial protection when the outer surface is moistened by exudate or external fluids and when the amount of exudates diminishes they become more adherent to the wound causing pain when remove. For all these reasons, traditional dressings should be used only in the case of clean and dry wounds or as secondary dressings to absorb exudates and provide protection to wounds; meanwhile the modern dressings are more indicated for the treatment of chronic wounds (*Boateng et al., 2008*).

### 1.2.2. Modern wound dressings

The classification of modern wound dressings is done according to the materials from which they are produced and generally occur in form of gels, thin films and foam sheets:

- *Hydrocolloid dressings*: are obtained from colloidal (gel forming materials as carboxymethylcellulose, gelatin and pectin) materials in combination with other materials such as elastomers and adhesives. Some examples already presented in the market are Granuflex™ and Aquacel™ (Conva Tec, Hounslow, UK), Comfeel™ (Coloplast, Peterborough, UK) and Tegisorb™ (3M Healthcare, Loughborough, UK). They are effective in the treatment of wounds that fail to respond to compression therapy alone and do not cause pain on removal, but they have an occlusive outer cover that prevents water vapour exchange between the wound and its surroundings, being disadvantageous for infected wounds that require a certain amount of oxygen to heal rapidly.
- *Alginate dressings*: are able to form gels when in contact with wound exudates. The high adsorption through a strong hydrophilic gel formation limits wound secretions and minimises bacterial contamination. Once applied to wounds, ions present in the alginate fibre are exchanged with these present in exudate and blood to form a protective film of gel, helping to maintain the lesion at optimum moisture content and healing temperature. Alginate dressings as Sorbsan™ (Maersk, Suffolk, UK), Kaltostat™ (Conva Tec), Tegagen™ (3M Healthcare) or Comfeel Plus™ remains on the wound for a longer period than hydrocolloids and are useful for all wound-healing stages. However, they cannot be used for dry and covered with hard necrotic tissue wounds because it could dehydrate them since they

only function properly in presence of moisture, thus, they are only useful for moderate to heavily exuding wounds.

- *Hydrogel dressings*: are insoluble and swellable hydrophilic materials made from synthetic polymers that can be applied as an amorphous gel or as a elastic, solid sheet or film. Some commercially available products are hydrogel/alginate combination dressings: Nu-gel™ (Johnson & Johnson, Ascot, UK) and Purilon™ (Coloplast). In general, hydrogel dressings possess almost all desirable characteristics of an “ideal dressing” since they are suitable for cleansing of dry, sloughed or necrotic wounds due to their ability for rehydrating dead tissues and enhancing the autolytic debridement. In addition, they are non reactive with biological tissue, they are permeable to metabolites, they do not irritate or adhere to the skin surrounding the wound, are malleable, do not leave residues and improve the reepithelialisation as well as are able to provide a cool environment that reduces the pain. Hydrogel dressings are suitable for all the 4 stages of wound healing with the exception of infected or heavily exuding wounds, because they are formed by a 70-90% of water so they cannot absorb a great amount of exudate. Furthermore, when they are applied as gel, a secondary covering is required so they need to be changed frequently and its low mechanical strength may make its handling difficult.
- *Semi-permeable adhesive film dressings*: are made from nylon derivatives supported in an adhesive frame of polyethylene that makes them occlusive. There are some available products as Cutifilm™ (B.D.F. Medical, Miltonkeynes, UK), Bioocclusive™ (Johnson & Johnson) and Tegaderm (3M Healthcare), but in general, they have low capacity to absorb exudates, leading to skin maceration, bacterial proliferation and risk of infection, so they should be frequently changed. In addition, they cannot be packed into deep or cavity wounds

because of its thin structure that make them only suitable for relatively shallow wounds.

- *Foam dressings*: are made from polyurethane and can be presented in form of porous foam or a foam film. Foam dressings as Tielle™, Lyofoam™ (ConvaTec) and Allevyn® (Smith and Nephew) may maintain the moisture around the wound and provide thermal insulation as well as absorb high amount of exudates. Furthermore, they are suitable for partial-or-full thickness wounds with minimal or moderate drainage to heavily exuding wounds due to its porous structure. However, they are not suitable for dry epithelializing wounds or dry scars.
- *Biological dressings or bioactive dressings*: include the biodegradable tissue engineered products derived from natural tissues or artificial sources. Usually they are a combination of different polymers (collagen, hyaluronic acid, chitosan, alginates and elastin) in which can be incorporated active compounds (antimicrobials or growth factors) for delivery to the wound site.
- *Tissue engineered skin substitutes*: are referred to the use of smart polymers (either in the natural biological form or semi-synthetic forms) that acts as scaffolds for tissue engineered substrates that replace lost tissue rather than facilitate wound healing, thus they are able to mimic normal physiologic responses to wound healing, because of that they are useful for chronic and third degree wounds that are difficult to heal and for the delivery of bioactive materials (growth factors or genetic materials) to a wound. However, they are still limited by the high cost involved, the risk of infection and antigenicity. Moreover, in some cases is necessary to create a second wound for harvesting patient's own cells to aid wound healing and the legal and ethical issues about

stem cells research makes the adoption of these dressings in routine clinical practice still rarely (*Han & Ceilley, 2017*).



**Figure 4. Some examples of commercially available modern wound dressings.**

### 1.3. Polymers for dressing applications

Synthetic and natural polymers are every time more used as excipients in the pharmaceutical field and its use depends on the kind of formulation and the route of administration. In fact, special attention is paid on those biocompatible and biodegradable since they can be readily hydrolysed into removable and non-toxic products, thus being eliminated through metabolic pathways. Some of the synthetic polymers commonly used for controlled release in dressing formulations are (*Englert et al., 2018*):

- Polyglycol acid (PGA): is an aliphatic polyester approved by the FDA for a wide range of applications. It is highly crystalline, fiber former, biocompatible, biodegradable and poorly soluble in organic solvents.

- Poly lactic-co-glycolic acid (PLGA): is a biodegradable copolymer formed by poly-lactic and poly-glycolic acid chains being its biodegradability modelled by variations in the composition ratio. Is one of the most accepted and approved materials for microparticles formation and commonly used for injectable micro-particulate systems.
- Poly-ε-caprolactone (PCL): is a non-toxic, biodegradable, semi-crystalline aliphatic polyester, which is approved by the FDA for several applications, e.g. drug delivery systems, sutures, long-term implants and adhesion barriers as well as new tissue scaffold host systems. It is hydrophobic, but soluble in several solvents, can be blended with a variety of other materials and degrades very slowly under physiological conditions (from months to years) compared to other polyesters.
- Polyvinylalcohol (PVA): is approved by the FDA and it can be obtained in a wide range of solubility, tensile strength and adhesiveness. The hydroxyl groups make them suitable for crosslinking to create hydrogel networks with low or high swelling behaviour in water.
- Polyvinylpyrrolidone (PVP): is used as a vehicle for drug dispersion and suspension and used as an adhesive in transdermal systems. The best example of PVP formulation is the disinfectant povidone-iodine.

On the other hand, in the last few years, polysaccharide-based polymers isolated from natural resources as plants, microorganisms, algae and animals, have attracted scientists attention due to their wide range of pharmacological activities (e.g. antitumor, antioxidant or anti-inflammatory effects) and properties since they are biocompatible, biodegradable, non-toxic and inexpensive excipients (*Yu et al., 2018*). Polysaccharides are polymeric

carbohydrate molecules formed by long chains of monosaccharide units bound together by glycosidic linkages and they can be divided in three groups:

- I. Homoglycans: polysaccharides formed by only one type of monosaccharides.
  - $\alpha$ -glucans: Pullulan is a  $\alpha(1\rightarrow4)$ ,  $\alpha(1\rightarrow6)$ -D-glucan biosynthesized from starch by the ubiquitous yeast-like fungus *Aureobasidium pullulans* (Dothioraceae) (*Mogoşanu et al., 2014*). It is soluble in water and has good water-uptake capacity and wound healing and antibacterial activities.
  - $\beta$ -glucans: is presented in the cell walls of yeasts, fungi and cereal plants. It consists on residues of D-glucopyranose linked through  $\beta(1, 3)$ -glucosidic linkages with one  $\beta(1, 6)$ -linked D-glucosyl group for every three glucose residues. It was found that have antibacterial and antiviral activities with skin wound healing properties (*Naseri-Nosar et al., 2018*).
  - Dextrans: are composed by a main chain of  $\alpha(1 \rightarrow 6)$ -linked glucopyranose units, which can be branched by  $\alpha(1\rightarrow2)$ ,  $\alpha(1\rightarrow3)$  or  $\alpha(1\rightarrow4)$  linkages, in a proportion lower than 50% (*Llamas-Arriba et al., 2019*). Dextran is soluble both in water and in organic solvents and is widely used in drug delivery and in scaffolds for tissue ingeneering applications (*Unnithan et al., 2015*).
  - Cellulose: is the most abundant polysaccharide available in nature and is composed by 1,4- $\beta$ -D-glucopyranosyl units. It is insoluble in water, thus limiting its use, but cellulose derivatives (semi-synthetic polymers obtained by alchilation and esterification of hydroxyl groups of cellulose polymeric chains) as hydroxyethyl cellulose (HEC) that is water-soluble,

are commonly used from drug release dressing formulations (*El Fawal et al., 2018*).

- Chitosan: obtained by the alkaline deacetylation of chitin extracted from shellfish, is a linear copolymer of  $\beta$ -(1  $\rightarrow$  4)-linked 2-acetamido-2-deoxy- $\beta$ -D-glucopyranose and 2-amino-2-deoxy- $\beta$ -D-glucopyranose. In acidic media, the amino groups are protonated thus being able to interact with different kinds of molecules. Therefore it can be used for different applications as in drug and gene delivery, cell encapsulation, protein binding, tissue engineered, wound healing, and as antibacterial, in textiles and food packaging, and antimicrobial in food additives (*Patrulea et al., 2015*).

II. Heteroglycans: polysaccharides formed by more than one type of monosaccharides.

- Pectin: is a structural heteropolysaccharide, formed by linear chains of  $\alpha$ -(1-4)-linked D-galacturonic acid, that is presented in the cell walls and it is extracted from citrus fruits. In presence of bivalent cations it gelifies ionotropically and the strength of the gelification depends on its methoxyl degree as well as on its amidation degree: amidated pectin of low methoxyl degree gelifies quickly in presence of liquids, as wound exudates (*Voragen et al., 2009*). Pectin is widely used as carrier of different drugs in controlled release formulations and also as carrier material in colon-specific drug delivery systems (for systemic action or a topical treatment of diseases such as ulcerative colitis, Crohn's disease and colon carcinomas) (*Sriamornsak, 2003*).

- Carrageenan: is obtained from seaweeds of the marine red algae family. It consists on alternating long linear chains of  $\alpha$ -(1, 3)-D-galactose and  $\beta$ 1, 4 3, 6-anhydro-galactose with ester sulphates (15–40%). It is used as emulsifier, gelling, thickening, stabilizing agent in pharmaceutical and

industrial applications. It has inflammatory and immunomodulatory properties and is used as anticancer, antihyperlipidemic agents as well as herpes and human papillomavirus inhibitors (*Yegappan et al., 2018*).

- Agar: is extracted from Gracilaria cell walls and from Gelidium and is composed of two major types of polysaccharide, namely, a rigid fibrillar structure consisting of cellulose and a matrix-like structure consisting of D-galactose, 3,6-anhydro-L galactose, and chromoprotein (phycocyanin and phycoerythrin). Agar gels are employed in different fields due to its biodegradability and its gelling, thickening and stabilizing properties, but its high costs limit its application (*Xiao et al., 2019*).

- Alginate: obtained from algae, is a linear copolymer consisting on 1 → 4 linked β-D-mannuronic acid (M) and its C-5 epimer α-L-guluronic acid (G). It is comprised of sequences of M-blocks and G-blocks residues interspersed with MG sequences. It was demonstrated that high mannuronic content alginate induce the production of cytokines in wound healing process (*Pawar et al., 2012*). Alginate is a very versatile polymer that can be used in a wide range of applications as injectable vehicles for tissue engineered; as topical drug delivery systems due to the previously mentioned properties; as buccal, ocular and gastrointestinal dosage forms due to its mucoadhesive properties; as vaccine adjuvants or coadjuvants to enhance bioavailability and immunogenicity of antigens after nasal and oral administration; and as gastro-retentive drug carriers due to its large surface areas when in form of microparticulate delivery systems (*Szekalska et al., 2016*).

III. Glycosaminoglycans: are highly sulphated polydisperse linear polysaccharides.

- Chondroitin sulphate: is composed of a linear chain of N-acetylgalactosamine and glucuronic acid. It promotes wound healing and

is commonly used in tissue engineering in the form of hydrogels or nanoparticles for drug delivery applications.

- Heparin: is composed by a linear backbone containing sulfonic, carboxylic and sulphanilamide groups. It has anticoagulant activity and has been considered as carrier for drug delivery systems since it can establish non-covalent bounds with different bioactive molecules as growth factors.

- Hyaluronan (HA): is made of glucuronic acid and N-acetylglucosamine linked via alternating  $\beta$ -1,3 and  $\beta$ -1,4 anhydroglycosidic bonds. It modulates the inflammatory response and promotes cell adhesion and growth being commonly used in the form of injectable hydrogel in tissue engineering (*Celikkin et al., 2017*).

In fact, there are different dressing formulations commercially available based on the use of polysaccharides as active excipients in wound healing. Alginate dressings, such as the previously mentioned Sorbsan<sup>TM</sup>, Kaltostat<sup>TM</sup>, Tegagen<sup>TM</sup> and Comfeel Plus<sup>TM</sup>, are effective for all healing stages but nevertheless they present some adverse effects as dehydration in wounds that are dry or covered with high necrotic tissue (*Boateng et al., 2008*). Chitosan-dressing formulations such as Axiostat® are effective for control bleeding of lacerations, minor cuts and abrasions but not for application in chronic wounds ([www.accessdata.fda.gov/cdrh\\_docs/pdf17/K172324](http://www.accessdata.fda.gov/cdrh_docs/pdf17/K172324)). For these reasons, novel formulations are required to overcome the problems of wound dressing devices already commercially available.

The main aim in the development of new dressings is to reach high standard in a cost/effectiveness analyses. Hence, the development of inexpensive wound dressings easy removable, able to be removable without trauma, that could completely fill the wound bed avoiding the bacterial proliferation and allowing at the same time the absorption of exudates and transpiration would

be an adequate approach to the formulation of new high cost effective dressings. Taking into account that, the development of “*in-situ*” gelling formulations, based on polysaccharide polymers as excipients, either in form of small powder particles with high surface areas (which can enhance the fluid uptake from wounds and improving the drug adsorption and the gelling rate after application) and in form of large aerogel particles, easily handled, with high porosities and surface areas also improving in this case the exudate absorption while forming a soft gel could be a promising approach to the production of a new generation of wound care devices.

#### **1.4. “*In-situ*” gelling formulations**

Hydrogels are suitable as protein delivery systems and as cell-entrapping scaffolds in tissue regeneration since they are soft and hydrophilic, but the traditional hydrogels obtained by chemical crosslinking of water-soluble polymers are incompatible with such kind of molecules. For this reason, is gaining attention the possibility of developing hydrogels able to spontaneously gel “*in-situ*” when in contact with biological fluids and able to increase the drug persistence in the site of action and controlling its release (*Van Tomme et al., 2008*). In the case of wound healing, the topical administration using the adequate excipients could promote the repairing process and avoid problems related with the stabilization of the drug and some problems related with systemic administration of drugs, as antibiotics resistance. Such kind of formulations are presented in form of micro- and nano-particulate systems in form of dry powders or aerogels, made from biocompatible and biodegradable excipients able to gellify when in contact with the wound fluids, gelling only on the lesion and not on the perilesional skin, thus avoiding problems related with traumatic removal and protecting the wound from the external environment and further infections. They are

able to maximize the drug persistence in the site of action and control the drug release thus allowing an easy, reproducible and accurate administration of the dose. (*De Cicco et al., 2014*).

### **1.5. Aerogels**

Aerogels were invented in the early 1930s by Steven Kistler (Stockton, California), and the term “aerogels” encompasses the nanostructured materials with up to virtually 100% overall porosity in the mesoporous range and with full pore interconnectivity that are obtained by the removal of the liquid component of a gel, subsequently substituted by a gas, avoiding the pore collapse phenomenon without damage the porous texture of the wet material (*García-González et al., 2011*). Aerogels are usually processed by the sol-gel methodology. Firstly, a gel is formed from a solution (sol) (i.e. formation of hydrogel from an aqueous solution) promoted by the action of a cross-linker that can be of chemical nature, as a cross-linker compound, or physical nature, as pH and temperature. In the following step, water presented in the gel structure is replaced by a solvent (alcohol) in order to obtain an alcogel. At the end, the aerogel material is obtained by the removal of the alcohol (usually ethanol) from the gel through the supercritical carbon dioxide (sc-CO<sub>2</sub>)-assisted drying (*Maleki et al., 2016; García-González et al., 2013*).

Aerogels are a class of nanoporous materials with particular structures and extraordinary materials characteristics: they simultaneously possess very high porosity ( $\approx 80-99.8\%$ ), high surface area ( $\approx 500-1200 \text{ m}^2/\text{g}$ ), ultra-low density ( $\approx 0.003-0.5 \text{ g}/\text{cm}^3$ ) and mesoporous (2-50 nm) pore size distribution. Furthermore, they possess other extraordinary characteristics as flexibility, transparency, low thermal conductivity, high mechanical strength and ultra-low dielectric constant. Due to all these characteristics they are suitable

materials for different applications: they are used as thermal insulation in building or construction; as materials for aerospace fabrications; in catalysis, filtration and environmental clean-up; as chemicals sensors, Cherenkov counters, piezoelectric devices, acoustic transducers, microwave electronics, metal casting molds, water repellent coatings and in battery applications (*Stergar et al., 2016*); in food related technologies, as packaging (*Mikkonen et al., 2013*); and, more recently, for medical and pharmaceutical applications as the controlled delivery of nonsteroidal anti-inflammatory drugs (*Del Gaudio et al., 2013*), the delivery of growth factors (*Díaz-Gómez et al., 2016*) or a steroidal anti-inflammatory drug (*Goimil et al., 2018*) from scaffolds, and the topical release of chitosan in chronic wounds (*López-Iglesias et al., 2019*) among others.

Aerogels morphology can be defined during the gelation process (molding, extrusion) or through the post-processing of the aerogels (milling, grinding) and they can be manufactured in a myriad of morphologies (beads, disks, powders, films or monoliths) and sizes. Polysaccharide-based aerogels are most commonly prepared in form of cylindrical monoliths by molding, but there is the possibility of obtaining them in form of beads in the millimeter/centimetre range. In the case of beads, the polysaccharide aerogel precursors are usually dropped, into the solution with the crosslinker or gelation promoter (e.g. a cationic solution, temperature or controlled pH) to trigger gelation. Instead, aerogel granules or powders can also be obtained by the conventional ball milling or by mechanical grinding of the initially fabricated monoliths without producing a severe distortion in its porous network and surface characteristics (*Maleki et al., 2016*).

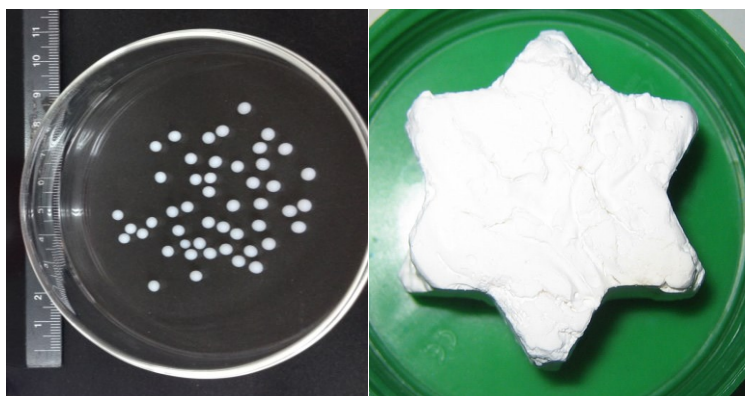


**Figure 5. Aerogel materials obtained in form of beads (left) and monolith with star-like shape (right).**

#### *1.5.1. Aerogels classification*

In accordance with their composition, aerogels can be classified into inorganic, organic or inorganic-organic hybrid aerogels (*Stergar et al., 2016*): the inorganic aerogels are those made from alkoxides including aerogels from some metallic oxides, being the silica aerogels the most widely studied because its suitability for many applications (*Schmidt & Schwertfeger, 1998*), especially as super-insulators, however they cannot be applied in life sciences because they are biocompatible but not biodegradable; the most studied organic aerogels are those of resorcinol-formaldehyde and melamine-formaldehyde, being also used as thermal insulators but, in this case, the toxic compounds involved in the manufacturing process limit its application in life sciences; however, organic molecules in combination with ceramic materials form the hybrid or composite aerogels that leads to a final material formed by an aerogel matrix and one or more additional phases. The easiest method for the production of composite aerogels is the previously mentioned sol-gel approach by incorporation of additional components as soluble organic or inorganic compounds, insoluble powders, polymers, biomaterials and pharmaceuticals (*Stergar et al., 2016*).

### *1.5.2. Aerogels for pharmaceutical application*

Since a few decades ago the advances and development of the aerogel science made that the interest for these materials in pharmaceutical sciences for drug delivery applications have been increased. The possibility of using of bio-based materials plays a key role in the development of new drug delivery formulations, especially the use of natural polysaccharides due to their stability, availability, low toxicity and low cost, as previously described. The aerogels made from polysaccharides (e.g. agar, nitrocellulose and cellulose) were already described by Kistler in 1931, however the research on them has been recently started, and is now also being extended to cosmetic, food and biotechnological fields (*García-González et al., 2011*). In literature was already reported the development of polysaccharide-based aerogels as potential carriers for drug delivery systems: the production of the starch aerogels from potato and corn resources obtained in form of monoliths (*Mehling et al., 2009*); the production of pectin aerogels from citrus peel both in form of powders (*White & Budarin et al., 2010*) and in form of monoliths (*White & Antonio et al., 2010*); the production of calcium-alginate aerogels in form of beads and microspheres (*Alnaief et al., 2011*) and also in form of monoliths (*Mehling et al., 2009*); the production of aerogel beads of K-carrageenan (*Quignard et al., 2008*) and of agar (*Robitzer & Tourrette et al., 2011*); the production of chitin (*Tsiptsias et al., 2009*; *Robitzer & Di Renzo et al., 2011*) and chitosan (*Chang et al., 2008*) monoliths as well as chitosan beads (*El Kadib et al., 2011*) and cellulose monoliths from different sources (*Innerlohinger et al., 2006*; *Liebner et al., 2010*). However, the possibility to produce polysaccharide-based aerogels in form of beads for administration in wounds, composed by an inner hollow part able to enhance the exudate adsorption capacity and in which can be encapsulated an API, and by a thin polymeric shell improving drug release, was not still developed nowadays.

For pharmaceutical applications, there are many different approaches based on the use of supercritical fluids technologies for the preparation of powders and aerogels as drug delivery vehicles and are further explained below.

### **1.6. Supercritical fluids technologies**

Supercritical fluids (SCFs) are substances used at pressure and temperature conditions beyond of its critical point. By this way, the fluid possesses the density and the solvent power of a liquid whereas the viscosity and the transport properties are common to those of a gas. Furthermore, the changes in temperature and pressure at the critical point allow to modify the density of the fluid thus being SCFs very versatile for different processes such micronization, extraction of natural compounds, chemical reactions or aerogels synthesis. There are different solvents and its mixtures that can be used as SCFs (table 2) being the carbon dioxide (CO<sub>2</sub>) commonly used on pharmaceutical field due to its mild conditions at the supercritical point (figure 6), 31°C and 73.8 bar, that hence are easy to reach and also because of its availability, safety, non-toxicity and low-cost. In conclusion, sc-CO<sub>2</sub> methodologies are considered as “green technologies” due to the possibility of CO<sub>2</sub> reutilization and release into the atmosphere at the end of the process (Tabernero *et al.*, 2012).

**Table 2. Temperature and pressure at the critical point for different solvents used as supercritical fluids.**

Solvent	T critical (K)	P critical (bar)
Carbon dioxide	304.3	74.0
Water	647.6	218.3
Methane	190.4	45.4
Ethane	305.3	48.1
Propane	369.8	41.9
Ethylene	282.4	49.7
Propylene	364.9	45.4
Methanol	512.6	79.8
Ethanol	513.9	60.6
Acetone	508.1	46.4

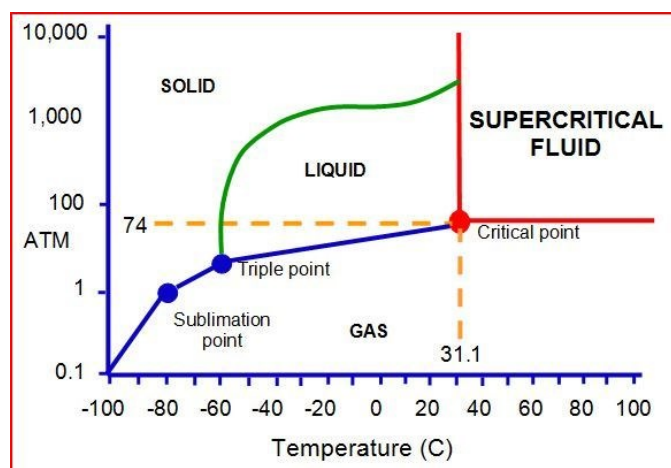


**Figure 6. Carbon dioxide phases diagram.**

In function of the role played by the supercritical fluid, in the pharmaceutical field the commonly used processes based on the utilization of supercritical fluids can be classified in three broad categories but there are numerous variations on them (Davies *et al.*, 2008):

- The Rapid Expansion of Supercritical Fluids (RESS): the fluid acts as a solvent for the drug and excipients that have some degree of

solubility into the supercritical fluid and are further precipitated at the end of the process.

- The Supercritical Assisted Atomization (SAA): the fluid acts as an atomization medium of the solution, containing the drug and excipients, and promoting its precipitation in form of micro/nano particles.
- The Supercritical Antisolvent Extraction (SAE): the fluid is used as antisolvent in combination with a co-solvent for the removing of the organic phase from gel formulations containing the drug and excipients and promoting the precipitation of both components.

#### *1.6.1. Supercritical Assisted Atomization (SAA)*

In the SAA process, the supercritical fluid acts as a co-solute. In fact, the supercritical fluid is solubilized in the liquid solution, consisting of the solvent and the solute to be micronized. This solution is injected through a nozzle placed at the top of a precipitation chamber, where evaporation of the solvent occurs by the utilization of warm nitrogen and the consequent formation of the particles takes place through a “decompressive atomization”, which consist on the production of smaller secondary droplets by the fast elimination of the solubilised CO<sub>2</sub> from the primary droplets. The presence of the supercritical fluid allows, in fact, reducing the viscosity and surface tension of the liquid in order to obtain drops and, consequently, particles, smaller than those obtained with traditional spray-drying processes. The possibility of having such small drops causes them to be quickly dried by a thermal carrier, leading to the formation of micrometric particles. The main limitation of this process lies in the temperatures required for drying, although working below atmospheric pressure can lower the working temperature (*Adami et al., 2011*). One of the main advantages of SAA is the possibility of using both organic solvents, in which the supercritical-CO<sub>2</sub> in

suitable process conditions is completely soluble, or aqueous solutions (or simply water) as process solvents, in which the sc-CO<sub>2</sub> is only partially soluble (up to the solubility limit at operating temperatures and pressures). The non-solubilized part acts as a "propellant" at the pressure drop caused by passing through the nozzle whereas the solubilized part causes the formation of an expanded liquid, characterized by a surface tension and a lower viscosity than a liquid in non-supercritical conditions. Therefore, there is a reduction in the cohesive forces (surface tension and viscosity) and the prevalence of the disintegration forces (friction and turbulence) at the injector where the atomization phenomenon takes place (*Reverchon, 2002*).

#### *1.6.2. Supercritical Antisolvent Extraction (SAE)*

Supercritical Antisolvent Extraction (SAE) or also called "supercritical drying" is an alternative drying process based on the use of SCFs, commonly CO<sub>2</sub>, and a co-solvent, usually ethanol or acetone, for removing the organic phase from solid formulations in order to produce aerogels from alcogels (*García-González et al., 2012*). Furthermore is a commonly used process for the extraction of many components as polyphenols from natural matrices (coffee beans, seeds) or catechins (*Reverchon et al., 2001*).

This process consist on introducing the material to be dried into a vessel of the apparatus with a proper amount of the co-solvent, close it hermetically and heating until the optimized temperature was reached. Once this occurs, the SCF is pumped into the vessel at the adequate temperature to maintaining it at supercritical conditions. The extraction process is carried out at a continuous flux of SFC and the organic solvent is completely removed from the dried formulation matrix. By means of this technique, supercritical fluid mixtures are formed in the gel pores, without remaining any liquid phase and avoiding the presence of an intermediate vapour-liquid phase that would promote surface tension in the gel pores and the collapse of the matrix

structure during solvent elimination as occurs in the case of conventional drying processes.

In general, supercritical drying of gels is the only process able to remove the solvent of the gel without damaging the gel network structure due to the intrinsic absence of surface tension in the pores of the gel (*García-González et al., 2012; García-González et al., 2013; Sanz-Moral et al., 2014*) since atmospheric drying of gels usually leads to the collapse of the pores due to the high capillary pressure gradients obtained upon the solvent removal, whereas the freeze drying of hydrogels often leads to cracks and the formation of large pores due to the increase in volume of water (i.e. the gel solvent) upon crystallization (*Betz et al., 2012; Jiménez-Saelices et al., 2017*). In the case of the supercritical drying of gels, the effects of an overestimation of the processing time on the end textural properties can be negligible or noticeable depending on the gel source (*Du et al., 2013; Pierre & Pajonk, 2002*). Overall, the choice of the drying method and the optimization of the drying process from the point of view of both materials performance and economy of the process will depend on each specific case of gel source and gelation mechanism. In addition, for the specific case of aerogels production in form of beads for topical administration in wounds it is necessary to produce the starting gel particles, to be submitted to the supercritical drying process, through a robust technique able to produce homogeneous and spherical gel beads in a narrow size distribution. For that, a suitable technique that meets all these requirements is the prilling or laminar jet break-up technology (*Del Gaudio et al., 2005*).

### **1.7. Prilling technology**

Prilling or laminar jet break-up technology is a process used for the production of microparticles in a narrow dimensional range and high encapsulation efficiency under mild operative conditions (room temperature

and atmospheric pressure). It consists on breaking apart a laminar jet of polymer solution into a row of mono-sized droplets by the application of a vibration force: when the vibration wavelength reaches its critical value, called the “Rayleigh wavelength”, the fluid is broken in spherical droplets by the action of surface tension that subsequently fall into a gelation solution thus forming the beads, but if the Rayleigh frequency is not reached or the amplitude of vibration is too low “satellite” liquid particles are formed (*Del Gaudio et al., 2005; Cerciello et al., 2017*).

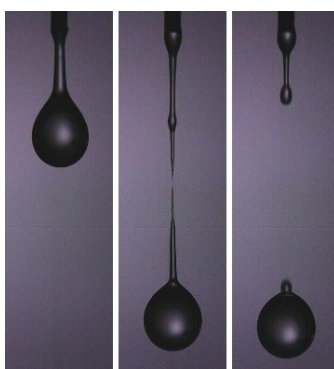


**Figure 7. Example of “satellite” particles formation.**

This technique was firstly developed by Joseph Plateau and Lord Rayleigh in 1878 through the study of linear stability analysis and nowadays is commonly applied for the encapsulation of chemicals, biological molecules, aromas and fragrances, pigments, extracts, drugs, cells and microorganisms due to its advantages as the production of high amounts of beads per second (up to 6000 beads according the encapsulation conditions and the polymeric blend) in an one-step process, the capability of operate at mild conditions, the high control of the narrow size distribution of the extruded droplets and the possibility to produce core-shell particles (*Whelehan & Marison, 2011; Serp et al., 2000; Fabien et al., 2016*).

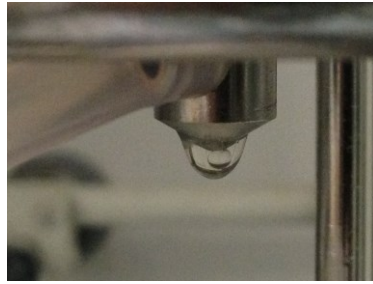


**Figure 8. Example of core-shell particle formation by co-axial prilling.**

In the pharmaceutical field, the use of prilling technique have been already reported for the development of drug delivery systems in form of beads (*Auriemma et al., 2013; Del Gaudio et al., 2015*) and core-shell microparticles (*Del Gaudio et al., 2014; Cerciello et al., 2016; Rodríguez-Dorado et al., 2018*) as well as it was reported the efficiency of the utilization of the prilling technique in tandem with the supercritical drying for the development of wound healing formulations (*Del Gaudio et al., 2013; De Cicco et al., 2016*).

### **1.8. Aims of the project**

Chronic wounds are increasing in the Western countries due to the continuous population ageing and to the incidence increase of non-communicable diseases as diabetes and cardiovascular-related maladies, the two main causes of non-healing wounds, that represent one of the major threat of health globally. Nowadays, there are different dressing materials commercially available for the treatment of chronic wounds, as hydrocolloids, foams, films or hydrogel dressings among others. The major technological challenge in formulating a new device for the treatment of chronic wounds is to find a compromise between the ability to absorb high amounts of exudate present in this kind of wounds (venous leg ulcers, diabetic foot ulcers and pressure sores) and the ability to maintain a proper moisturized environment. Moreover, in order to obtain an active wound healing device, formulations should be able to tailor the delivery of a loaded active pharmaceutical ingredients (APIs) directly to the wound. In addition, aspects related to the fitting of a dressing on the wound bed and the adequate removal without causing pain, are critical for the patient compliance.

In order to overcome these issues, this PhD project has been focused on the development of technological approaches based on supercritical fluids for the production of polymeric micro-nano particulate systems for wound healing by using natural biopolymers, as high mannuronic content alginate, low molecular weight chitosan and low methoxyl grade pectin amidate, as biocompatible and low-cost excipients able to tailor the delivery of drugs and to overcome the problems related to conventional devices (traumatic removal, dehydration, occlusiveness, high costs).

The general objectives of this PhD thesis were:

- Designing and developing new active topical formulations, in form of dry powders or aerogels, able to control release rate of APIs to wounds, ulcers and bedsores, acting as an efficient non-traumatic dressing.

- The evaluation of processes based on SC-CO<sub>2</sub> (SAA and SAE) and/or in combination with the laminar jet break-up technique (prilling) to produce wound healing formulations loaded with different APIs.
- To determine the mechanisms involved in the particles production, the kinetic of release from the polymeric carrier and the influence of the polymer properties on the release kinetic of the API cargo.
- Investigation on the technological properties of the formulations focused on chemico-physical, morphological and mechanical properties, size distribution, gelling rate, fluid uptake and moisture exchange properties, as well as API release profile in simulated wound fluid (SWF).
- Determination of the healing properties of the powders and aerogels through in vitro tests, carried out in Franz cells using SWF, and in vivo assays with mice, and/or rats.

In particular the PhD program involved the development and characterization of:

- “In-situ” gelifying powders loaded with doxycycline obtained through Supercritical Assisted Atomization (SAA) for wound healing applications.
- Aerogel formulations able to uptake higher amounts of exudate obtained by Prilling in tandem with Supercritical Antisolvent Extraction (SAE). In particular, this part of the work involved the production of alginate aerogels in form of spheres, and the production of hollow aerogels loaded with a BCS Class I drug (ketoprofen lysinate). The optimization of the different drying process for the production of the alginate aerogel beads and the aerogel loaded-capsules with high specific surface areas and porosities was carried out during a research period of 7 months in the University of Santiago de Compostela (Spain).

The formulations were characterized in terms of textural properties (nitrogen adsorption porosimetry, helium picnometry), morphology and size distribution (SEM, DLS), beads hardness (dynamometry), solid state (DSC, FT-IR) and drug content and encapsulation efficiency (UV, HPLC).



## **2. MATERIALS AND METHODS**



## 2.1. Chemicals

- Medium viscosity sodium alginate (MMW, 120 kDa, 1% viscosity 40 mPa·s; mannuronic acid content 70%) was kindly donated by Dompè Pharma (Dompè S.p.A., L'Aquila, Italy).
- High viscosity sodium alginate from brown algae (HMW, 180 kDa, 1% viscosity 65 mPa·s; mannuronic acid content: 70%) was purchased from Carlo Erba reagents (Milan, Italy).
- High viscosity sodium alginate Kelton LVCR (1% viscosity 35 mPa·s; mannuronic acid content 60%) was kindly donated by Dompè Pharma (Dompè S.p.A., L'Aquila, Italy).
- Chitosan of low molecular weight (200-300 cP viscosity; 75-85% deacetylated) was purchased from Sigma-Aldrich (Milan, Italy).
- Pectin of low methoxyl degree and high amidate degree was obtained from Herbstreith & Fox KG (Neuenburg, Germany).
- Doxycycline Hyclate was purchased from Unione Commerciale Lombarda (Brescia, Italy).
- Ketoprofen Lysinate was kindly donated by Dompè Pharma (Dompè S.p.A. L'Aquila, Italy).
- Sunflower seed oil was purchased from Oleificio del Golfo (Latina, Italy).
- Tween<sup>TM</sup> 85 and Span<sup>®</sup> 85 were purchased from Sigma-Aldrich (Milan, Italy).
- Polyvinyl alcohol (PVA) was purchased from Sigma-Aldrich (Milan, Italy).
- Calcium chloride, CaCl<sub>2</sub> (93% purity) was obtained from Sigma-Aldrich (Milan, Italy).
- Dichloromethane was purchased from Carlo Erba (Milan, Italy).

- Absolute ethanol was purchased from VWR (Llinars del Vallés, Spain).
- Carbon dioxide (99.8 % purity) from Praxair (Madrid, Spain) was used for the supercritical drying of the gels.
- All other reagents were purchased from Sigma-Aldrich (Milan, Italy) and employed as received.

## 2.2. Methods

### 2.2.1. Encapsulation technique: laminar jet break-up or prilling

For the production of core-shell microparticles by inverse gelation using artificial intelligent tools (SECTION B 3.2.2) the prilling apparatus used was the Nisco Encapsulator® var. D (Nisco Engineering Inc., Zurigo CH) in co-axial configuration. The Nisco Encapsulator is formed by:

[1] A control unit for regulating the frequency, vibration amplitude, feed solution rate and stroboscopic lamp intensity.

[2] A membrane vibration system.

[3] A stainless steel nozzle or combination of them (co-axial configuration) with different diameters (100-600  $\mu\text{m}$ ).

[4] A syringe/s containing the feed solution/s.

[5] A piston pump/s (Model 200 Series, Kd Scientific Inc., Boston, MA, USA).

[6] A gelling bath.

[7] A magnetic stirrer.

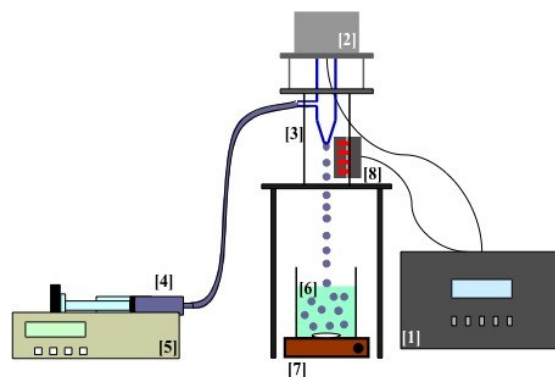


**Figure 9. Nisco Encapsulator apparatus**

For the production of alginate beads (SECTION B 3.2.1) and core-shell microparticles loaded with Ketoprofen Lysinate (SECTION B 3.2.3) the prilling apparatus used was the Büchi Encapsulator B-390 (Büchi Labortechnik AG, St. Gallen, Switzerland) that is composed by:

- [1] A bottle containing the feed solution.
- [2] The beads production unit.
- [3] The vibration unit.
- [4] The nozzle.
- [5] An electrode.
- [6] A control dispersion system.
- [7] A vibration control unit.
- [8] A stroboscopic LED.
- [9] A gelation bath.
- [10] A magnetic stirrer.
- [P] Compressed air.



**Figure 10. Büchi encapsulator B-390 apparatus**

## ***2.2.2. Supercritical Fluids-based technologies***

### ***2.2.2.1. Supercritical Assisted Atomization (SAA)***

For the production of “in-situ” gelling powders (SECTION A), a supercritical assisted atomization plant was used. This plant include the following parts:

- CO<sub>2</sub> and N<sub>2</sub> bottles.
- Two peristaltic pumps (mod. 305, Gilson, Middleton, MO, USA): one for pumping the liquid feed solution and the other one for the delivery of carbon dioxide.

- A mixing chamber of 25 cm<sup>3</sup> internal volume with stainless steel perforated saddles. It is linked to the precipitation chamber by an 80 μm nozzle and it is the only part of the implant where high pressures (80-100 bar) are applied.
- A precipitation chamber heated by electrical resistances in which droplets evaporation takes place by a controlled flow of N<sub>2</sub> heated until 85°C in an electric heat exchanger (mod. CBEN 24G6, Watlow, St. Louis, MI, USA).
- A filter on the bottom of the precipitation chamber that allows the powders collection and the gas stream out.

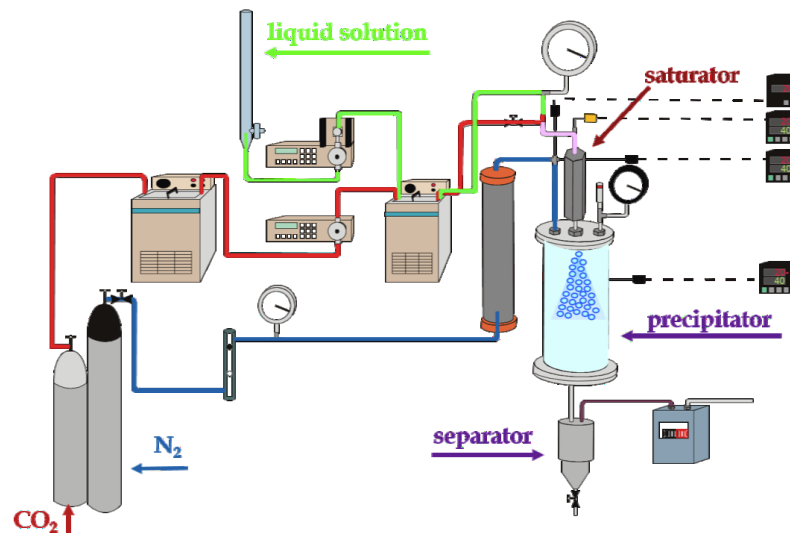


**Figure 11. General scheme of a SAA apparatus.**

#### 2.2.2.2. Supercritical Antisolvent Extraction (SAE) or “supercritical drying”

For the aerogels production (SECTION B), a supercritical drying laboratory plant (figure 12) composed by a 100 mL stainless steel vessel (Thar Technologies, Pittsburg, PA, USA) was used. The implant is divided in three sections composed by the following components:

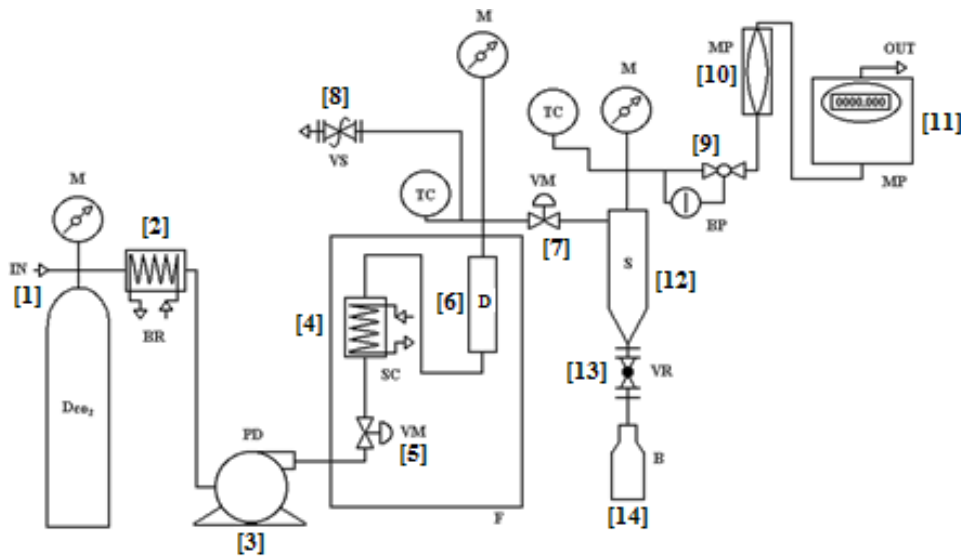


**Figure 12. Scheme of SAE plant.**

- Pumping section:
  - 1) A CO<sub>2</sub> bottle reservoir.
  - 2) A cooling bath.
  - 3) A membrane pump (Milton Roy mod. Milroyal B) modified by using a cooling circuit of the head of the pump and of the CO<sub>2</sub> aspiration line.
- Drying section:
  - 4) A oven that is heated by connective air.
  - 5) A micrometric valve that allows the CO<sub>2</sub> entrance into the drying vessel.
  - 6) A stainless steel vessel where drying takes place.
  - 7) A micrometric valve at the drying vessel exit.
  - 8) A three direction security valve.
  - 9) A back pressure valve at the end of the separator.
  - 10) A rotameter.
  - 11) A roll counter of the CO<sub>2</sub> flow.

- Separation section:
  - 12) A conic stainless steel separator.
  - 13) An on/off valve at the bottom of the separator (for withdrawing the solvent during the process).
  - 14) A glass flask to collect the extracted solvent.

In the plant are also included manometers and thermocouples to control operative temperatures and all the controls are localized in a specific electronic panel.

### ***2.2.3. Artificial Intelligence (AI) tools***

The database of the different formulations in (SECTION B 3.2.2) was modeled using two commercial software, FormRules® v4.03 and INForm® v5.01 (Intelligensys Ltd., UK) which implement neurofuzzy logic and Artificial Neural Networks together with genetic algorithms, respectively. They allow the generation of knowledge related to the influence of the different variables on the characteristics of the core-shell particles and the selection of the optimal values to obtain the best results of the process. The common training parameters used by FormRules® v4.03 were the following: ridge regression factor of  $1 \text{ e}^{-6}$ , number of set densities: 2, set densities: 2 and 3, maximum inputs per submodel: 4, maximum nodes per input: 15, adapt nodes: true: The statistical fitness criteria selected was Structural Risk Minimisation (SRM) ( $C1 > 0.74$  and  $C2 = 4.8$ ) because gave an excellent fitting together with simples and intelligible rules, consisting on a set of “if...then” fuzzy rules. These rules are made up of two parts: the initial one, which includes the input or inputs explaining a specific output, followed by the second part describing the output characteristics, which are defined by a word and its correspondent membership degree (*Colbourn et al., 2005*). For ANN model generation the database was randomly split in two groups: 39 records for training, 4 to test the error. Training parameters used by

INForm® were the following: Momentum = 0.8, Learning Rate = 0.7, Target Interactions = 1000, Target MS Error = 0.0001, Random Seed = 10,000, Network Structure (7 inputs, 1 hidden layer, transfer functions = asymmetric sigmoid and linear), Back Propagation Type = RPROP. Separate models were developed with FormRules® and INForm® for each property, the accuracy of which was assessed using the parameter R<sup>2</sup> and ANOVA f-ratios for each output:

R<sup>2</sup> is defined as follows:

$$R^2 = \left( 1 - \frac{\sum_{i=1}^n (y_i - y_i')^2}{\sum_{i=1}^n (y_i - \bar{y})^2} \right) \times 100$$

where y is the actual point in the data set, y' is the value calculated by the model and  $\bar{y}$  is the mean of the dependent variable. The larger the value of the train set R<sup>2</sup>, the more the model captured the variation in the training data. Values for R<sup>2</sup> > 70% are indicative of reasonable model predictabilities (Colbourn *et al.*, 2005). Computed f ratio values higher than critical f values for the degrees of freedom of the model, indicate no statistical significance between predicted and experimental results and hence, good model performance.

#### **2.2.4. Analytical technologies**

##### *2.2.4.1 Scanning Electron Microscopy*

The morphology and size distribution of the formulations was studied by Scanning Electron Microscopy (SEM) using a Carl Zeiss EVO MA10 microscope provided with a secondary electron detector (Carl Zeiss SMT Ltd., Cambridge, UK) and equipped with a LEICA EMSCD005 metallizator

producing a deposition of 200-400 Å thick gold layer. Powder and aerogel samples were dispersed on a carbon tab previously stuck to an aluminium stub (Agar Scientific, Stansted, UK). Samples were coated with a gold layer using a sputter coater (mod. 108 Å, Agar Scientific, Stansted, UK) at 35 mA during 155 seconds. At least 20 SEM images were taken into account for each sample.



**Figure 13. Scanning Electron Microscope.**

#### *2.2.4.2 Nitrogen Adsorption Porosimetry*

The textural properties of aerogels and cryogels (SECTION B) were studied by nitrogen adsorption-desorption analysis in an ASAP 2000 apparatus (Micromeritics, Norcross, GA, USA). Specific surface area ( $S_a$ ) and pore size distribution of aerogel and cryogel particles were calculated by the Brunauer-Emmett-Teller (BET) and Barret, Joyner and Halenda (BJH) methods, respectively. The overall specific pore volume ( $V_{pBJH,d}$ ) and the mean pore diameter ( $D_{pBJH,d}$ ) were also obtained by the BJH method. Samples were previously outgassed ( $<10^{-5}$  mbar) at 60°C for at least 20 h before the analysis.



**Figure 14. Nitrogen Adsorption Porosimetry ASAP 2000 apparatus.**

#### *2.2.4.3 Differential Scanning Calorimetry (DSC)*

Thermal characteristics of dry powders and raw materials (SECTION A) were studied by differential scanning calorimetry (DSC) using a Mettler Toledo DSC 822e apparatus controlled by a Mettler StarE software, Columbus, Ohio). A proper amount of samples (>1.5 mg) was crimped in a standard aluminium pan that was pierced and heated from 25°C to 350°C at a scanning rate of 10°C/min for doxycycline and dry powders obtained in SECTION A. All assays were performed in nitrogen atmosphere at a flow rate of 150 mL/min. The characteristic peaks were recorded and the specific heat of the melting endotherm was evaluated.



**Figure 15. DSC 822e Mettler Toledo apparatus.**

#### 2.2.4.4 FTIR-ATR spectroscopy

Infrared analysis were performed in a FT-IR/NIR Frontier Spectrophotometer, Perker Elmer, MA, USA) equipped with a single reflection horizontal ATR accessory having a diamond coated ZnSe top-plate crystal fixed at incident angle of 90° (Universal ATR Accessory, Perkin Elmer, MA, USA). Samples were analysed using 64 scan with a 1 cm<sup>-1</sup> resolution step.



**Figure 16. FTIR spectrophotometer apparatus.**

#### 2.2.4.5 Fluorescent Microscopy

Fluorescent microscopy (FM) assays were conducted by analysing core-shell particles (SECTION B 32.2) in a ZeissAxiophot fluorescent microscope with an Apochroma 20×1,4NA no-oil immersion objective (Carl ZeissVision, München-Hallbergmoos, Germany) using standard optic filters: Rhodamine adsorbing yellow radiation (max 551 nm) and emitting an orange fluorescence (max 573 nm) to highlight the core of the particles, and a standard DAPI filter (4', 6-diamidino-2-phenylindole) optics adsorbing violet radiation (max 372 nm) and emitting a blue fluorescence (max 456 nm) to highlight the particles shell. Texas Red, adsorbing yellow radiation (max 586 nm) and emitting an orange fluorescence (max 605 nm), and FITC (fluorescein-isothiocyanate), adsorbing blue radiation (max 495 nm) and emitting green fluorescence (max 519 nm) were also used for analysing

microparticles of SECTION B 3.2.3.

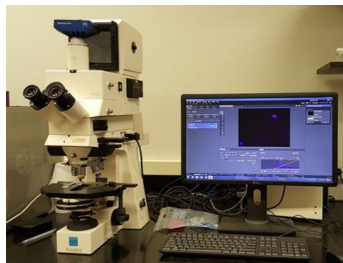


**Figure 17. ZeissAxiophot fluorescent microscope**

Projection diameter of the core-shell particles from SECTION B 3.2.2 was obtained by image analysis (Image J software, Wayne Rasband, National Institute of Health, Bethesda, MD, USA). A minimum of one hundred bead images were analysed for each formulation in order to calculate length-number mean and relative standard deviation for at least three prilling processes. Perimeter and projection surface area of core-shell particles were obtained by image analysis and used to calculate Sphericity Coefficient (SC) by the following equation (1) (*Del Gaudio et al., 2009; Maleki et al., 2016*), in order to associate to each batch shape a specific score, between 1 and 10, while 0 was associated to very irregular shaped particles.

$$(1) SC = 4\pi A/P^2$$

where A is the projected bead surface area and P its perimeter.

#### *2.2.4.6 Density measurements*

The skeletal density ( $\rho_{\text{skeletal}}$ ) of aerogels was measured by helium pycnometry (Micropycnometer Quanta-Chrome MPY-2, Boynton Beach, FL, USA) at room temperature using helium as the displacement gas due to its size and inert behaviour. A sealed chamber of known volume containing a previously

weighted amount of sample was pressurized with helium to 1.20 bar and, once stabilized, the pressure was recorded. Then, a valve was open to expand the gas into a reference chamber of known volume and also this pressure was recorded when stabilized. This pressure drop ratio was compared to the behaviour of the system when a known volume standard underwent the same process. Helium picnometer was previously calibrated using two metallic spheres of known weight and volume.



**Figure 18. Quanta-Chrome MPY-2 Helium Micropycnometer.**

The envelope density ( $\rho_{envelope}$ ) of aerogel beads (SECTION B 3.2.1) was calculated from the equation (2), being  $m$  and  $V$  the average weight and volume of an aerogel bead, respectively, and  $N$  the number of beads for each aerogel sample. The envelope density ( $\rho_{envelope}$ ), referred to the volume of the solid material including open and closed pores, was determined for a single and consolidate quantity of material, thus there are no interparticle voids between packed particles.

$$(2) \rho_{envelope} = \frac{m}{V X N}$$

Overall porosity ( $\varepsilon$ ) of aerogel beads (SECTION B 3.2.1) was obtained from the bulk and skeletal densities data by the equation (3):

$$(3) \varepsilon = \left(1 - \frac{\rho_{envelope}}{\rho_{skeletal}}\right) \times 100$$

Density of aerogel capsules from SECTION B 3.2.3 was calculated by the following equation (4):

$$(4) \quad \frac{1}{\rho} = \frac{V_{total}}{g} = \frac{1}{\rho_{skeletal}} + \frac{1}{\rho_{envelope}} + \frac{V_{macropore}}{g}$$

being  $1/\rho_{envelope}$  the desorption pore volume ( $\text{cm}^3/\text{g}$ ) obtained by the BJH method. The shell thickness and the particles radius were obtained by means of image analysis and allowed to calculate the different volumes (macropore, mesopore and solid volumes). In consequence, the overall porosity was calculated from the equation (5):

$$(5) \quad \varepsilon (\%) = \left( \frac{\frac{V_{macropore}}{g} + \frac{1}{\rho_{envelope}}}{\frac{1}{\rho}} \right) \times 100$$

#### 2.2.4.7 Beads hardness assays

To determine the breaking strength of the gel beads of SECTION B 3.2.2 to compression, individual beads from several batches have been tested with an electronic dynamometer (AG/MC2, Acquati, Arese, Italy) equipped with a 5 daN load cell. Beads were placed in a custom-built clamp with an opening of 2.5 mm, which closed at a rate of 5 mm/min when the instrument was operated in compression mode. The first peak force recorded by the software (LabChart 7, ADInstruments, Bella Vista, NSW, Australia) corresponding to the bursting of the bead was collected for at least 20 beads for each batch. Three batches were analysed for each experiment. Statistical analysis was conducted with SPSS software.



**Figure 19. Electronic dynamometer AG/MC2.**

#### *2.2.4.8. Dynamic Light Scattering (DLS)*

Particle size distribution of powders from SECTION A was evaluated by dynamic light scattering (DLS) (N5, Beckman Coulter, Miami, Florida). Each sample was diluted in dichloromethane and analyzed with a detector at 90° angle. For each batch, mean diameter and size distribution were the mean of three measures. The effectiveness of the particle dispersion was verified performing the measurement after different sonication times ranging between 5 and 30 min. Results were expressed as  $d_{50}$  in all time intervals.



**Figure 20. Dynamic Light Scattering.**

#### *2.2.5. Experimental procedures*

##### *2.2.5.1 Dry powders preparation*

The aqueous feed solutions to be atomized through SAA process (SECTION A 3.1) for the obtaining of dry powders were produced by combinations of alginate, pectin and doxycycline at different ratios, taking as reference the solution containing all polymers and doxycycline in which the ratio between

polymers and drug (7:1) was kept constant even when not all the excipients were used (table 3). Percentage of doxycycline was fixed at 1.43% (w/w). For each type of formulation, both the solutions containing the active and the analogous solutions containing only the polymeric excipients were processed, and then used as reference to evaluate the influence of the drug on the chemical-physical characteristics of the formulations produced.

**Table 3. Feed solutions composition (P = pectin; A = alginate; C = chitosan; D = doxycycline).**

Feed Solution	Alginate (w/v)	Amidated pectin (w/v)	Chitosan (w/v)	Doxycycline (w/w)	Polymer/drug ratio
<b>PACD</b>	0,50%	0,50%	0,25%	1,43%	P:A:C:D 3:3:1:0,1
<b>PAD</b>	0,50%	0,50%	-	1,43%	P:A:D 3,5:3,5:0,1
<b>ACD</b>	0,50%	-	0,25%	1,43%	A:C:D 5,25:1,75:0,1
<b>PAC</b>	0,50%	0,50%	0,25%	-	P:A:C 3:3:1
<b>PA</b>	0,50%	0,50%	-	-	P:A 3,5:3,5
<b>AC</b>	0,50%	-	0,25%	-	A:C 5,25:1,75

The aqueous solution formed by the excipients and the drug was added to the mixing chamber, where different pressures were tested between 78 and 110 bar, then pumped to the saturator where it was mixed with the sc-CO<sub>2</sub>, thus forming a quaternary system (carrier/drug/solvent/sc-CO<sub>2</sub>). The supercritical-CO<sub>2</sub> was dissolved in the feed solution by testing different Gas-to-Liquid Ratios (GLR) between 1.8-2.5 and different temperatures at the saturator (60-85°C). The solution obtained in the saturator was sprayed through the injection nozzle into the precipitation chamber, being the droplets at the

outlet of the injector formed by both solutes dissolved in the solvent. The temperature and the pressure at the precipitation chamber were studied in the ranges 70-105°C and 1.3-2.4 bar, respectively. After solvent evaporation, the precipitated microparticles in form of dry powders were collected.

#### 2.2.5.2 Aerogels preparation

For the manufacturing of alginate aerogels of SECTION B 3.2.1, stock aqueous alginate solutions were prepared at different concentrations (1.25, 1.50, 2.00 and 2.25 % (w/v)). Batches from different molecular weight alginates, both obtained from brown algae, were used: high molecular weight (HMW) sodium alginate and medium molecular weight (MMW) sodium alginate. Gel beads were prepared using a prilling apparatus (Büchi Encapsulator B-390) equipped with a 400 µm-diameter nozzle. Alginate solutions (60 mL) were pumped at a flow rate of 8 mL/min. Nozzle vibration was set at a frequency of 350 Hz and an amplitude of 100 %. CaCl<sub>2</sub> 0.3 M in either aqueous or ethanolic solution was used as gelling agent (*Cerciello et al., 2015*). The distance between the nozzle and the gelling bath was set at 8 cm. After the droplets fall into the bath, the hydrogel beads formed were stirred (ageing time) for 5 min considering the zero time the end of the prilling process, whereas the alcogel beads were immediately collected after the end of the prilling process; thereafter, they were rinsed with either distilled water or ethanol depending on the type of solution used as gelling bath, leading to the production of hydrogels and alcogels, respectively. MMW<sub>x</sub> samples denote those prepared from medium molecular weight alginate and HMW<sub>x</sub> those prepared from high molecular weight alginate, being *x* the concentration of alginate in the 1.25% - 2.25% (w/v) range. Before the drying of all the produced batches, a direct solvent exchange process to replace water or ethanol with absolute ethanol was conducted

twice. Once the beads were conditioned, supercritical drying for the obtaining of aerogel beads was carried out in a scale-up 100 mL stainless steel autoclave (Thar Technologies, Pittsburg, PA, USA). The drying process by sc-CO<sub>2</sub> was carried out at 40°C and 120 bar during 210 minutes using a CO<sub>2</sub> flow of 7 g/min during the first hour and then 5 g/min until the end of the process. Drying experiments were carried out in triplicate. These operating conditions were chosen in accordance to the vapor-liquid equilibrium data for the binary system ethanol-CO<sub>2</sub> in order to operate at conditions above the mixture critical point. Under these conditions an adequate extraction of the organic solvent of the gel is obtained whilst preserving the internal gel structure (*Della Porta et al., 2013*). In addition, for comparative studies, oven-drying at 60°C until constant weight was reached and freeze-drying of the beads were carried out. Freeze-drying was carried out at ca. -80°C and 0.01 mbar in a Telstar Lyo Quest Plus - 85°C/ECO apparatus (Barcelona, Spain) over 24 hours. Hydrogel and alcogel beads were previously cooled to -20°C and -80°C, respectively, and followed by further chilling with liquid nitrogen (-196 °C).

For the manufacturing of core-shell microparticles of SECTION B 3.2.2, water-in-oil (W/O) emulsions were prepared by stirring mixtures of 30 mL of an aqueous calcium chloride solution, in the concentration range between 20 and 50 g/L and 100 mL of sunflower oil using an Ultra-Turrax® T25 (IKAWorks GmbH & Co. Staufen, Germany) homogenizer at ≈12,000 rpm for 10 min. In order to decrease the oil/water interfacial tension, non-ionic surfactants were used at different concentrations. Tween™ 85 (ranging from 0 to 0.625%) and Span® 85 (0.5%) were added to the CaCl<sub>2</sub> solution and the sunflower oil, respectively (*Pouton & Porter, 2008*). Alginate solutions were also made at a concentration ranging from 1 to 2% w/v. The prilling apparatus Nisco Encapsulator connected to a double pump and equipped with

a coaxial nozzle of 400  $\mu\text{m}$  and 600  $\mu\text{m}$  inner and outer diameter, respectively, was used. Immediately upon preparation, the emulsion and the alginate solution were introduced into each syringe and pumped into the coaxial nozzle. The emulsion was pumped through the inner nozzle while alginate solution into the annular one and then extruded. Additionally, an aqueous solution of calcium chloride (0.3 M) and Tween<sup>TM</sup> 85 (ranging from 0 to 0.5%) was used as an external bath. Batches of microcapsules were produced at different flow rates (Q) of alginate solution and emulsion, in the ranges of 7-17 mL/min and 1-7 mL/min, respectively, as well as at different frequencies of vibration (230-300 Hz). Once parameters were optimized by the utilization of the different software based on the artificial intelligence tools, as previously described, the produced core-shell microparticles were submitted to different supercritical drying processes on a 100 mL stainless steel autoclave (Thar Technologies, Pittsburg, PA, USA) at 40°C and at 120 bar during 210 minutes (sc-drying 1) or at 140 bar during 270 minutes (sc-drying 2) to produce void aerogels.

For the manufacturing of core-shell loaded-microparticles of SECTION B 3.2.3, alginate solutions at different concentrations (1.50% - 2.25%, (w/v)) were used to form the shell of the gel beads and an (O/W/O) emulsion was used to form the core. A primary O/W emulsion was formed by 1 mL dichloromethane and a 15 mL  $\text{CaCl}_2$  aqueous solution at different concentrations (13.4 g/L, 26.8 g/L) and different percentages of PVA (0.5%, 1.0%, (w/v)) used as surfactant in the aqueous phase. This primary emulsion was added to 30 mL sunflower oil containing 0.5% Span<sup>®</sup> 85 (v/v) under gentle magnetic stirring. For the production of drug-loaded microparticles, ketoprofen lysinate was added at 10% and 20% (w/w) regarding the amount of polymer used. With the purpose to manufacturing uniform core-shell beads in a narrow size distribution, concentric nozzles of different diameters

were tested (300-900  $\mu\text{m}$ ). Alginate solutions flow rate was tested in the range 10-49 mL/min whereas the emulsion flow rate was tested in the range 4-6 mL/min. The vibration frequency was tested in the range 280 Hz-400 Hz and the use of the electrode in the range 500-2500V. The obtained gel-beads were collected in a 0.3M  $\text{CaCl}_2$  ethanolic solution placed at different distances (3-5 cm) from the nozzle exit and maintained under gentle stirring during 5 minutes before being rinsed and collected in absolute ethanol. Previously at the sc- $\text{CO}_2$  drying process, a solvent exchange was carried twice in order to eliminate the possible traces of water. The sc- $\text{CO}_2$  drying was carried out in a 100 mL stainless steel autoclave (Thar Technologies, Pittsburg, PA, USA) at 40°C and at a  $\text{CO}_2$  flow rate of 7 g/min during the first hour and at 5 g/min during the rest of the process. Different assays were carried out at 120 bar during 210 minutes (sc- $\text{CO}_2$  drying 1), and 140 bar during 270 minutes (sc- $\text{CO}_2$  drying 2) for the production of void aerogels loaded with ketoprofen lysinate.

#### *2.2.5.3 Swelling and fluid uptake studies*

The gelling and swelling capacities of the various powder formulations (SECTION A) were evaluated when in contact with the simulated wound fluid (SWF). For this study a Franz vertical diffusion cell (Hanson research, USA) formed by an acceptor compartment of 5 ml volume in contact with a membrane on which a carefully weighed quantity of powder is placed (donor compartment) was used. A polyvinylidene fluoride (PVDF) membrane for biological solutions (MerckMillipore) with pores with a diameter of 0.45  $\mu\text{m}$ , previously set with the same solution present in the acceptor compartment, was used. The solution used to simulate the wound fluid (SWF) is composed of a 50% maximum recovery diluent, MRD (Sigma Aldrich, Milan, Italy, containing peptone, peptide digestion of animal tissue, 0.1% (w/v) and

chloride of sodium 0.9% (w/v)) and a 50% fetal calf serum (Sigma Aldrich, Milan, Italy) (Bowler *et al.*, 2001). The acceptor compartment was thermostated at  $37^{\circ}\text{C} \pm 0.5$  and several times, during the experiment, fluid was added to the Franz cell to keep the volume constant. A magnetic stirrer was also introduced to ensure constant agitation. About 8 mg of powders have been placed on the already set and previously weighed membrane. The weight of the gel formed was measured at regular intervals until reach constant weight. All experiments were performed in triplicate. The fluid uptake over time, defined by the ratio between the weight of the gel at a generic time  $t_x$  and the weight of the dry powders at the time  $t_0$  was obtained.

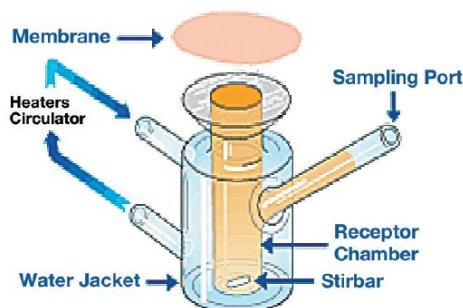


**Figure 21. Scheme of a Franz vertical diffusion cell.**

Fluid uptake ability of the aerogel capsules (SECTION B 3.2.3) was evaluated as the weight ratio of the formed hydrogel and starting aerogel and at different time points when formulations were in contact with simulated wound fluid (SWF), composed of a 50% maximum recovery diluent, MRD (Sigma Aldrich, Milan, Italy, containing peptone, peptide digestion of animal tissue, 0.1% (w/v) and chloride of sodium 0.9% (w/v)) and a 50% fetal calf serum (Sigma Aldrich, Milan, Italy) (Bowler *et al.*, 2001). The weight of the gel formed was measured at regular intervals until reach constant weight. All experiments were performed in triplicate.

#### 2.2.5.4 Permeation in vitro assays

In vitro permeation studies were performed using the previously described Franz type vertical diffusion cells (Hanson research, USA) (Figure 21). The donor compartment was filled with simulated wound fluid (SWF) and placed in a water bath at a temperature of  $37^{\circ}\text{C} \pm 0.5$ . In this compartment a magnetic stirrer has been introduced to ensure constant agitation. The release tests were performed using a polyvinylidene fluoride (PVDF) membrane (MerckMillipore) with pores with a diameter of  $0.45\ \mu\text{m}$ , previously set with the same solution. At the beginning of each experiment a carefully weighted amount of powder formulation (about 15 mg) was placed on the membrane and the release was followed for 36 hours, taking samples at pre-established times. The amount of taken sample ( $200\ \mu\text{l}$ ) was replaced by an equal amount of SWF to maintain the constant volume in the cell. The sample was then diluted to 1 ml, filtered to remove the protein part, and analysed with HPLC-UV technique using a Kinetex C18 (AN 50 mm,  $100\ \text{\AA}$ ) column, and using a concentration gradient (table 4) to allow the chromatographic separation of doxycycline (Kogawa & Salgado, 2012). The obtained data have been reported as percentage of drug released as a function of time elapsed. Each experiment was performed in duplicate.

**Table 4. Concentration gradient used for HPLC-UV analysis (A = 10 mM PBS solution; B = metanol for HPLC analysis).**

Time (min)	%A	%B	Flow (mL/min)
0	70	30	0.15
3	70	30	0.15
6	0	100	0.15
8	0	100	0.15
9	70	30	0.15

#### 2.2.5.5 Drug content and encapsulation efficiency

The drug content of powder formulations (SECTION A) was calculated by two different methods. The first technique consisted on dissolving a carefully weighed quantity of powder (about 7 mg) into 5 ml of a 100 mM PBS solution. The produced solution thus was filtered (filter pores 0.22  $\mu\text{m}$ ), to remove the polymer matrix, and subsequently analysed by the UV-Vis spectrophotometer (Evolution 201 UV-Vis Double Beam Spectrophotometer Thermo Scientific, Waltham, MA) at a wavelength of 351 nm. Each analysis was conducted in triplicate and the results were then expressed in terms of average value. In the second method the HPLC-UV technique was used instead. A carefully weighed amount of powder (about 7 mg) was dissolved in a 10 mM PBS solution; the solution thus obtained was centrifuged for 10 min at 6000 rpm to remove the polymer matrix. The supernatant collected was then analysed by HPLC using the method previously defined in table 4. The drug content was calculated as the ratio in percentage between the amount of drug obtained experimentally by UV or HPLC and the amount of powder weighed for analysis (equation 6).

$$(6) \text{ Drug content, \%} = \frac{\text{experimental amount of drug}}{\text{weighed amount of powder}} \times 100$$

The encapsulation efficiency was calculated as the ratio in percentage between the amount of drug obtained experimentally through UV and the theoretical amount of drug presented in the feed solution used for the SAA process (equation 7).

$$(7) \text{ Encapsulation efficiency, \%} = \frac{\text{experimental amount of drug}}{\text{theoretical amount of drug}} \times 100$$

The drug content and the encapsulation efficiency analysis of Ketoprofen-loaded aerogels (SECTION 3.2.3) were carried out by the UV-Vis spectrophotometer (Evolution 201 UV-Vis Double Beam Spectrophotometer Thermo Scientific, Waltham, MA) at a wavelength of 254 nm. Approximately 10 mg of each formulation were added to 2.5 mL PBS (100 mM, pH 7.4) under vigorous stirring for 30 minutes, then filtered and centrifuged at 6000 rpm during 30 minutes. After that, the supernatant was measured at the spectrophotometer. Each analysis was done in triplicate and the drug content and the encapsulation efficiency were calculated by the equations (6) and (7).

#### *2.2.5.6 Stability tests under storage*

A known amount of alginate aerogel samples (ca. 50 mg) of SECTION 3.2.1 were placed on top of a platform inside sterile and hermetic glass vessels containing a sulphuric acid solution (37% (v/v)) at the bottom and placed in an oven at 25°C to maintain the required relative humidity (65%) and mimic the International Conference on Harmonisation (ICH) climatic conditions of zone II (Mediterranean/subtropical zone) for stability studies of drug formulations (*Kommanaboyina & Rhodes, 1999*). The vessels were stored under these conditions during 1 and 3 months. Once the storage period was over, the aerogels were collected for further characterization.





### **3. RESULTS AND DISCUSSION**



## **SECTION A**

### **3.1. “*IN-SITU*” GELLING POWDER FORMULATIONS FOR WOUND HEALING**



The main goal of this part of the project was to assess the feasibility of the Supercritical Assisted Atomization (SAA) technique in the development of a new formulation in form of dry powders with the adequate physico-chemical and morphological properties, as well as release characteristics, for wound healing application. These formulations have been designed to gelify “*in-situ*” when in contact with the wound environment rich in exudate thus, moving from solid to gel fit rapidly the wound bed, while reducing the amount of exudates into the wound cavity and allowing a controlled release of an encapsulated API. This work was carried out in collaboration with the research group of Prof. Reverchon (in the person of Dr. Renata Adami) from the University of Salerno.

Sodium alginate with high mannuronic content (A) and amidate pectin with low methoxyl grade (P) were selected as primary excipients for the development of such formulations. In fact, A can form a soft and flexible hydrophilic gel, due to its high mannuronic content, through a ionic exchange Ca/Na process when in contact with the wound exudates and can induce the production of inflammatory cytokines thus improving the healing process (Szekalska *et al.*, 2016). By the other hand, P can gelify ionotropically when in contact with bivalent cations presented in the exudate due to its low methoxyl grade thus enhancing the “*in-situ*” gel-forming rate (Sriamornsak *et al.*, 2004). Moreover, a third polysaccharide, low molecular weight chitosan (C), was added to the AP blend in order to provide protection against bacterial infection and also because it is known that chitosan can promote the granulation by inducing proliferation of dermal fibroblasts and can favour the expression of growth factors, as TGF- $\beta$ 1, involved in wound healing. In addition, chitosan (Patrulea *et al.*, 2015) induce a different interaction with APIs due to the formation of a polyelectrolyte complex that reduces free charges on the polysaccharides chains.

The selected API for these specific formulations was the Doxycycline (figure 22), an inexpensive broad-spectrum of action antibiotic from the family of tetracyclines, approved by the FDA, that is efficient against gram-positive and gram-negative bacteria, both presented on infected wounds. Furthermore, it has the ability of inhibit the MMP-2 and MMP-9 metalloproteases thus promoting the improvement of the healing process by reducing inflammation and protease activity (*Anumolu et al., 2010*).

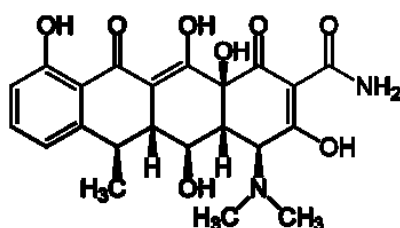


**Figure 22. Doxycycline molecule**

A first series of experiments were conducted in order to set some of the operating variables, mainly related to the ratio between the various polysaccharides and the optimal doxycycline concentration. In fact, high drug concentrations would lead to the formation of powders with unnecessarily high dosages of doxycycline, from which would be difficult to evaluate the physiological effects and the contribution of the different polysaccharides in modifying the release of the active agent from the powders.

Different feed solutions were prepared maintaining in all cases the same ratio between polymers and the drug, as it was shown in table 3, while setting doxycycline concentration at 1.43% (w/w) referring to the polysaccharides. The ratio between the polymers was fixed, however, taking into account the possibility of formation of non-soluble polyelectrolyte complexes during the formation of the feed solutions, due to the interaction between the cationic groups of chitosan and the anionic groups of alginate and pectin, that can lead to the formation of a precipitate that could not be processed by SAA. In fact, when chitosan amount was increased in solutions containing alginate

and chitosan (PACD and ACD) some feeds demonstrated Tyndall effect typically related to the formation of a colloidal suspension (*De & Robinson, 2003*).

For the optimization of the operating conditions to be used in the SAA process, in the early stages of the work, process studies were conducted using blank feed solutions, using temperatures and pressures that allowed a safe and rapid evaporation of the solvent. Considering the fact that feeds were aqueous solutions, the first outlet temperature was set at 105°C. The gas-liquid ratio (GLR) was initially set at a specific value able to avoid the anti-solvent effect. A high ratio between sc-CO<sub>2</sub> and the liquid, in fact, could lead to the solubilisation of the liquid in sc-CO<sub>2</sub> with possible formation of precipitates in the mixing chamber. Subsequently, other studies were conducted to identify the minimum temperature at which it was possible to obtain complete evaporation of the solvent in order to obtain a micro-submicroparticulate dry powder. The temperature gradient set between 70°C-80°C in the chamber resulted as the lower limit beyond which the process cannot be carried out. This gradient was however suitable for formulations containing doxycycline since the degradation temperatures of the components used are well above of these values as for many other active biomolecules (even thermolabiles). Furthermore, it must also be considered that exposure to these temperatures is relatively short, so it can be assumed that these operating conditions are also applicable to active ingredients with lower degradation temperatures. The GLR was then increased in order to facilitate the evaporation of the solvent despite the lowering of the temperatures, up to the limit value, thus obtaining complete evaporation but at the same time avoiding the anti-solvent effect.

**Table 5. Process yield for polysaccharides blend based powder obtained by SAA using optimized process parameters.**

Feed Solution	T inlet (C°)	Mixer Pressure (bar)	T outlet (C°)	Chamber Pressure (bar)	GLR	Yield (%)	EE (%)
PA	80	87	70	1.4	2.5	50.1	-
PAD	80	78	70	1.4	2.5	50.9	42.0
AC	80	81	70	1.4	2.5	75.8	-
ACD	80	86	70	1.4	2.5	83.9	61.0
PAC 10	85	88	100	1.5	2.5	89.0	-
PAC 11	80	83	80	1.3	2.5	87.4	-
PAC 12	80	84	70	1.4	2.5	76.7	-
PACD 12	80	81	70	1.4	2.5	71.8	52.0

Once the operating conditions were optimized (table 5), they were used for the preparation of the different formulations containing the different polymeric excipients containing the doxycycline and also for processing the feed solutions without active, to be used as a reference. All experiments were carried out in triplicate and in all cases high yields of the process (50.1-89.0%) and encapsulation efficiencies were achieved (42.0-61.0%).

Scanning Electronic Microscopy (SEM) analyses was conducted on both blank and doxycycline loaded formulations immediately after their production by SAA technique in order to assess morphology of the particles as well as to have a brief indication on particles size distribution and its relation to the feed composition. As shown in figure 23, the different composition of the feeds significantly affected the morphology of the obtained particles. The most notable difference was observed in the formulations containing chitosan (AC, PAC) that showed higher roughness compared to those containing only alginate/pectin blend. Moreover, in the formulations containing chitosan it was possible to clearly identify microparticles deriving from the fusion of nanoparticles still partially visible

on their surface, due to the interactions created between the amino residues of chitosan and the carboxylic groups of the alginate during the phase of feed solutions preparation (Kim *et al.*, 1999).

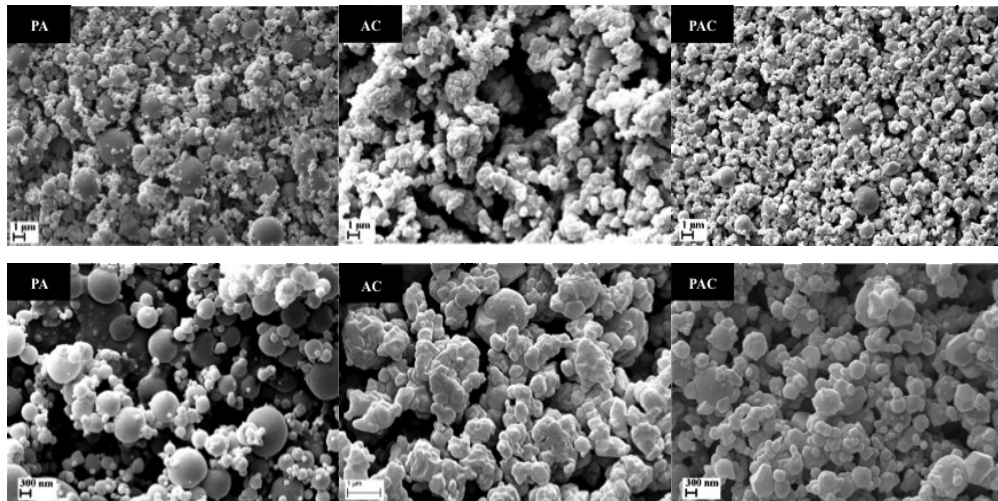


**Figure 23. SEM images of particles obtained by SAA containing: alginate/chitosan (AC), pectin/alginate (PA) and pectin/alginate/chitosan (PAC).**

The presence of doxycycline did not affect particles morphology as it is shown in figure 24 where presence of particles with smooth or rough surface related to the chitosan content, is still visible.

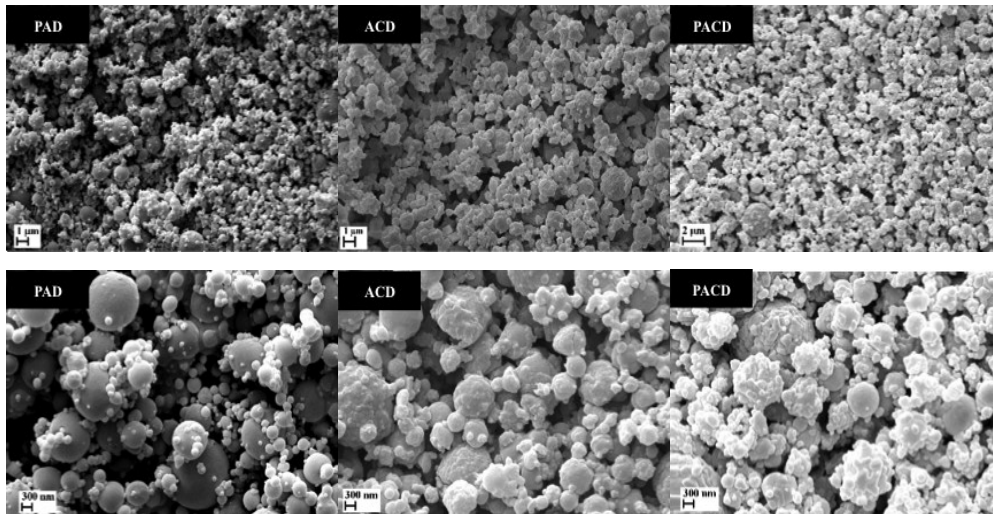


**Figure 24. SEM images of particles obtained by SAA containing: alginate/chitosan/doxycycline (ACD), pectin/alginate/doxycycline (PAD) and pectin/alginate/chitosan/doxycycline (PACD).**

In all formulations, most of the particles showed size of a few microns, but it was also possible to visualize particles with a smaller diameter in the range 300-800 nm, as shown in figure 25.

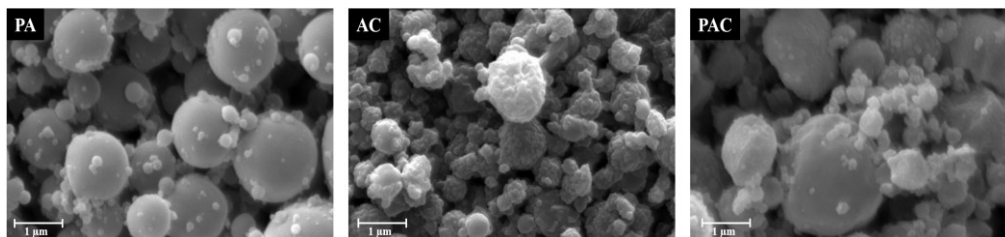


**Figure 25. Magnification of SEM images (figure 24) of particles obtained by SAA containing: alginate/chitosan (AC), pectin/alginate (PA) and pectin/alginate/chitosan (PAC).**

The formulations containing all the polymers (PAC, PACD) showed a more homogeneous size distribution compared to those without chitosan, which showed a bimodal dimensional distribution, where it was possible to detect the presence of particles of the order of a few microns in diameter and the

simultaneous presence of particles with diameters even below 200 nm, an evident consequence of a higher secondary atomization, normally related to the SAA process.

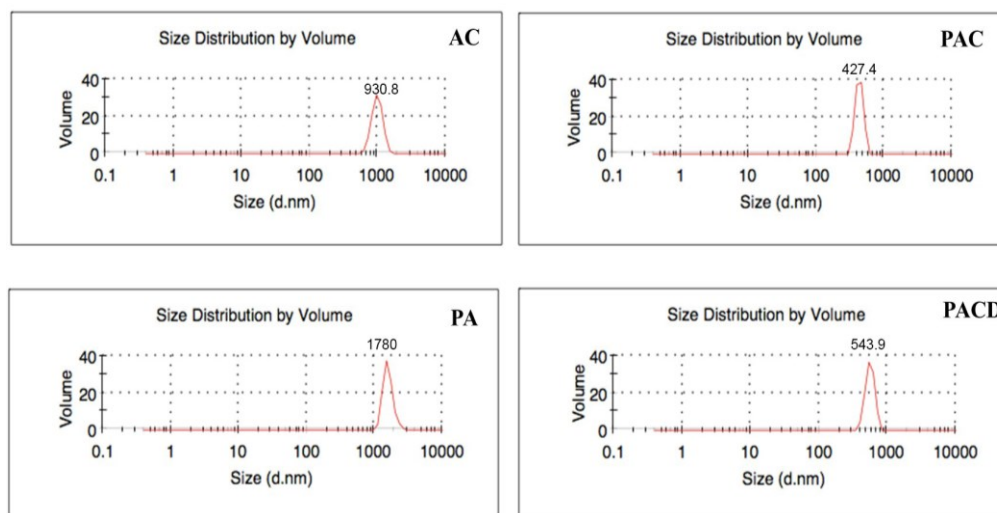


**Figure 26. Size distribution of powder formulations AC, PA, PAC and PACD.**

Calorimetric analyses were conducted for all the formulation batches containing only the excipients (figure 27) and for the formulations containing also the doxycycline (figure 28). The individual polymers showed exothermic peaks due to degradation at 250°C for pectin and alginate and at 300°C for chitosan. Moreover, the endothermic peaks, presented immediately before the exothermic degradation peaks of the various polymers, correspond to the melting temperature of each polymer. Pectin also presented several endothermic peaks due to the different melting points of the various crystalline and amorphous domains. This fusion was also found in the profiles of the formulations containing pectin (PAC and PA), even if at different temperatures, being such variation probably due to the formation of the polymer matrix in the particles. All formulations showed an endothermic

peak between 50 and 100°C, due to the loss of residual moisture present in the particles. The formulation containing alginate and chitosan (AC) presented this endothermic peak at the lowest temperature among the three formulations. Nevertheless, the formulation that showed the analogous peak at higher temperatures was that formed by alginate and pectin (PA) whereas at intermediate temperature there was the peak of the formulation containing all the polymers (PAC).

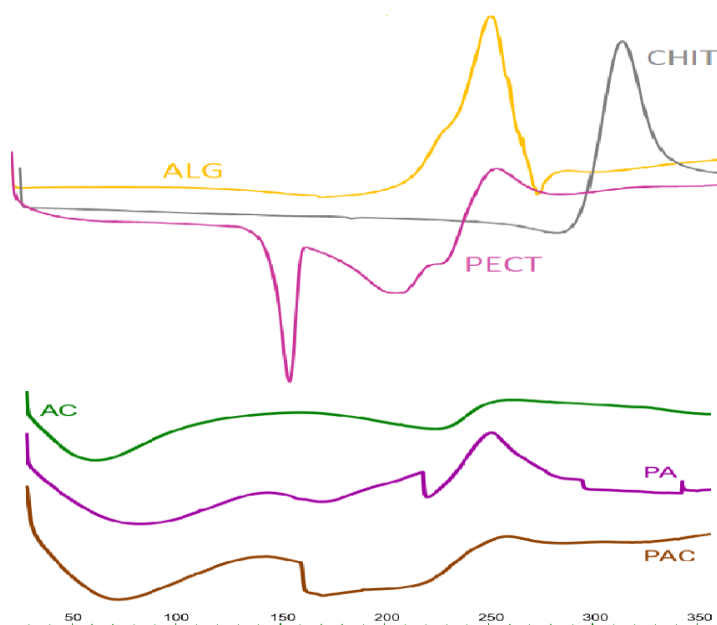


**Figure 27. Calorimetric profiles from pure alginate, chitosan and amidated pectin and from formulations containing alginate/chitosan (AC), pectin/alginate (PA) and pectin/alginate/chitosan (PAC).**

From this information it was possible to demonstrate a strong interaction between the functional groups present in alginate and chitosan, as previously described. The evaporation of water at lower temperatures indicates in fact a lower interaction between water and the functional groups of the polymers, a sign that in the formulation containing alginate and chitosan (AC) there is a

greater interaction between the polymers. In the case of exothermic degradation peaks, in the formulations containing chitosan (AC and PAC) two identical peaks were found, at a slightly higher temperature than the degradation temperature of alginate and pectin, while there was no chitosan exothermic peak around 300°C; also this aspect is an indication of the interaction between chitosan and alginate, while in the formulation without chitosan (PA) there was an exothermic peak at the same values of pectin and alginate (about 250°C). In general, the absence of the individual peaks of the polymers in the calorimetric profiles of the formulations confirmed the successful interaction between them in the formation of the polymeric matrix constituting the microparticles. Calorimetric analyses carried out for the formulations containing doxycycline did not show differences between those ones without the drug, probably due to its low concentration in relation to the polymers concentration.

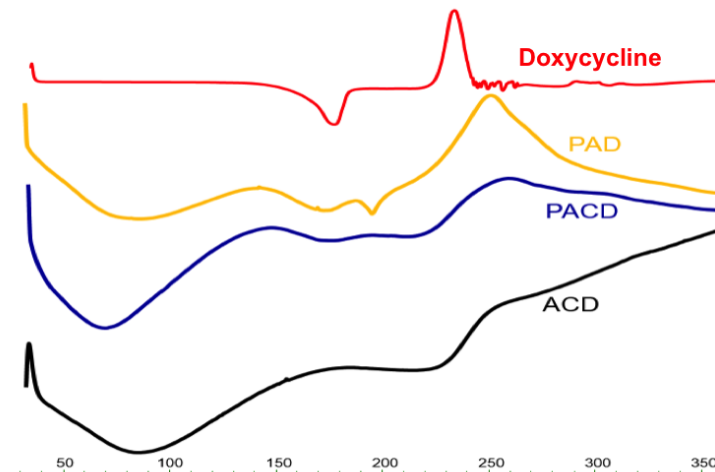


**Figure 28. Calorimetric profiles from pure doxycycline and from formulations containing: alginate, chitosan and doxycycline (ACD); pectin, alginate and doxycycline (PAD); and pectin, alginate, chitosan and doxycycline (PACD).**

Infrared spectroscopy analyses allowed analysing the effect of the interaction between the components presented in the produced particles. The analysis of the particles without doxycycline allowed to identify the differences with the raw materials not processed. Moreover, the comparison with the same samples containing the active ingredient allowed verifying possible interactions within the polymeric matrix due to the presence of doxycycline. As it is shown in figure 29, there were observed some differences in the stretching bands of the polymers. The  $1730\text{ cm}^{-1}$  peak that was presented exclusively in formulations containing pectin (PACD and PAD) is probably related to the antisymmetric stretching of the carboxylic alginate group, which is influenced by the amide group presented in the amidated pectin. There was also observed a peak at  $850\text{ cm}^{-1}$  only in the case of formulations containing pectin, probably due to the methyl group of the pectin methoxyl influenced by the carboxyl groups of chitosan. However, a further peak presented only in the presence of chitosan was observed at about  $1520\text{ cm}^{-1}$  and is probably due to the symmetrical stretching of the carboxylic alginate group which is influenced by the amino group of chitosan. The analyses conducted on the formulations containing doxycycline did not show significant differences compared to the formulations without containing the drug, probably due to the high ratio between polymers and drug.

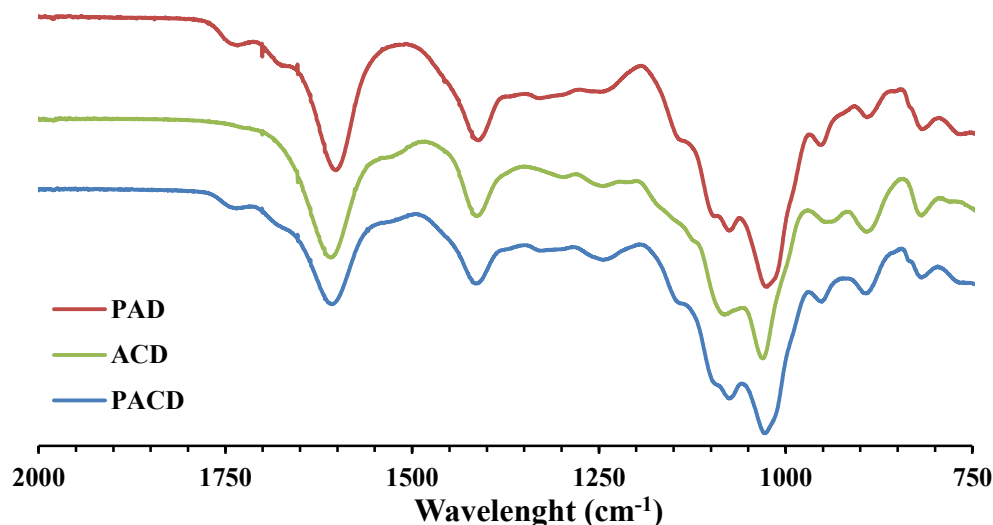


**Figure 29. Comparison between the infrared spectroscopy analyses of the ACD, PAD and PACD formulations.**

One of the most interesting features of the produced formulations is their ability to rapidly gel and swell when in contact with fluids that are normally present into chronic wounds. This phenomenon, called “*in-situ*” gelling is due to the presence in the exudate of divalent cations able to reticulate, gelifying alginate and pectin, and of phosphates able to gel the chitosan present in the formulations. The powders transformation into a gel allows a complete filling of the wound bed and promotes the prolonged release of the API at the site of action by increasing the diffusion pathway of the active ingredient through the gel barrier. Moreover, the formation of an hydrogel at the wound site able to remain hydrated over time can promote a non-traumatic removal at the end of the therapeutic action. Therefore, the gelling rate of the formulations was considered an end point parameter for the evaluation of the quality of the formulation in terms of effectiveness and compliance of the patient since a powder with a slow gelling or with incomplete gelling could cause difficulties during its application or even

cause its unsolicited removal. To determine this parameter, fluid uptake studies were carried out using simulated wound fluid (SWF) to evaluate the gelling speed and fluid uptake necessary for the gelling of the powders produced by SAA. The fluid uptake capacity was evaluated as the ratio between the weight of the formulation after the gel formation “*in-situ*” and the weight of the powder in the initial dry state. In all cases, the absorption of SWF was very quick. As it is shown in figure 30, the formulations containing pectin (PACD and PAD) completed the gelling process in just three minutes, reaching 10 times and 16 times the initial weight, respectively, whereas the formulation composed of alginate and chitosan (ACD) reached the maximum of swelling after one minute from the contact with the fluid, with an increase of 6 times compared to the initial weight.

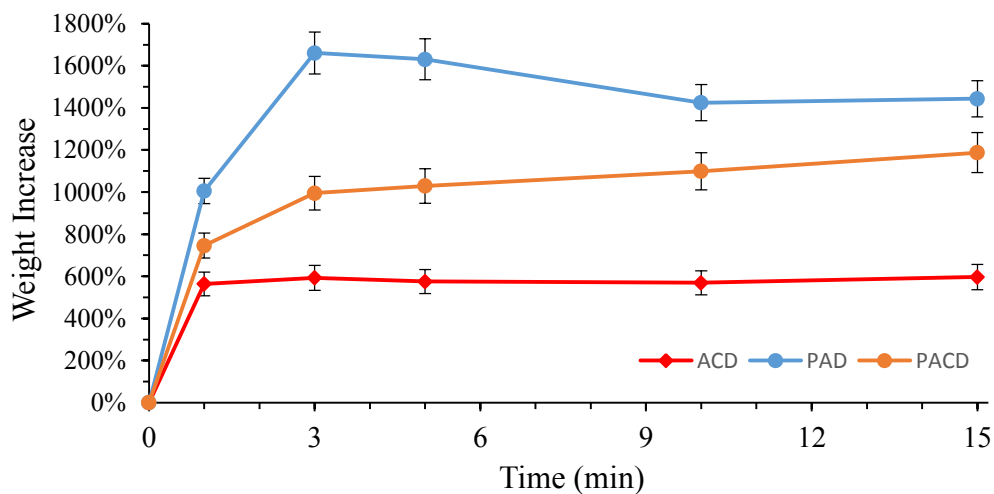


**Figure 30. Simulated wound fluid uptake by powders microparticles produced through SAA containing alginate/chitosan/doxycycline (ACD), pectin/alginate/doxycycline (PAD), pectin/alginate/chitosan/doxycycline (PACD).**

The formulation composed of pectin, alginate and doxycycline (PAD) showed a greater fluid absorption capacity, compared to other formulations, in terms of quantity, but reached the maximum swelling point slowly than the formulation composed of alginate, chitosan and doxycycline (ACD). Nevertheless, the formulation composed of all polymers and doxycycline (PACD) showed an intermediate behaviour. These results can be explained considering that, among the three polymers, chitosan is the one that has a lower gelling capacity while the pectin is the polymer that has the highest gelling capacity. Instead, for reaching the point of maximum swelling, the higher speed showed by the formulation containing exclusively alginate, chitosan and doxycycline (ACD) can be explained from the greater surface area of the particles, as previously described in the analysis of morphological characteristics, since these particles showed a very high roughness due to the presence of chitosan, and a high roughness is associated with a high surface area allowing to reach faster the point of maximum swelling. Therefore, in the case of the formulation composed of alginate, pectin and doxycycline (PAD), which being free of chitosan, showed a lower roughness, its lower gelling speed was associated to its lower surface area. Accordingly the gelling speed and the maximum swelling are directly attributable to the relationship between the particle size, the surface roughness and the chemical and physical characteristics of the polymers presented in the formulations. The formulation containing all the polymers showed an intermediate behaviour and it was perhaps the best formulation in terms of compliance and effectiveness. In fact, the gelling speed is important from the point of view of patient compliance since with a lower gelation speed, less waiting time will be needed once the formulation has been applied. Moreover, the extent of gelling is also important since influencing the prolonged release of the drug over time. The gelling capacity of the powders over time has also been assessed from the qualitative point of view, at regular time intervals. In fact,

photos of the powders placed in contact with the simulated wound fluid were taken at different times and it was observed a complete gelling of all the formulation within 3 minutes (figure 31).

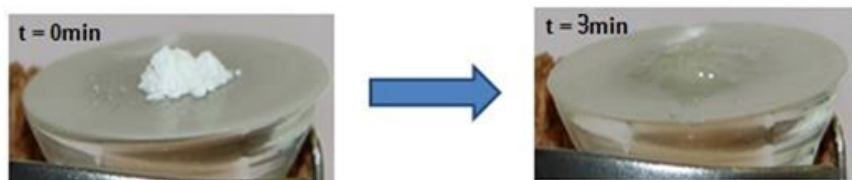


**Figure 31. Evolution of the powders gelation process.**

As “*in-situ*” powder gelling involves a diffusion mechanism of active release, it was necessary to compare the release rate of the unprocessed doxycycline with respect to that of the various formulations. The release profiles were evaluated *in vitro* by the use of vertical diffusion Franz cells, using simulated wound fluid (SWF) in the acceptor compartment, as it was previously described in section 2.2.5.4.

Figure 32 shows the release profiles of doxycycline from the various formulations compared with those of pure doxycycline alone. The main advantage observed was the prolonged release of doxycycline over time from the various formulations compared to the pure doxycycline alone, which permeated within 5 minutes and whose release was completed in about 30 minutes.

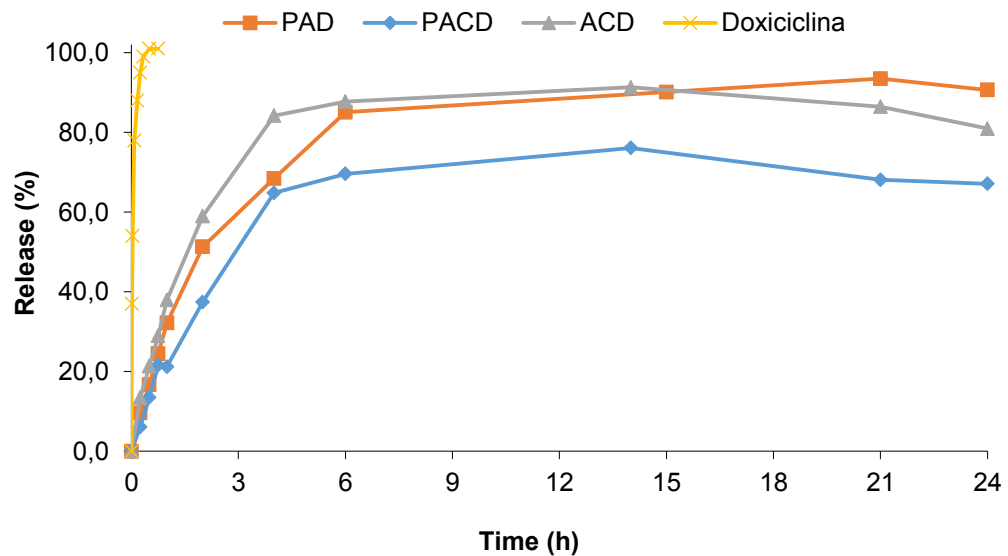


**Figure 32. Permeation profiles of pure doxycycline and of formulations containing alginate, chitosan and doxycycline (ACD); pectin, alginate and doxycycline (PAD) and pectin, alginate, chitosane and doxycycline (PACD).**

In all formulations was observed a fast release during the first two hours after application. This phenomenon was presumably due to the permeation of the amount of doxycycline that is close to the gel surface once it was completely swollen and therefore able to spread faster through it. The doxycycline presented in the innermost part of the gel is then released by diffusive release. The release of a high amount of active in the early stages after application is called “burst effect” and can be an advantage to reduce the spread of infection at the beginning of a local therapy. The various formulations have shown a continuous release, up to 15 hours for ACD and PACD formulations and up to 21 hours for the PAD formulation. The release, as it was expected, was faster for the formulation containing alginate and chitosan due to its higher surface area promoted by a higher roughness. In

addition, even the minor gelling capacity of this formulation favoured a quicker release of the drug. However, the formulation without chitosan, containing pectin, alginate and doxycycline (PAD) showed a more prolonged release over time due to both the high share of amidated pectin that, among the three polymers, has the greater gelling capacity and also due to its lower surface area compared to the other formulations, due to a lower roughness.

In conclusion, this experimental work has demonstrated the applicability of SAA technology in the production of polysaccharide-based dry powders containing doxycycline, having characteristics suitable to the dressing of infected wounds. These formulations, in fact, from the data obtained, are more effective, compared to the unformulated doxycycline, to increase patient compliance thanks to their prolonged release over time.





## **SECTION B**

### **3.2. AEROGELS FORMULATIONS FOR WOUND HEALING**



### 3.2.1. Alginate aerogel beads

*Based on the article: **Rodríguez-Dorado, R.**, López-Iglesias, C., García-González, C., Auriemma, G., Aquino R. P., Del Gaudio, P. “Design of aerogels, cryogels and xerogels of alginate: effect of alginate molecular weight, gelation conditions and drying method on particles’ micromeritics”. *Molecules* **2019**, 24(6), 1049.*



The use of small powder particles, as those previously described on SECTION A have numerous advantages when applied as wound healing formulations nevertheless there is a technological paradox since particles for topical administration must be large enough in order to be easily handled for application on wounds. Thus, an alternative approach can be the use of aerogel particles in the range of a few millimetres size since this kind of materials are very porous and have high surface areas, thus being able to absorb high amount of exudates from wounds while immediately forming a soft gel when in contact with the wound bed. Thus, in this section, the work was focused on the production and characterization of alginate aerogels as promising materials for topical administration in wounds.

Processing and shaping of dried gels have attractive properties in several fields. Namely, alginate aerogel beads as highly porous and nanostructured particles are of high interest in biomedical applications. The alginate properties and the drying method are the parameters influencing the characteristics of the dried gel particles as well as the solvent used in the gelation solution. In this part of the project, aerogel beads were prepared from different alginate molecular weight (120 kDa and 180 kDa) and concentrations (1.25, 1.50, 2.0 and 2.25%) as through different gelation conditions (aqueous and ethanolic  $\text{CaCl}_2$  0.3M solutions) and drying methods (supercritical drying, freeze-drying and oven drying) in order to obtaining particles with a broad range of physicochemical and texture properties. The study of the physicochemical properties of these alginate-based materials as a function of the processing variables (alginate concentration, gelation conditions, drying method) is of utmost importance. The analysis of the state-of-the-art unveils a paucity of information on the effect of the alginate physicochemical properties (molecular weight, M-G ratio, etc.) and gelation conditions on the textural properties of the resulting aerogels. Moreover, the effect of the drying method on the textural properties

of alginate gels has not been studied yet and, particularly, this is the first time that the freeze-drying of alcogels is explored for polysaccharides.

In order to produce homogeneous beads with narrow size distribution, before the drying process, a robust production technique must be taken into account. In this phase of the project, alginate beads were produced by prilling technique from alginates of different molecular weight, namely medium molecular weight (MMW) and high molecular weight (HMW) as well as using different solution concentrations (1.25% - 2.25%, w/v) to evaluate their influence on the physicochemical and textural properties of the resulting alginate aerogel beads. Moreover, both hydrogel and alcogel alginate particles were obtained by gelation of alginate solution droplets in either aqueous or ethanolic  $\text{CaCl}_2$  0.3M solution. Diameter of alginate beads obtained by prilling is the result of various variable concurring in producing a gelled matrix from alginate droplets. Hydrogel beads diameters (2.18 – 2.64 mm) were mainly larger than those of alcogels (2.31 – 2.46 mm), with differences in beads diameter behaviour depending on alginate molecular weight. In fact, as is shown in table 6, using MMW alginate the difference in size reduced when concentration of the alginate solution increased, whereas, using HMW alginate the increase in concentration of the processed solution led to an increase in size difference between hydrogel and alcogel beads. This behaviour can be explained taking into account the different formation of association structures through interpolymer bridging in aqueous or ethanolic gelling bath that leads to variations in viscosity of the gelling droplet and consequently to a variation in its gelation rate (*Tkalec et al., 2016*). Such phenomenon also influenced the particle size of aerogels from with a slightly lower diameter for high molecular alginate (HMW) than for MMW aerogels. Moreover, HMW alginate gel beads experimented a higher shrinkage after the supercritical drying process (*Mallepally et al., 2013*), thus they also resulted to be less porous than aerogels obtained with MMW alginate.

**Table 6. Average diameter (mm) of native gel beads (hydrogel and alcogel) and aerogels, volume shrinkage and porosity (%) of each batch after supercritical drying. Mean  $\pm$  SD; (n=6).**

Sample	d (mm) $\pm$ sd		%Vol shrinkage	% Porosity	d (mm) $\pm$ sd		%Vol shrinkage	% Porosity
	Hydrogel	Aerogel			Alcogel	Aerogel		
MMW125	2.64 $\pm$ 0.20	2.52 $\pm$ 0.19	13.3	99.7 $\pm$ 0.0	2.31 $\pm$ 0.13	2.77 $\pm$ 0.23	43.0*	99.8 $\pm$ 0.0
MMW150	2.51 $\pm$ 0.15	2.20 $\pm$ 0.10	32.5	99.5 $\pm$ 0.0	2.38 $\pm$ 0.16	2.51 $\pm$ 0.16	14.5*	99.7 $\pm$ 0.0
MMW200	2.45 $\pm$ 0.09	2.36 $\pm$ 0.16	6.7	99.5 $\pm$ 0.0	2.44 $\pm$ 0.13	1.86 $\pm$ 0.02	60.9	97.6 $\pm$ 0.1
MMW225	2.41 $\pm$ 0.11	2.33 $\pm$ 0.14	10.8	99.3 $\pm$ 0.0	2.37 $\pm$ 0.13	1.96 $\pm$ 0.10	43.7	98.7 $\pm$ 0.0
HMW125	2.18 $\pm$ 0.14	1.93 $\pm$ 0.08	30.9	99.3 $\pm$ 0.0	2.46 $\pm$ 0.23	1.81 $\pm$ 0.02	60.8	99.2 $\pm$ 0.0
HMW150	2.34 $\pm$ 0.14	1.73 $\pm$ 0.02	60.3	98.4 $\pm$ 0.0	2.32 $\pm$ 0.12	1.55 $\pm$ 0.06	71.2	98.6 $\pm$ 0.0
HMW200	2.56 $\pm$ 0.13	2.03 $\pm$ 0.13	50.6	99.5 $\pm$ 0.0	2.33 $\pm$ 0.09	1.81 $\pm$ 0.03	53.7	99.5 $\pm$ 0.0
HMW225	2.40 $\pm$ 0.13	1.92 $\pm$ 0.08	49.3	99.2 $\pm$ 0.0	2.33 $\pm$ 0.10	1.90 $\pm$ 0.08	46.3	99.3 $\pm$ 0.0

(\*)These values indicate a swelling behaviour instead of shrinkage after the sc-CO<sub>2</sub> drying. Values of aerogels skeletal density, obtained by helium pycnometry and used for calculate the porosity, are shown in table S1 in supplementary material.

Alcogels MMW125 and MMW150 showed a swelling behaviour instead of shrinkage after the sc-CO<sub>2</sub> drying process as it is indicated with a (\*) in table 6. This could be due to the immediate contraction in volume of the polymer matrix in the CaCl<sub>2</sub> ethanolic solution (*Tkalec et al., 2015*) during the prilling step, thus reducing the subsequent shrinkage during the supercritical drying. The specific BET-surface areas ( $S_a$ ) of aerogels obtained by supercritical drying (figure 33a) were in the range 271.0-537.3 m<sup>2</sup>/g. Aerogels obtained from gel beads formed in ethanolic CaCl<sub>2</sub> solutions showed higher  $S_a$  values than aerogels derived from gel beads formed in aqueous CaCl<sub>2</sub> solutions. The ethanolic gelling bath promoting the shrinkage of the polymeric matrix structure during the gel beads formation lead to smaller particles and subsequently to aerogel with higher specific surface area as shown in figure 33a, with the exception of the HMW200 sample. Moreover,  $S_a$  was also depending on alginate molecular weight used to produce beads: higher  $S_a$

values were obtained in the case of aerogels produced with HMW alginate (306.2-537.3 m<sup>2</sup>/g) than those produced with MMW alginate (271.0-419.6 m<sup>2</sup>/g). Pore size distribution in the alginate aerogels (figure 33b) was studied from the N<sub>2</sub> adsorption-desorption measurements using the BJH-method. Aerogel beads derived from alcogels presented higher BJH cumulative desorption pore volumes (V<sub>pBJH,d</sub>), in the range 0.80–3.02 cm<sup>3</sup>/g, than the aerogels derived from hydrogels (0.64-1.83 cm<sup>3</sup>/g). Differences in gelation rate due to the presence of more carboxylic groups on a single polymeric chain was also responsible of the V<sub>pBJH,d</sub> variation between aerogels produced from MMW or HMW alginate. For HMW alginate aerogels there is a smaller amount of internal gaps due to a major packing between the polymer chains. A similar trend was also observed for the BJH desorption average pore diameter (D<sub>pBJH,d</sub>) (figure 33c), with the exception of HMW125 and HMW150 aerogels where no significant differences between aerogels from hydrogels and from alcogels were obtained. In all cases, aerogels pore diameter (9.21-25.78 nm) was obtained in the mesoporous range, as it was expected.

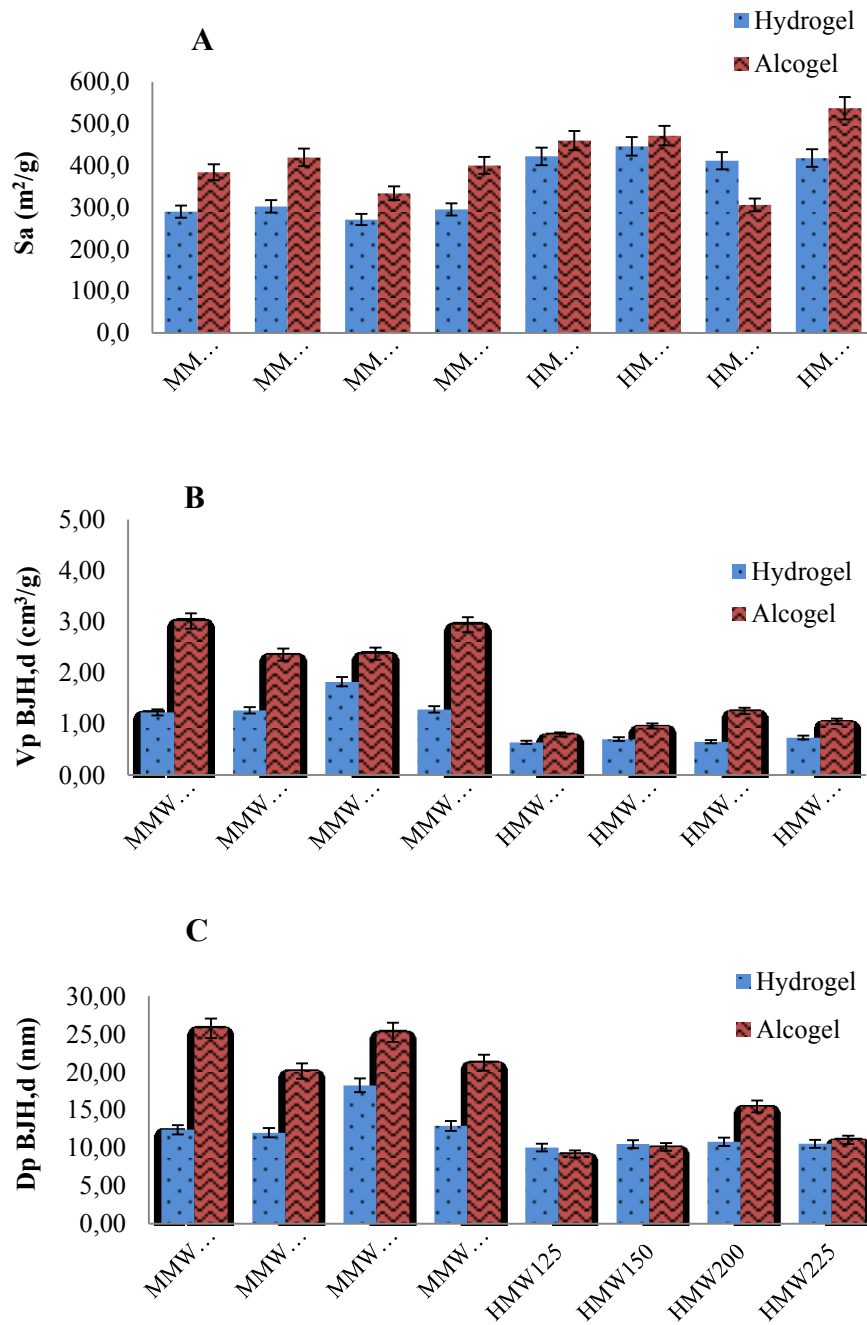


**Figure 33. Panel A: Specific surface area ( $m^2/g$ ),  $S_a$ ; Panel B: BJH cumulative desorption pore volume ( $cm^3/g$ ); Panel C: BJH cumulative desorption pore diameter (nm) of aerogel samples obtained from both hydrogel and alcolgel beads of different alginate molecular weight and concentration.**

In order to make a comparison, hydrogel and alcogel beads were also freeze-dried and the obtained cryogels showed lower specific surface areas ( $0.8\text{-}245.6\text{ m}^2/\text{g}$ ) than its aerogel counterparts, while textural properties of the xerogels (oven-dried gels during  $\geq 48\text{h}$ ) could not be studied since their porosity was below the detection limit of the  $\text{N}_2$  adsorption-desorption equipment. As expected, freeze dried particles showed lower mesoporosity and a reduction in the average pore diameter in comparison to the aerogel counterparts:  $V_{\text{pBJH,d}}$  ranged between  $0.10\text{-}0.65\text{ cm}^3/\text{g}$  and  $0.03\text{-}0.80\text{ cm}^3/\text{g}$  in the case of cryogels obtained from hydrogels and from alcogels, respectively; and  $D_{\text{pBJH,d}}$  ranged between  $3.3\text{-}9.5\text{ nm}$  and  $2.5$  and  $10.0\text{ nm}$  for cryogels obtained from hydrogels and from alcogels, respectively.

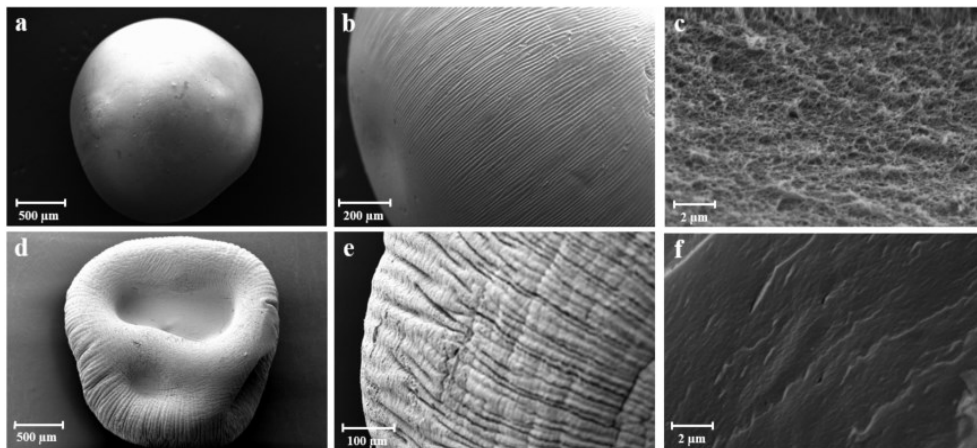


**Figure 34. SEM images of HMW225 alcogel: spherical bead (a), magnification on the smooth surface (b), inner porous network (c) of aerogels; collapsed structure (d), magnification of the surface (e) and inner structure (f) of cryogels.**

In addition, SEM images demonstrated the sphericity of the obtained aerogel beads (figure 34a), the presence of the characteristic smooth surface of alginate aerogels (figure 34b) as well as the preservation of the porous nanostructure of the matrix (figure 34c). On the contrary, cryogel beads

obtained from alcogels exhibited partial collapsed structure (figure 34d) and reduced porosity (figure 34f). In addition it was also observed an intense white colour of the alginate beads treated with supercritical drying indicating a complete purification of the original alginate (*Della Porta et al. 2013*) whereas the cryogel beads showed pale yellow colour (figure S1).

The stability under storage of aerogels (figure 35) was tested after 1 and 3 months under the humidity and temperature conditions of ICH-climatic zones II. These conditions are usually taken for stability test of drug products to cover the climatic zones I and II corresponding to mosts of the territory of Europe, USA and Japan (*Kommanaboyina & Rhodes, 1999*). Differences in stability between aerogels obtained from hydrogels and alcogels were evaluated using samples produced at the same concentration and alginate molecular weight (HMW150). Moreover aerogels obtained from alcogels at the same polymer concentration (2.25%, w/v) were used to assess the influence of alginate molecular weight on aerogel stability. After one month of storage, aerogels did not show significant differences in weight whereas an increase in weight between the 3.6% and 32.5% was observed after 3 months, probably due to the uptake of humidity. The gain in weight upon a 3-month storage of HMW150 aerogels obtained from the hydrogel and the alcogel showed an increase of 3.6% and 13.1%, respectively. This phenomenon can be explained by the fact that starting aerogels ( $t=0$ ) obtained from alcogels have higher specific surface areas and pore volumes than those obtained from hydrogels, thus conferring them a higher ability to uptake humidity and, as a consequence, their weight increase easier. The gain in weight for 2.25% alginate concentration aerogels was higher for alginates of higher molecular weight (32.5% in the case of HMW225 and 21.2% in the case of MMW225). These differences can be explained considering that the starting aerogels obtained from HMW alginate have higher specific surface areas and pore

volumes than those ones obtained from MMW alginate due to the presence of more carboxylic groups for a single chain of alginate able to interact with the  $\text{Ca}^{2+}$  ions during the prilling production of the gel beads.

Specific surface area ( $S_a$ ) decreased in all cases after 3 months of storage probably due to the increasing in pore size related to the uptake of humidity. For HMW150 aerogels, the reduction was higher in aerogels produced from alcogels (ca. 50%) due to the fact that the originating alcogels demonstrated higher surface areas than hydrogels, leading to higher adsorption capacity being able to uptake higher amounts of humidity. The effect of alginate molecular weight on the  $S_a$  values was less pronounced after 3-months storage with variations of 18.5% and 28.0% for MMW225 and HMW225, respectively (figure 35). BJH pore volume and pore diameter of the beads demonstrated similar behaviour during the storage conditions showing main variations after 1-month storage. Aerogels obtained by hydrogels with the lowest concentration in alginate demonstrated the highest increase whereas its homologous obtained by alcogels showed only slight variations in BJH pore volume (about 10%) while pore diameter increased of about 45% after one month then it remained almost constant over time, as shown in figure 35b and figure 35c.

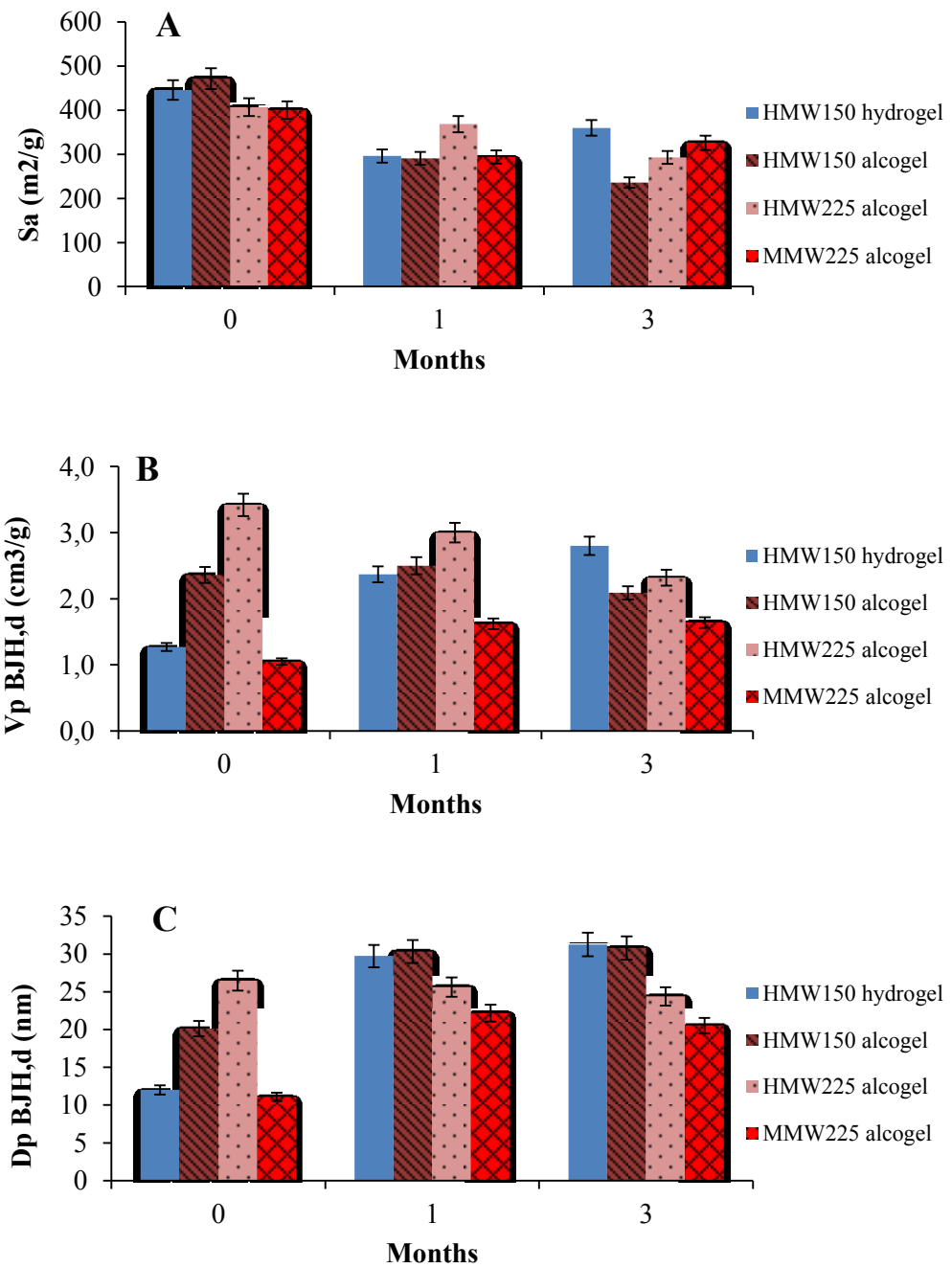


**Figure 35. Effect of stability tests under storage (25°C, 65% r.h) during 3 months on textural properties of alginate aerogels: (a) specific surface area (m<sup>2</sup>/g), S<sub>a</sub>; (b) BJH cumulative desorption pore volume (cm<sup>3</sup>/g); (c) BJH cumulative desorption pore diameter (nm). Mean values ± SD.**

In this work, alginates with different molecular weight were used for the production of gel beads through the prilling technique in single nozzle configuration, using both aqueous and ethanolic calcium chloride solutions as gelling agent obtaining hydrogel and alcogel beads in a very narrow size distribution (ca 2.4 mm  $\pm$  6.0% for each formulation). Supercritical CO<sub>2</sub> drying of these gels allowed to obtain aerogel particles with spherical shape. Gelation in ethanolic media promoted the formation of aerogels with superior textural properties in comparison with the aerogels derived from particle gellified in aqueous media. The textural properties of aerogels were far higher than those obtained from cryogels and xerogels obtained by freeze-drying and oven drying, respectively. The alginate molecular weight had an important effect on the degree of shrinking and the porosity during the production of alginate aerogels. The use of medium molecular weight was the most suitable to reduce shrinkage and leading to aerogels with higher porosity. On the contrary, aerogels with higher surface areas were obtained when high molecular weight alginate was used. Alginate aerogels may reduce their textural properties upon storage at 25°C and 65% of relative humidity depending on the formulation, being aerogels produced with medium molecular weight alginate especially stable after 3 months of storage under these conditions. In conclusion, the size and the high specific surface areas and porosities of those materials make them suitable as carriers for topical administration of drugs, since they are easily manageable and due to their textural properties. High surface area, in fact, allows fast adsorption of biological fluids that could be useful to set controlled drug release hydrogels or by absorbing high quantities of exudates once applied on a wound could produce a first line wound dressing.





### **3.2.2. Core-shell microparticles obtained by inverse gelation optimized by artificial intelligent tools for aerogels production**

*Based on the article: **Rodríguez-Dorado R**, Landín M., Ayça A., Russo P., Aquino P., Del Gaudio P. “A novel method for the production of core-shell microparticles by inverse gelation optimized with artificial intelligent tools”. *International Journal of Pharmaceutics*, **2018**, 538, 97-104.*



Regarding the optimal textural properties of alginate aerogels obtained in section 3.2.1 that make them suitable as particle formulations for wound healing applications, the next step of this work was studying the possibility of manufacturing aerogels formed by a hollow inner cavity in order to increase the fluid uptake capacity and the gelling rate. For that, in this work it was developed a new approach to obtaining core-shell microparticles by inverse gelation, using directly the coaxial nozzle of a prilling apparatus, and then submitted to a supercritical drying for the production of hollow aerogels. Furthermore, the possibility of produce a new structure of aerogel based on natural polysaccharides as thin layer microcapsules with a void inner part is a concept not yet developed that could increase interaction with biological fluids compared to other formulations thus being very useful in biomedical applications. For this work, sunflower oil was used as model for hydrophobic substances or carrier for hydrophobic active ingredients due to its high versatility in food, cosmetic and pharmaceutical industry (*Gutierrez et al., 2008; Rowe et al., 2006*) as well as for its numerous health benefits and functional properties including antioxidant, anti-inflammatory, anti-vasoconstrictive, antiarrhythmic, antithrombotic, anticancer, antidiabetic, antidepressant (*Bakry et al., 2016*). Microencapsulation of hydrophobic compounds into a hydrophilic matrix is a useful approach to protect and deliver bioactive substances susceptible to degradation in presence of light, low pH or oxidative environmental conditions (*Fang & Bhandari., 2010; Leong et al., 2016; Madene et al., 2006*). Different techniques, as coacervation and spray drying, the most commonly used methods to encapsulate oils, in combination with the use of specific polymeric excipients, allow the encapsulation of APIs with poor bioavailability, undesired taste or volatile while enabling the controlled release of the API leading to its compartment-specific distribution (*Freiberg & Zhu, 2004; Xu et al., 2007*), despite the fact that in some cases these techniques do not assure

high stability of the produced particles (*Chan, 2011; Drusch & Berg, 2008*). However, have been recently proposed an innovative approach, referred as inverse gelation, for the encapsulation of oils in alginate capsules with desired size and morphology as well as with proper membrane thickness (*Abang et al. 2012; Tsai et al., 2017; Wu et al., 2017*) in which an emulsion of calcium chloride solution in oil was dropped in an alginate solution to produce Ca-alginate capsules but, in some cases, an additional external force was needed to control droplets size (*Martins et al., 2015*). Instead, in this work, a calcium chloride aqueous solution-sunflower oil emulsion was pumped through the inner nozzle of the prilling apparatus while an alginate solution came out from the annular one for the production of core-shell particles by inverse gelation in a one step process immediately out of the nozzle without needing the application of external forces. In order to reduce the number of experimental trials, AI tools (Artificial Neural Networks and fuzzy logic in combination with genetic algorithms) on the understanding and selection of the optimal operating conditions of the prilling process were used. By this way, it is presented for the first time, the optimization of the production of core-shell particles by prilling based on AI tools using the results of preliminary experiments categorized and scored after the simple observation of the produced core-shell particles.

Preliminary experiments were carried out to set up the prilling process and to establish the limits of the different variables in order to find the responsible of size, shape and oil distribution of the core-shell beads and, ultimately, to optimize the production process of spherical microparticles of homogeneous size and with a single oil core in their inside.  $\text{CaCl}_2$  solution concentration into the emulsion was set between 20 and 50 g/L in order to understand the optimal amount of gelling agent necessary to reach the ionotropic gelation between the alginate chains and the divalent cations of  $\text{Ca}^{2+}$  during the

formation of the core-shell droplet at the nozzle, as well as its effect on water droplet size and shear force between them into the emulsion (*Márquez et al., 2010*). Alginate concentrations were also tested (in the range 1.0% - 2.0%) since viscosity at nozzle plays a crucial role in core-shell particles production by prilling due to the need of the outer solution to completely wrap the inner one to promote homogeneous core-shell beads formation (*Del Gaudio et al., 2013; Routh & Russel, 1999*). Viscosity of the solutions coming out of the nozzles are dependent on flow rates then both alginate solution and emulsion flow rates was varied during the setting of the experiments in order to determine the proper flow rate combination for proper particle production. Flow rate of the alginate solution, independently from its concentration, was varied between 4 and 17 mL/min while emulsion flow rate ranged between 1 and 7 mL/min. At the lower flow rates, the particles resulted elongated containing an irregular oily core, and while applying the highest flow rates smaller and more spherical core-shell particles were obtained. The amounts of Tween<sup>TM</sup> 85 (0.200–0.625%, v/v) and Span<sup>®</sup> 85 (0.5%, v/v) into the emulsion were also studied to determine the best mixture to avoid the deformation or breakage of the particles core at the oil-water interface due to shear forces at nozzle and to obtain proper stability of the emulsion in order to control the diffusion/permeation of a proper amount of Ca<sup>2+</sup> through the oil layer during the formation of the particles (*Cheng et al., 2007*).

Table 7 presents the conditions used in the production of each batch of microparticles. Three properties of microparticles (shape, oil content and oil distribution) for each batch were assessed and scored between 0 and 10. Score 10 was attributed to spherical particles, narrow-size distributions and a single drop of oil inside the alginate shell. The further away from these optimum properties, the lower the score assigned (score definitions are presented in table 7).

**Table 7. Conditions used for the production of preliminary batches and scores for properties of the produced microparticles.**

Batch	ALG %(w/v)	Emulsion		Q <sub>ALG</sub>	Q <sub>EM</sub>	F (Hz)	SCORE		
		[CaCl <sub>2</sub> ] (g/L)	[TW85] %(v/v)	(mL/min)	Shape		Oil content	Oil distribution	
1	2.00	50	0.500	17.0	7.0	300	7	5	5
2	2.00	50	0.500	14.0	6.0	300	4	5	5
3	2.00	50	0.500	12.0	5.0	300	0	0	0
4	1.50	50	0.500	11.0	5.0	300	3	0*	0*
5	1.50	50	0.500	9.0	4.0	300	0	0	0
6	1.50	50	0.500	9.0	4.0	250	1	2	2
7	1.50	50	0.500	5.0	2.0	250	1	2	2
8	1.50	50	0.500	4.0	2.0	250	0	0	0
9	1.00	50	0.500	5.0	2.0	250	0	0	0
10	1.00	50	0.500	7.5	3.0	250	0	0	0
11	1.00	50	0.500	15	5.0	250	0	0	0
12	1.00	50	0.500	17.0	7.0	250	1	2	2
13	1.00	30	0.500	17.0	7.0	250	8	8	8
14	1.00	30	0.500	14.0	7.0	250	8	8	8
15	1.00	30	0.500	14.0	6.0	250	8	8	8
16	1.00	30	0.500	12.0	6.0	250	8	8	8
17	1.00	30	0.500	8.0	1.0	250	8	8	8
18	1.25	30	0.500	8.0	1.0	250	4	6	8
19	1.25	25	0.500	8.0	1.0	250	4	6	8
20	1.50	30	0.500	8.0	2.0	250	0	0	0
21	1.50	20	0	8.0	4.0	250	6	6	7
22	1.50	20	0.625	8.0	4.0	250	2	4	4
23	1.50	20	0.625	7.0	4.0	250	2	4	4
24	1.50	20	0.625	8.0	3.0	250	2	1	1
25	1.50	20	0.625	12.0	6.0	250	6	7	7
26	1.50	20	0.625	14.0	8.0	250	6	7	7
27	1.00	20	0.200	8.0	6.0	250	0	0	0
28	1.00	35	0.200	10.0	6.0	250	0	0	0
29	1.00	35	0.200	9.0	6.0	250	0	0	0
30	1.00	35	0.200	8.5	6.0	250	0	0	0
31	1.00	35	0.200	8.2	6.0	250	0	0	0
32	1.25	35	0.200	10.0	6.0	250	3	2	2
33	1.12	35	0.200	10.0	6.0	250	0	0	0
34	1.12	35	0.200	8.5	6.0	250	0	0	0
35	1.12	35	0.200	8.5	6.0	300	0	0	0
36	1.12	35	0.200	8.5	6.0	230	0	0	0
37	1.12	35	0.200	10.0	6.0	230	0	0	0
38	1.12	35	0.200	11.0	6.0	230	2	2	2
39	1.12	35	0.200	9.0	6.0	230	5	6	6
40	1.12	35	0.200	8.8	6.0	280	4	5	1
41	1.12	35	0.200	8.7	6.0	280	4	5	1

\*particles without oily phase into the core

Some of these experiments led to spherical particles of homogeneous size, with a defined oil nucleus whereas others produced particles with significant deviations from what is considered optimal particle properties or even did not give rise to particles. Figure 36 presents core-shell particles produced with increasing amount of alginate solution and as it can be seen, some particles are spherical (figure 36a) but some exhibit an elongate shape (figure 36b), or even a double core (figure 36c).

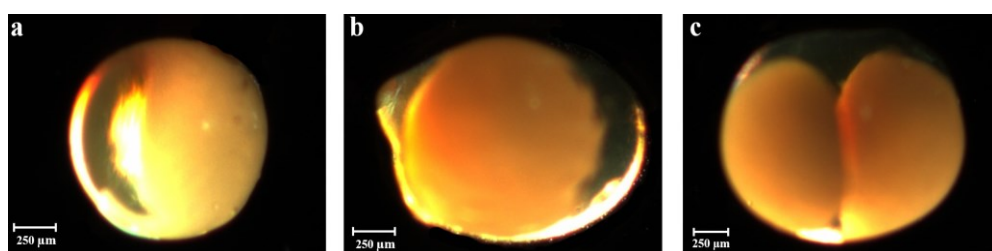


**Figure 36. Core-shell particles of different shapes and oil distribution obtained by prilling in co-axial configuration with alginate outer solution concentration between 1.0% and 2.0% (w/v): batch 13 (a), batch 21 (b), and batch 1(c).**

The conditions for the production of microparticles together with their shape, oil content and oil distribution scores from the preliminary experiments (table 7) were compiled in a database that was successfully modeled with FormRules®, that combines artificial neural networks and fuzzy logic technologies. Neurofuzzy logic systems allow to determine the inputs that explain the variability of the outputs and express the results as “if...then” rules (Landin & Rowe, 2013). Seven variables were introduced as inputs: alginate percentage ([ALG]), concentration of CaCl<sub>2</sub> solution in the emulsion ([CaCl<sub>2</sub>]), percentage of Tween<sup>TM</sup> 85 in the emulsion ([TW85]), percentage of Tween<sup>TM</sup> 85 in the receptor bath ([TW85<sub>RB</sub>]), flow rates of alginate (Q<sub>ALG</sub>) and emulsion (Q<sub>EM</sub>) and frequency of vibration (Hz). The three categorized

characteristics of the produced particles (shape, oil content and oil distribution) were introduced as outputs. All the results regarding shape, oil content and oil distribution were categorized as indicated in the supplementary material in tables S2, S3 and S4, respectively; and the significant inputs and the parameters indicative of the quality of the models (predictability and accuracy) for each property are represented in table 8.

**Table 8. Significant inputs for the neurofuzzy logic models for each output and parameters to assess their quality (the most important submodel is highlighted).**

Output	Submodels	Inputs from neurofuzzy logic submodels	R <sup>2</sup>	Calculated f value	Degrees of freedom	f critical for $p < 0.01$
Shape	Submodel 1	[CaCl <sub>2</sub> ] · Q <sub>ALG</sub> x Hz	81.96	9.08	14 and 42	2.53
	Submodel 2	Q <sub>EM</sub>				
	<b>Submodel 3</b>	<b>[ALG] · [TW85]</b>				
Oil content	<b>Submodel 1</b>	<b>[CaCl<sub>2</sub>] · [TW85]</b>	70.07	11.36	7 and 41	3.11
	Submodel 2	Q <sub>EM</sub>				
Oil distribution	<b>Submodel 1</b>	<b>[CaCl<sub>2</sub>],[TW85] · Q<sub>EM</sub></b>	82.95	11.76	12 and 41	2.65

The high training R<sup>2</sup> values (R<sup>2</sup> ≥ 70.07) obtained together with calculated f values of the ANOVA higher than critical f values for the degrees of freedom of the models are indicative of good model predictabilities and accuracies. The complete set of “If ...then” rules allows the understanding of the effect of the different variables on the properties of the core-shell particles. As it can be seen, variations in shape can be mainly explained by the interaction of the concentration of alginate and the Tween<sup>TM</sup> 85 in the emulsion. The

interaction between the concentration of calcium chloride, the flow of alginate solution and the frequency as well as the single effect of the emulsion flow can also influence the particles shape. Oil content and distribution depend on the concentration of calcium chloride, the concentration of Tween<sup>TM</sup> 85 in the emulsion and the flow of the emulsion during the prilling process. The incorporation of Tween<sup>TM</sup> 85 in the gelling bath had not effect on the parameters studied.

Alginate solution concentration strongly influenced sphericity of the particles. SC values of all particles ranged between 0.82 and 0.98 with higher values associated to alginate concentration between 1.0% and 1.5% (w/v); such values were used to score the particles in a range between 1 and 10. The effect of the concentration of alginate on the shape of the particles is explained by its influence on the rheological properties of the produced solutions. In fact, it has been described that the viscosity of the alginate solution, directly related to its concentration, plays a crucial role in the production of core-shell particles by prilling (*Heinzen et al., 2002; Routh & Russel, 1999*). The combination of proper alginate concentration and concentration of Tween<sup>TM</sup> 85 medium (0.15–0.5%) gave the maximum sphericity coefficient due to the surface-active properties of the Tween<sup>TM</sup> 85, that at low concentrations (< 1%), can be internalized into the particles promoting homogeneous distribution of the oily phase, then spherical shape of the particles (table S2, rule 15). The rheological properties of the solutions coming out from the nozzles are also dependent on both flow rates of alginate solution and emulsion. At the lower flow rates, the produced particles were elongated and amorphous, containing an oily coiled wire as internal core, probably due to a slower gelation process. When applying higher flow rates, smaller and more spherical core-shell particles were obtained (table S2, rules 5, 6, 8 and 10).

The effect of the interaction of flow of alginate and calcium concentration and frequency was another aspect to be considered. The amount of calcium contributes to the stabilization of the size of the water droplets within the emulsion and the shear force between them. In fact, when the calcium concentration was lower than 25 g/L, the particles were unable to form in the short time window represented by the falling of the droplets into the receiving bath, whereas when the concentration exceeded 35 g/L, the emulsion was very unstable and led to the co-axial nozzle stuck by the rapid gelation of the alginate coming out of the annular nozzle.

The oil content and its distribution within the particles was mainly determined by the interaction between the concentration of calcium chloride and Tween<sup>TM</sup> 85 present into the emulsion, which is indicative of the important role of emulsion stability in obtaining particles with optimal characteristics (tables S3 and S4). In fact, the presence of the non-ionic surfactants improved the oil-water interfacial tension reducing the deformation of oily phase into the droplet coming out from the coaxial nozzle (*Cheng et al., 2007*).

The complexity of the models indicated by the neurofuzzy logic software showed that the optimization of the production of core-shell particles by prilling process cannot be carried out considering one variable at time but all of them simultaneously. This was possible through the use of INForm® software that combines artificial neural networks with genetic algorithms. ANNs models also had high predictability ( $R^2$  ranging between 78 and 94% for both training and test data) for the three parameters studied. ANN models were used to find the proper conditions to obtain particles of the optimal characteristics. In order to show the software what is considered optimum, desirability functions were designed for each output using the parameters in table 9. As an example, the desirability function for the oil content score is

shown in figure 37.

**Table 9. Parameters involved in the definition of desirability functions for the optimization process by INForm®.**

Output	Weight	Function	Min	Mid	Max
Shape Score	8	UP	0	6	9
Oil Content Score	9	UP	0	6	10
Oil Distribution Score	10	UP	0	6	8

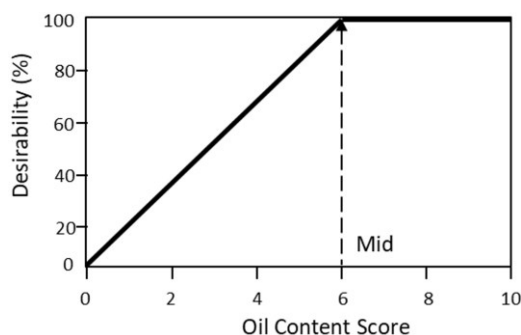


**Figure 37. Example of desirability function for parameter Oil Content Score designed using the parameters from table 9.**

ANN models were asked for finding the optimal combination of ingredients and process operation conditions in order to get simultaneously the highest score for oil distribution (unique drop of oil inside), oil content (maximum oil encapsulation) and shape (spherical particles). The optimal conditions selected by INForm® are presented in table 10 which also includes the predicted score for each output. All of them reached the maximum of desirability. Optimized parameters from table 10 were used to set the prilling process operating conditions in order to validate the procedure. Spherical double-layered beads with a narrow size distribution and homogenous oil distribution into the particle core were obtained without any struck of the prilling process, as shown in figure 38.

**Table 10. Optimized parameters and predicted score obtained by INForm® data optimization on prilling core-shell particles generation process.**

Input	[ALG] (w/v)	[CaCl <sub>2</sub> ] (w/v)	[TW85] (v/v)	[TW85 <sub>RB</sub> ] (v/v)	Q <sub>ALG</sub> (mL/min)	Q <sub>EM</sub> (mL/min)	Frequency (Hz)
Weight	1.47	26.82	0.44	0.41	17.0	4.9	300
Output	Predicted Score		Desirability				
Shape Score	6.9		100				
Oil Content Score	6.7		100				
Oil Distribution Score	6.7		100				

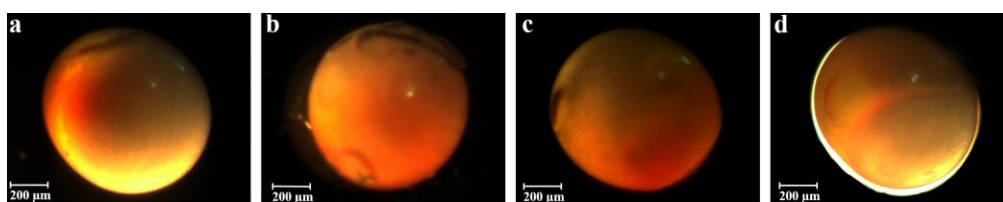


**Figure 38. Sunflower oil loaded core-shell microparticles obtained by prilling in co-axial configuration set with operative conditions obtained by ANN based approach (a) and particles produced with variation in solutions flow rate ratio: 10% (b, c); 12% (d).**

The good results in terms of particles desired properties obtained with small adjustment of the inner and annular solutions flow rate ratio (about 10%) were also showed in figure 38. Higher variations lead to particles with undesired properties, mainly in inhomogeneous oil distribution, probably due to the slow release of Ca<sup>2+</sup> from emulsion that enable to stabilize the core of the particles during shell gelation (*Pays et al., 2001*). Ca<sup>2+</sup> concentration into the emulsion and alginate concentration are also responsible of the core-shell polymeric membrane thickness. In fact, calcium ions diffusing into the alginate solution at the interface between the two phases forms the membrane

coating the oil drop. Differently from other inverse gelation approaches where membrane thickness is depending only on calcium diffusion rate (*Abang et. al., 2012; Martins et. al., 2017*) in prilling inverse gelation approach the alginate plays an active role in determining the particle membrane thickness due to the fact that its amount coming out from the annular nozzle can be precisely set. Therefore, both calcium ions and not yet cross-linked alginate depletion determine the rate and thickness of the polymeric membrane. Optimized condition selected by INForm® allowed to obtain homogeneous shell thickness around 110  $\mu\text{m}$ , as shown in figure 39. In order to increase production rate some tests were conducted using the optimized parameters with the only exception of the increased vibration frequency (from 300 Hz till 350 Hz) and very good particles were obtained when frequency reached 340Hz. Fluorescent microscopy analyses pointed out homogeneous oil distribution into the core of the particles and thinner alginate shell, about 95  $\mu\text{m}$  (figure 39b and 39c). This phenomenon can be explained taking into account both faster detachment of the droplet from the coaxial nozzle and faster gelation of the alginate shell due to the reduced ionic junctions of the polymer membrane (*González-Rodríguez et al., 2002; Koyama & Seki, 2004*). Different values of vibration frequency led to core-shell particles with insufficient shell homogeneity and thinner polymer membrane, the higher the frequency the lower the shell thickness, as shown in figures 39d and 39f.

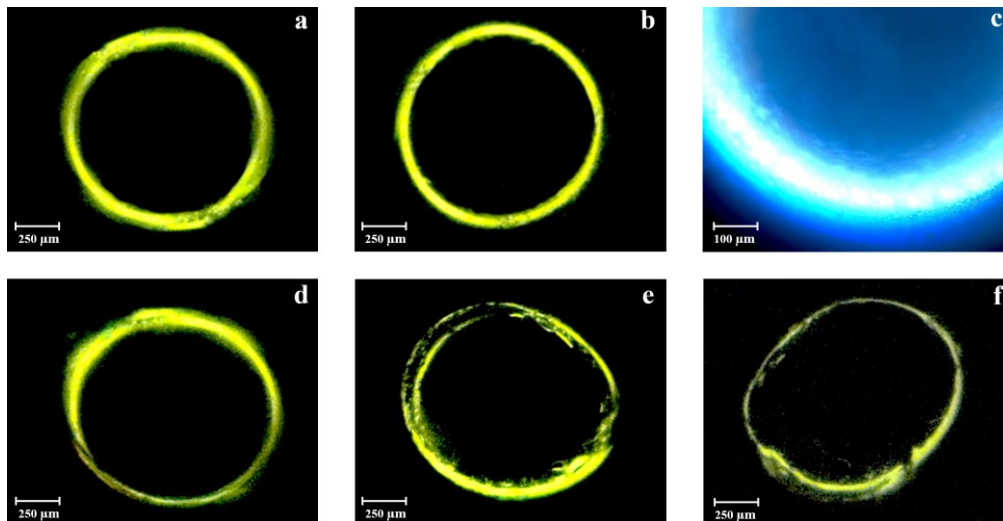


**Figure 39. Fluorescent microscopy images of core-shell particles obtained by ANN optimized prilling operative conditions at different frequency of vibration: 300 Hz (a), 340 Hz (b) and a magnified detail of the shell (c), 320 Hz (d) 330 Hz (e) and 350 Hz (f).**

In order to evaluate the resistance of the particles during further manipulation and storage, hardness of core-shell particles from several batches were tested. Core-shell beads (CSB) demonstrated a breaking strength between 222 mN and 295 mN. Particles with the highest resistance (294.84 mN) were obtained with alginate concentration set at 1.47% (w/v) and optimized operating conditions using 300 Hz as frequency of vibration, while the use of different process parameters led to smaller values, not statistically different ( $p=0.063$ ). The increase of the frequency of vibration led to the reduction in shell thickness and consequently to a reduction in particles hardness, as shown in figure 40. As expected, beads hardness decreased significantly ( $p < 0.05$ ) when particles were produced with lower alginate concentrated solutions reaching its minimum at 222.14 mN for particles obtained with 1.0% (w/v) alginate solution. According to such results, we demonstrated that alginate concentration plays a very important role in increasing hardness of the beads due to increased alginate shell thickness and homogeneity while optimized

manufactured parameters can contribute to tailor particle resistance allowing both their handling in different processes and suitability for different administration route.

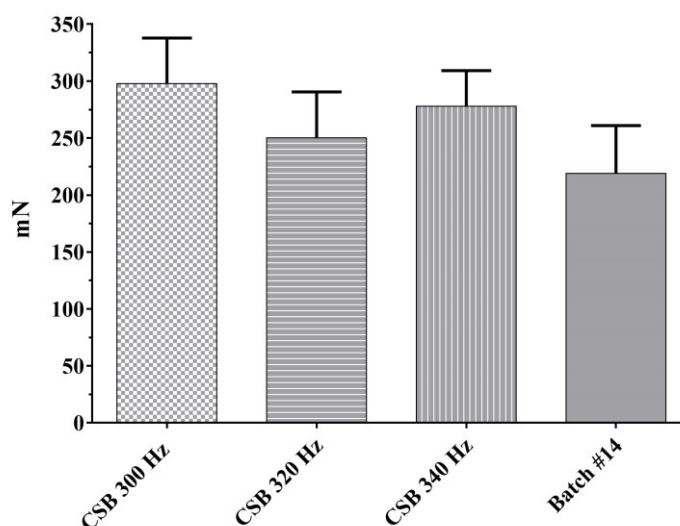


**Figure 40. Hardness of core-shell particles obtained by prilling and optimized operative conditions at different frequency of vibration. Particles obtained with no optimized parameters (Batch #14) were used as comparison. Data represents mean  $\pm$  SD with significance  $p < 0.05$ .**

Once obtained the optimized parameters for the production of core-shell beads, these were manufactured both in aqueous and ethanolic  $\text{CaCl}_2$  0.3M solutions, in order to get hydrogels and alcogels, respectively. The obtained microparticles were submitted to two different supercritical drying processes at 120 bar during 210 minutes (sc- $\text{CO}_2$  drying 1) and at 140 bar during 270 minutes (sc- $\text{CO}_2$  drying 2), both at 40°C and at a flow rate of 7 g/min during the first 60 minutes and at 5 g/min until the end of the process with the purpose to obtaining aerogel capsules (aerogels formed just by a external layer covering a void inner part). The drying at higher pressures was able to dry the core-shell gels slightly faster. Supercritical drying allowed the

extraction of ca. 99% of all the ethanol initially presented in the autoclave ( $\approx$  20 mL), in contact with the gel beads, in just 40 min for all the cases. Oil traces from the gel core were not observed in the autoclave or in the aerogels at the end of the process, thus indicating that the oil was properly eliminated from the particles upon drying. Morphology of aerogel capsules obtained from the hydrogel beads and alcogel beads presented some differences in both shape and surface roughness (figure 41). Aerogel capsules obtained from the hydrogels were almost spherical with smoother surfaces (figures 41a-c), whereas those obtained from alcogels showed a partially collapsed structure (figures 41d-f). The use of ethanol in the gelling bath solution might have reduced the interaction between  $\text{Ca}^{2+}$  ions and the carboxylic groups of the alginate leading to a more significant shrinkage of the beads during gelation and ageing. SEM images confirmed that supercritical drying of core-shell gel beads allowed the production of hollow aerogels (capsules) with a shell thickness of ca. 27  $\mu\text{m}$  and with no significant differences between hydrogel and alcogel processed beads. Oven drying at 60°C was used as alternative drying method on all the produced particle batches prolonging the procedure until constant weight was reached. Oven drying was not able to remove completely the oil phase from beads even after 30 hours. Moreover, oven drying altered the morphology of the particles leading to deformed and collapsed beads, as shown in figure 41g-i. Oven-dried beads presented some voids embedded through the collapsed polymeric matrix (figure 41h).

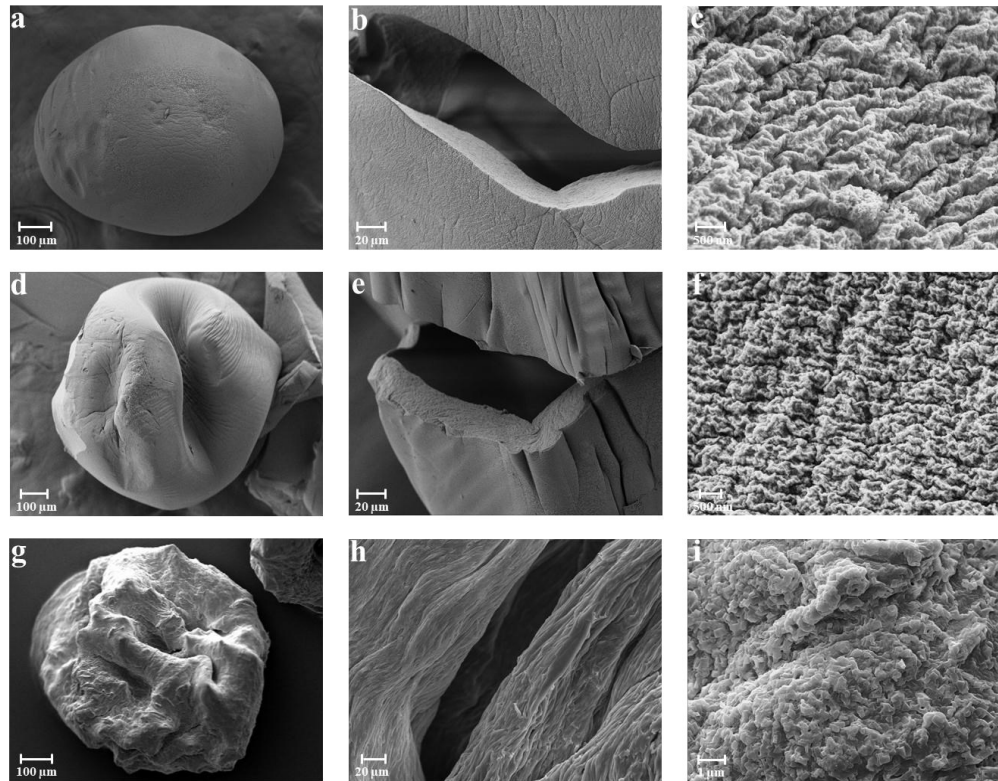


**Figure 41. SEM micrographs of dried MMW alginate gel beads at different magnifications: aerogels obtained from beads gelled in  $\text{CaCl}_2$  0.3M (a-c) aqueous and (d-f) ethanolic solutions; (g-i) beads gelled in aqueous solution and oven-dried. From left to right: whole particles, cryo-fractured cross-section of the particles and surface magnification.**

The specific BET surface area ( $S_a$ ), BJH cumulative desorption pore volume ( $V_{p_{\text{BJH,d}}}$ ), BJH desorption average pore diameter ( $D_{p_{\text{BJH,d}}}$ ) and average volume of aerogel capsules derived from core-shell hydrogels (CSH) and core-shell alcogels (CSA) were evaluated (table 11). The obtained  $S_a$  values were in the 306-407  $\text{m}^2/\text{g}$  range, being higher in the case of aerogel capsules obtained with the sc- $\text{CO}_2$  drying 2, with a longer drying time and higher pressure. Aerogel microcapsules derived from alcogels (CSA) showed higher values of  $S_a$ ,  $V_{p_{\text{BJH,d}}}$  and  $D_{p_{\text{BJH,d}}}$  than those derived from hydrogels (CSH)

thus following the same trend previously observed for alginate aerogel beads in SECTION 3.2.1.  $D_{p_{BJH,d}}$  obtained values were between 7.2 and 14.9 nm, which is in the mesoporous range (2-50 nm) according to the IUPAC classification. Alginate aerogel capsules with higher porosity were obtained through the sc-CO<sub>2</sub> drying 1, which is the fastest one and it requires the use of lower pressure than in sc-CO<sub>2</sub> drying 2.  $V_{p_{BJH,d}}$  and  $D_{p_{BJH,d}}$  values for aerogel capsules were both higher than those in alginate aerogel beads.

**Table 11. Textural properties of aerogel capsules obtained from supercritical drying of hydrogels (CSH) and from alcogels (CSA), indicating with -1 and -2 the sc-CO<sub>2</sub> drying 1 and the sc-CO<sub>2</sub> drying 2, respectively.**

<b>Aerogel</b>	<b>Sa (m<sup>2</sup>/g) ± SD</b>	<b>V<sub>p<sub>BJH,d</sub></sub> (cm<sup>3</sup>/g)</b>	<b>D<sub>p<sub>BJH, d</sub></sub> (nm)</b>
CSH1	306.2 ± 15.3	1.26 ± 0.06	14.6 ± 0.7
CSH2	339.2 ± 17.0	0.60 ± 0.03	7.2 ± 0.4
CSA1	371.2 ± 18.6	1.58 ± 0.08	14.9 ± 0.7
CSA2	407.2 ± 20.4	0.83 ± 0.04	8.2 ± 0.4

In conclusion, sunflower oil microencapsulation in calcium-alginate capsules was successfully carried out by the development of an innovative inverse gelation approach in which the ionotropic gelation was reached immediately at the co-axial nozzle exit of a prilling encapsulator apparatus. By this methodology, core-shell microcapsules were obtained in a single step process after the setting of all the operating variables involved in the process by means of the implementation of artificial intelligence tools based on ANNs, neurofuzzy logic and genetic algorithms. Particles were then obtained with the desired size and morphology containing a single and homogeneous oily core. The optimized parameters by AI tools allowed to manufacturing of spherical core-shell beads (sphericity coefficient about 0.98) with diameter

about 1.1. mm and a narrow size distribution containing the oily droplet wrapped by a thin a regular alginate layer (about 95  $\mu\text{m}$ ). The use of AI tools allowed the optimization of prilling operating conditions through a reduced number of preliminary experiments permitting, for the first time, the manufacturing of microcapsules by inverse gelation using this methodology. The results demonstrated that proper interaction between  $\text{Ca}^{2+}$  presented into the W/O emulsion and alginate can be tailored to produce core-shell beads with different hardness that could be loaded with oil or drugs dispersed into lipids useful in various kind of applications. In addition, with the purpose to obtaining aerogel capsules formed by a void inner cavity, suitable for increase the fluid uptake in wound healing applications, the optimized core-shell microparticles were submitted to a supercritical drying that led to microcapsules with thin aerogel shell (about 27  $\mu\text{m}$ ) and high specific surface areas, pore volumes and pore diameters due to the presence of a void core in the particles after the oil removal. Such kind of formulation could be potentially used to load hydrophobic active ingredients into alginate aerogels.



**3.2.3. Supercritical drying of core-shell microparticles  
for the manufacturing of ketoprofen lysinate loaded  
aerogels**



Previous studies in SECTION 3.2.2 allowed to develop a new inverse gelation methodology carried out directly at the co-axial nozzle of the prilling apparatus for the production of core-shell microparticles as carriers of APIs with different nature. These formulations in form of gel capsules are good candidates for the manufacturing of aerogel capsules as new carriers of drugs for being topically administrated in the treatment of chronic wounds since polysaccharide-based aerogel beads are highly porous materials, with high specific surface areas and with an extremely low density that are able to uptake great amounts of fluids (*García-González et al., 2011; Maleki et al., 2016; López-Iglesias et al., 2019*). Furthermore, the fact that an emulsion composes the inner phase of the microparticles, could allow the encapsulation of either hydrophilic or hydrophobic APIs. For these reasons this work was focused in the development of loaded-aerogel capsules manufactured by prilling in tandem with sc-CO<sub>2</sub> drying. In this case the manufacturing of the core-shell microparticles through the inverse gelation methodology previously described, was carried out by the Büchi encapsulator B-390, with concentric nozzles, and using an O/W/O emulsion as internal hydrophobic phase and an alginate solution as the external hydrophilic layer of the microparticles. Hydrophobic core / hydrophilic shell microparticles were loaded with a non-steroidal anti-inflammatory drug (ketoprofen lysinate) used as model drug, in the aqueous phase of the O/W/O emulsion. For the O/W/O preparation, different concentrations of aqueous CaCl<sub>2</sub> solution were tested since it was necessary to study the proper concentration to get the inverse gelation at the nozzle exit allowing the proper formation of the jet droplets without blocking and also different amounts of PVA used as surfactant in the aqueous phase with the purpose of reducing the interfacial tension. In order to obtain a spherical core covered by a thin layer of alginate both flow rate of the emulsion and of the alginate solution were tested at different rating, evaluating that higher flow rate values were needed for the

alginate solution (10-49 mL/min) compared to the rate of the emulsion feed (4-6 mL/min). Different vibration frequencies were tested in order to understand how the jet could be properly broken up into uniform droplets containing both phases and the possibility to use the electrode in order to favour the dispersion of the droplets. Initially, the operating prilling variables tested were those optimized by AI tools in the SECTION 3.2.2, but the presence of the drug into the inner phase destabilized the formation of the particles and subsequent experiments were tried. As it is shown in figure 42, non-optimized conditions lead to the formation of non-spherical and non-homogeneous in size and shell distribution particles (figure 42a) as well as multi-core (figure 42b) or with a non-centered core (figure 42c) and with a too dense shell (figure 42d). After the study of all operative conditions, the selected nozzles were those of 450  $\mu\text{m}$  diameter at the inner and 900  $\mu\text{m}$  diameter at the outer one, in order to get particles with sizes  $> 1\text{mm}$ , easily to handle during topical application directly into the wound bed. In consequence, the use of the electrode had no effect in the production of particles of such sizes thus it was no used. With the purpose to manufacturing particles with a single centered core recovered of a thin shell (figure 43) the selected operative conditions resulted to be: 1.75% (w/v) alginate concentration being pumped at a 31 mL/min flow rate whereas the emulsion was pumped at 6 mL/min; 13.4 g/L  $\text{CaCl}_2$  concentration at the aqueous phase of the emulsion containing 1.0% (w/v) PVA; 3 cm of falling distance between the nozzle exit and the collecting bath and the vibration frequency set at 340 Hz. The optimized beads were collected in  $\text{CaCl}_2$  (0.3 M) in absolute ethanol, in order to avoid the presence of water in the subsequent supercritical drying process and the smallest drop distance (3 cm) was chosen for the purpose of reduce the fall times and avoid the lengthening of the drops.

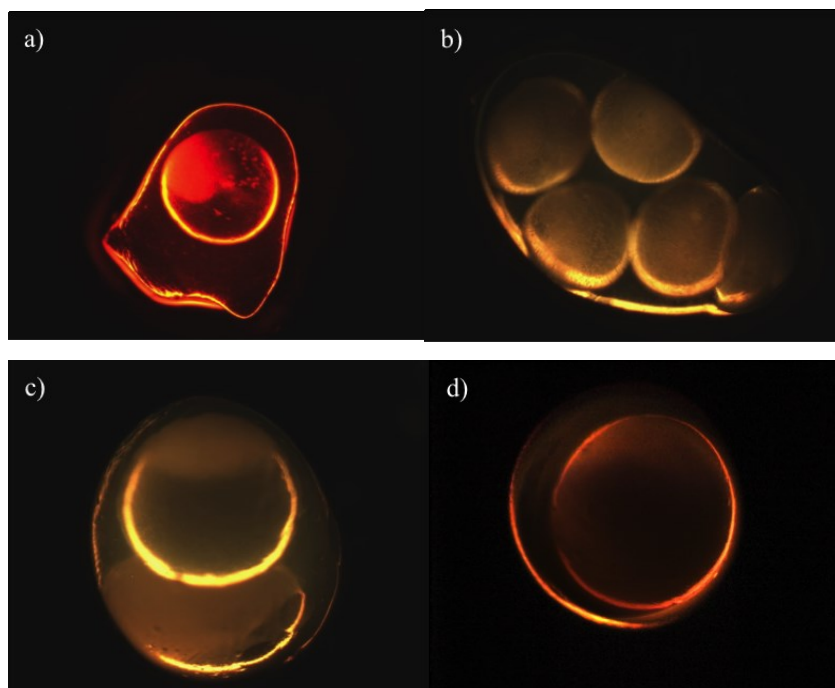


**Figure 42. Non-optimized core-shell particles.**

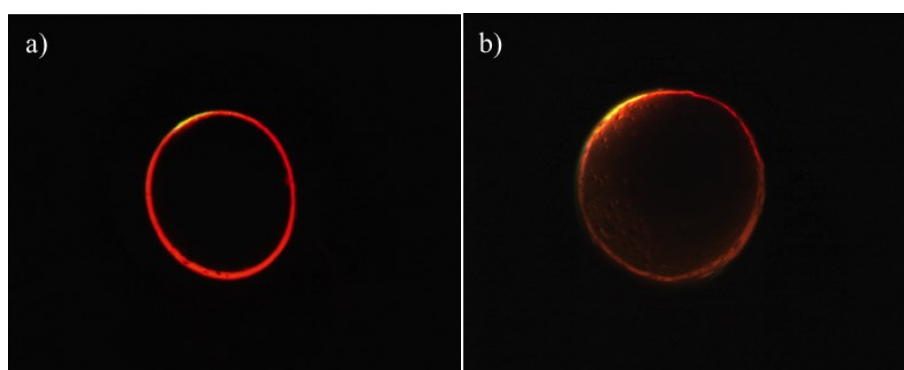


**Figure 43. Core-shell microparticles obtained with the optimized parameters at different alginate concentrations: (a) 2.00% (w/w) and (b) 1.75% (w/w).**

Fluorescent microscopy assays confirmed the emulsion encapsulation at the inner part of a thin alginate layer thus developing homogeneous and spherical core-shell beads with a single centered core, able to being submitted to a

subsequently sc-CO<sub>2</sub> drying for the manufacturing of aerogels. Therefore, once optimized all the parameters, core-shell beads were produced loading 10% (F1) and 20% (F2) of ketoprofen lysinate and successive experiments were only conducted on these formulations.

Previously at the sc-CO<sub>2</sub> drying process, a solvent exchange was carried twice in order to eliminate the possible traces of water. The sc-CO<sub>2</sub> drying was carried out at 40°C and at a SC-CO<sub>2</sub> flow rate of 7 g/min during the first hour and at 5g/min during the rest of the process. Different assays were carried out at 120 bar during 210 minutes (sc-CO<sub>2</sub> drying 1), and 140 bar during 270 minutes (sc-CO<sub>2</sub> drying 2). After sc-CO<sub>2</sub> drying 1, the obtained aerogels were analysed by nitrogen adsorption porosimetry in order to determine its textural properties (BET specific surface area ( $S_a$ ), BJH cumulative desorption pore volume ( $V_{p_{BJH,d}}$ ) and BJH cumulative pore diameter ( $D_{p_{BJH,d}}$ )) and it was observed that they had very low  $S_a$  and pore volumes (table 12).

**Table 12. Textural properties of formulations F1 and F2 after supercritical-CO<sub>2</sub> drying 1 (40°C, 120 mbar, 210 minutes).**

SC-CO <sub>2</sub> drying 1	Surface area ( $S_a$ ) (m <sup>2</sup> /g)	Pore volume ( $V_{p_{BJH,d}}$ ) (cm <sup>3</sup> /g)	Pore diameter ( $D_{p_{BJH,d}}$ ) (nm)
F1	14.5 ± 0.7	0.10 ± 0.00	26.90 ± 1.34
F2	27.5 ± 1.4	0.30 ± 0.02	31.23 ± 1.56

In addition, SEM images showed that supercritical drying does not modify the sphericity of the beads (figure 44a), but in this case it was also observed from the cryo-fractured beads (figure 44b) that some kind of “bubbles” are presented in the internal void part of the beads that could be oil droplets from the emulsion. However, as it is shown in figure 44c, ketoprofen crystals were presented into the polymeric matrix, thus indicating that the solvent

elimination through supercritical drying was able to remove the oily phase without nick the amount of the encapsulated ketoprofen.

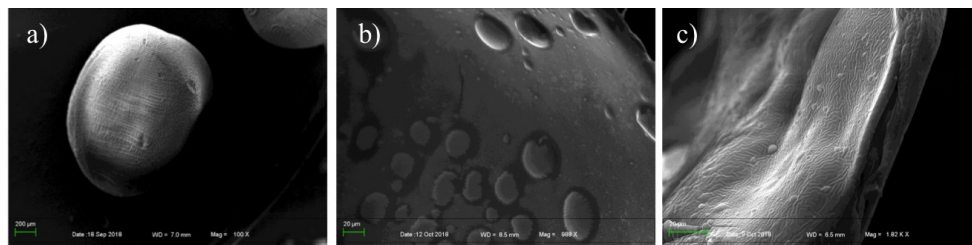


**Figure 44. SEM images of aerogels after SC-CO<sub>2</sub> drying 1: (a) single bead; (b) inner part of a bead; (c) ketoprofen crystals at the inner part.**

Accordingly with the results showed in table 12 and the SEM images of figure 44, a subsequent sc-CO<sub>2</sub> drying process (2) was carried out using higher pressure (140 bar) and longer time of drying process (270 min). In this case, the aerogels obtained showed higher specific surface areas and pore volumes as well as pore diameters in the mesoporous range, being this values (table 13) more appropriate for this kind of materials.

**Table 13. Textural properties of formulations F1 and F2 after the sc-CO<sub>2</sub> drying 2 (40°C, 140 mbar, 270 minutes).**

SC-CO <sub>2</sub> drying 2	Surface area (S <sub>a</sub> ) (m <sup>2</sup> /g)	Pore volume (V <sub>pBJH,d</sub> ) (cm <sup>3</sup> /g)	Pore diameter (D <sub>pBJH,d</sub> ) (nm)	Density (g/cm <sup>3</sup> )	Porosity (%)
F1	242.7 ± 12.1	1.96 ± 0.10	25.37 ± 1.27	0.107	89.9
F2	368.4 ± 18.4	2.35 ± 0.12	25.62 ± 1.28	0.068	93.1

SEM images of aerogels obtained from sc-CO<sub>2</sub> drying 2 confirmed again that the supercritical drying conditions do not modify the sphericity of the beads (figures 45a and 45d) and allowed to produce very porous materials (figures 45b and 45e) with a thin alginate shell (figures 45c and 45f), but in this case

ketoprofen crystals were not observed in the matrix as in the drying process number 1.

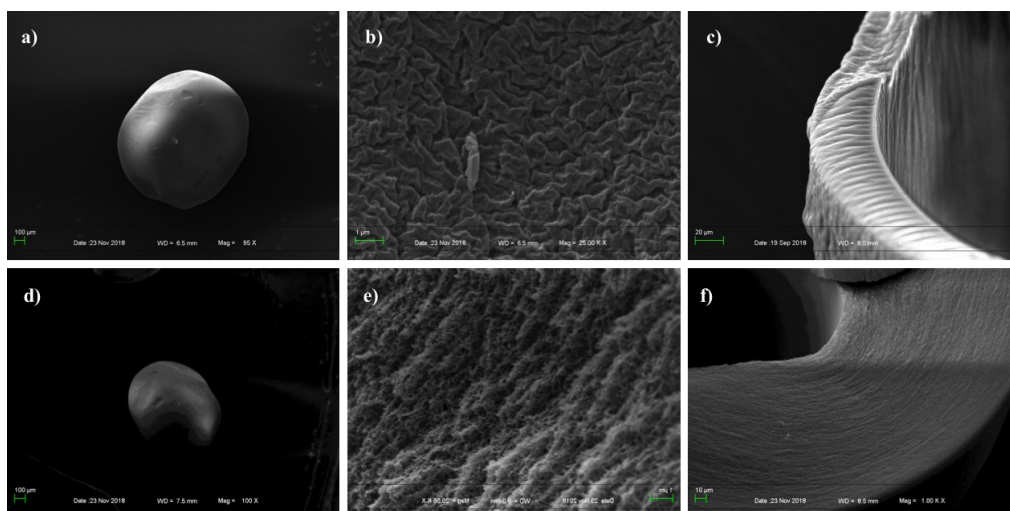


**Figure 45. SEM images of F1 (a, b, c) and F2 (d, e, f) aerogels obtained after SC-CO<sub>2</sub> drying 2: (a, b) single bead; (b, e) porous structure; (c, f) shell.**

Fluid uptake ability of the aerogel capsules was evaluated as the weight ratio of the formed hydrogel and starting aerogel and at different time points when formulations were in contact with SWF. As expected, fluid uptake was directly related to surface area. In fact, formulations exhibited an increase in weight ranging from 480% to 505% the initial weight of the aerogel for F1 and F2, respectively. Moreover, shrinking of the particles was observed before the swelling phase. This phenomenon is due to the partial collapse of the alginate shell and was more significant and faster for formulations with higher surface area. However, as shown in figure 46 gelling rate was very fast for all formulations with a total gelling time reduced to 6 seconds for F2 aerogel beads.

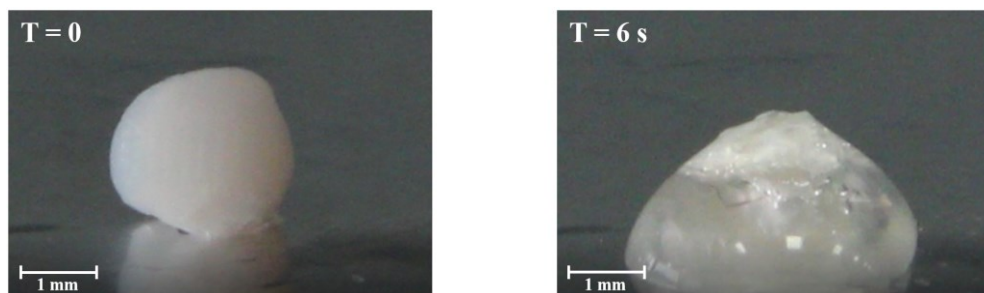


**Figure 46. Fluid uptake of F2 formulation moving from aerogel to hydrogel when in contact with a single droplet of simulated wound fluid. Pictures shot at different time point, 0 and 6 seconds.**

Accordingly with these results, quantification analyses of the encapsulated drug were carried out by UV-Vis spectrophotometry and the obtained results showed a ketoprofen content and encapsulation efficiency of 0.09% and 1.04% in the case of F1 and 0.31% and 1.86% in the case of F2. Thus, it was verified the presence of the drug into the aerogel formulations although at low amount, but instead its disappearance as crystals could be explained from the results obtained by infrared spectroscopy (FTIR-ATR) showed in figure 47, in which the spectra of the pure ketoprofen, the alginate, and the loaded-aerogel containing the 20% of ketoprofen are shown. Two peaks were observed in the stretching region (C=O) for the pure ketoprofen, between 1667 and 1555  $\text{cm}^{-1}$ , that represents the vibrational stretching of the carboxylic group and the vibrational stretching of the carbonyl in the ketonic group, respectively. In the loaded-aerogels these peaks were not presented and this could be to its shift to lower wavelength numbers being covered by the stretching of the alginate carboxylic group, due to the formation of hydrogen bonds between the alginate and the ketoprofen and to the formation of interactions between hydroxyl groups of ketoprofen and the  $\text{Ca}^{2+}$  presented in the gellified matrix of the polymeric particles.

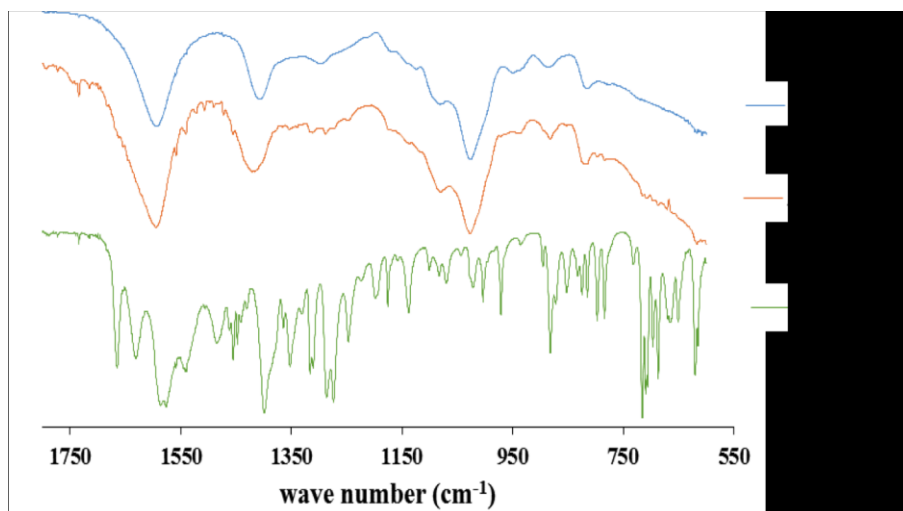


**Figure 47. FTIR-ATR spectra of the alginate, the pure ketoprofen and the loaded-aerogel.**

In conclusion, it was developed a robust manufacturing method for the production of core-shell beads by prilling technique in tandem with supercritical drying for the production of loaded-aerogels using ketoprofen lysinate, a BCS class I non-steroidal anti-inflammatory drug (NSAID), as model drug. The obtained optimized gel beads produced by prilling showed a single spherical core encapsulated into an alginate thin shell and had a size > 1 mm, thus being easily handled. These optimized beads loaded with ketoprofen lysinate were successfully dried by supercritical-CO<sub>2</sub> assaying different conditions of pressure and time of drying process, and those aerogels obtained by using the more drastic conditions (140 bar pressure and 270 minutes of drying process) showed higher surface areas and porosities. Furthermore, the SEM images corroborated the high porosity of these materials and the presence of the drug into the alginate matrix, thus being formulations able to absorb high amount of exudate and easily-handled improving in this manner the patient compliance, although those are preliminary studies and a compromise between the supercritical drying

process and the encapsulation efficiency of the drug into the aerogels should be further studied.



## **4. CONCLUSIONS**



This PhD Project was focused on the development of novel inexpensive technological approaches based on the use of supercritical carbon dioxide (sc-CO<sub>2</sub>) for the production of polymeric micro-nanoparticulate systems made by biocompatible and biodegradable polysaccharide-based excipients (alginate, pectin and chitosan) for the manufacturing of new wound dressing formulations. In particular, the project focused on the development and characterization of “*in-situ*” gelling powders obtained by Supercritical Assisted Atomization (SAA) and of alginate aerogel formulations, either in form of beads and capsules, obtained by Supercritical Antisolvent Extraction (SAE) in tandem with prilling.

The SAA technique allowed to obtain micro- and nanoparticulate powders loaded with doxycycline, used as model drug with high yield process and encapsulation efficiency. Powders made with a blend of polysaccharide, showed proper technological characteristics to be administered directly to the wounds, since they were able to totally gel when in contact with the fluids present into the wound bed, in about three minutes. The formation of the gel made by excipients in the repairing tissue at wound site was able to prolong the drug release after an initially burst effect release.

The optimization of processing parameter of SAE technique in tandem with prilling allowed to efficiently obtain alginate aerogels in form of beads and capsules. Aerogel capsules loaded with ketoprofen lysinate, used as model drug, with a thin nanoporous layer of alginate, were obtained. Moreover, in this work has been demonstrated, for the first time, that the application of artificial intelligence based software can be a powerful tool for the optimization of parameters involved in the prilling process. Hollow aerogel capsules showed good properties in terms of specific surface areas and porosities. Moreover, the properties of the alginate layer strongly promoted fast uptake of high amounts of exudate, moving from aerogel to a soft

hydrogel, in less than 10 seconds to total gelation. Such results suggest that both in situ gelling powders and alginate aerogel capsules could be administered as self-consistent dosage forms in the treatment of both acute and chronic wounds.

## References

- Abang, S., Chan, E. S., & Poncelet, D. (2012). Effects of process variables on the encapsulation of oil in ca-alginate capsules using an inverse gelation technique. *Journal of microencapsulation*, 29(5), 417-428.
- Adami, R., Liparoti, S., & Reverchon, E. (2011). A new supercritical assisted atomization configuration, for the micronization of thermolabile compounds. *Chemical Engineering Journal*, 173(1), 55-61.
- Alnaief, M., Alzaitoun, M. A., García-González, C. A., & Smirnova, I. (2011). Preparation of biodegradable nanoporous microspherical aerogel based on alginate. *Carbohydrate Polymers*, 84(3), 1011-1018.
- Anumolu, S. S., DeSantis, A. S., Menjoge, A. R., Hahn, R. A., Beloni, J. A., Gordon, M. K., & Sinko, P. J. (2010). Doxycycline loaded poly (ethylene glycol) hydrogels for healing vesicant-induced ocular wounds. *Biomaterials*, 31(5), 964-974.
- Auriemma, G., Mencherini, T., Russo, P., Stigliani, M., Aquino, R. P., & Del Gaudio, P. (2013). Prilling for the development of multi-particulate colon drug delivery systems: Pectin vs. pectin–alginate beads. *Carbohydrate polymers*, 92(1), 367-373.
- Bakry, A. M., Abbas, S., Ali, B., Majeed, H., Abouelwafa, M. Y., Mousa, A., & Liang, L. (2016). Microencapsulation of oils: a comprehensive review of benefits, techniques, and applications. *Comprehensive Reviews in Food Science and Food Safety*, 15(1), 143-182.
- Betz, M., García-González, C. A., Subrahmanyam, R. P., Smirnova, I., & Kulozik, U. (2012). Preparation of novel whey protein-based aerogels as drug carriers for life science applications. *The Journal of Supercritical Fluids*, 72, 111-119.

- Boateng, J. S., Matthews, K. H., Stevens, H. N., & Eccleston, G. M. (2008). Wound healing dressings and drug delivery systems: a review. *Journal of pharmaceutical sciences*, *97*(8), 2892-2923.
- Bowler, P. G., Duerden, B. I., & Armstrong, D. G. (2001). Wound microbiology and associated approaches to wound management. *Clinical microbiology reviews*, *14*(2), 244-269.
- Celikkin, N., Rinoldi, C., Costantini, M., Trombetta, M., Rainer, A., & Świążzkowski, W. (2017). Naturally derived proteins and glycosaminoglycan scaffolds for tissue engineering applications. *Materials Science and Engineering: C*, *78*, 1277-1299.
- Cerciello, A., Auriemma, G., Del Gaudio, P., Sansone, F., Aquino, R. P., & Russo, P. (2016). A novel core-shell chronotherapeutic system for the oral administration of ketoprofen. *Journal of Drug Delivery Science and Technology*, *32*, 126-131.
- Cerciello, A., Auriemma, G., Morello, S., Pinto, A., Del Gaudio, P., Russo, P., & Aquino, R. P. (2015). Design and in vivo anti-inflammatory effect of ketoprofen delayed delivery systems. *Journal of pharmaceutical sciences*, *104*(10), 3451-3458.
- Cerciello, A., Del Gaudio, P., Granata, V., Sala, M., Aquino, R. P., & Russo, P. (2017). Synergistic effect of divalent cations in improving technological properties of cross-linked alginate beads. *International journal of biological macromolecules*, *101*, 100-106.
- Chan, E. S. (2011). Preparation of Ca-alginate beads containing high oil content: Influence of process variables on encapsulation efficiency and bead properties. *Carbohydrate polymers*, *84*(4), 1267-1275.
- Chang, X., Chen, D., & Jiao, X. (2008). Chitosan-based aerogels with high adsorption performance. *The Journal of Physical Chemistry B*, *112*(26), 7721-7725.

- Cheng, J., Chen, J. F., Zhao, M., Luo, Q., Wen, L. X., & Papadopoulos, K. D. (2007). Transport of ions through the oil phase of W1/O/W2 double emulsions. *Journal of colloid and interface science*, 305(1), 175-182.
- Colbourn, E., & Rowe, R. C. (2005). Neural computing and pharmaceutical formulation. *Encyclopedia of Pharmaceutical Technology*. New York, USA: Marcel Dekker, 145-157.
- Cutting, K. F. (2003). Wound exudate: composition and functions. *British journal of community nursing*, 8(Sup3), S4-S9.
- Davies, O. R., Lewis, A. L., Whitaker, M. J., Tai, H., Shakesheff, K. M., & Howdle, S. M. (2008). Applications of supercritical CO<sub>2</sub> in the fabrication of polymer systems for drug delivery and tissue engineering. *Advanced drug delivery reviews*, 60(3), 373-387.
- De Cicco, F., Reverchon, E., Adami, R., Auriemma, G., Russo, P., Calabrese, E. C., Porta, A., Aquino, R. P., & Del Gaudio, P. (2014). In situ forming antibacterial dextran blend hydrogel for wound dressing: SAA technology vs. spray drying. *Carbohydrate polymers*, 101, 1216-1224.
- De Cicco, F., Russo, P., Reverchon, E., García-González, C. A., Aquino, R. P., & Del Gaudio, P. (2016). Prilling and supercritical drying: A successful duo to produce core-shell polysaccharide aerogel beads for wound healing. *Carbohydrate polymers*, 147, 482-489.
- De, S., & Robinson, D. (2003). Polymer relationships during preparation of chitosan–alginate and poly-l-lysine–alginate nanospheres. *Journal of Controlled Release*, 89(1), 101-112.
- Del Gaudio, P., Auriemma, G., Mencherini, T., Della Porta, G., Reverchon, E., & Aquino, R. P. (2013). Design of alginate-based aerogel for nonsteroidal anti-inflammatory drugs controlled delivery systems using prilling and supercritical-assisted drying. *Journal of pharmaceutical sciences*, 102(1), 185-194.

- Del Gaudio, P., Auriemma, G., Russo, P., Mencherini, T., Campiglia, P., Stigliani, M., & Aquino, R. P. (2014). Novel co-axial prilling technique for the development of core-shell particles as delayed drug delivery systems. *European Journal of Pharmaceutics and Biopharmaceutics*, 87(3), 541-547.
- Del Gaudio, P., Colombo, P., Colombo, G., Russo, P., & Sonvico, F. (2005). Mechanisms of formation and disintegration of alginate beads obtained by prilling. *International journal of pharmaceutics*, 302(1-2), 1-9.
- Del Gaudio, P., De Cicco, F., Sansone, F., Aquino, R. P., Adami, R., Ricci, M., & Giovagnoli, S. (2015). Alginate beads as a carrier for omeprazole/SBA-15 inclusion compound: A step towards the development of personalized paediatric dosage forms. *Carbohydrate polymers*, 133, 464-472.
- Del Gaudio, P., Russo, P., Lauro, M. R., Colombo, P., & Aquino, R. P. (2009). Encapsulation of ketoprofen and ketoprofen lysinate by prilling for controlled drug release. *Aaps Pharmscitech*, 10(4), 1178.
- Della Porta, G., Del Gaudio, P., De Cicco, F., Aquino, R. P., & Reverchon, E. (2013). Supercritical drying of alginate beads for the development of aerogel biomaterials: optimization of process parameters and exchange solvents. *Industrial & Engineering Chemistry Research*, 52(34), 12003-12009.
- Diaz-Gomez, L., Concheiro, A., Alvarez-Lorenzo, C., & García-González, C. A. (2016). Growth factors delivery from hybrid PCL-starch scaffolds processed using supercritical fluid technology. *Carbohydrate polymers*, 142, 282-292.
- Drusch, S., & Berg, S. (2008). Extractable oil in microcapsules prepared by spray-drying: Localisation, determination and impact on oxidative stability. *Food Chemistry*, 109(1), 17-24.

- Du, A., Zhou, B., Zhang, Z., & Shen, J. (2013). A special material or a new state of matter: a review and reconsideration of the aerogel. *Materials*, 6(3), 941-968.
- El Fawal, G. F., Abu-Serie, M. M., Hassan, M. A., & Elnouby, M. S. (2018). Hydroxyethyl cellulose hydrogel for wound dressing: Fabrication, characterization and in vitro evaluation. *International journal of biological macromolecules*, 111, 649-659.
- El Kadib, A., Molvinger, K., Cacciaguerra, T., Bousmina, M., & Brunel, D. (2011). Chitosan templated synthesis of porous metal oxide microspheres with filamentary nanostructures. *Microporous and Mesoporous Materials*, 142(1), 301-307.
- Englert, C., Brendel, J. C., Majdanski, T. C., Yildirim, T., Schubert, S., Gottschaldt, M., Windhab, N., & Schubert, U. S. (2018). Pharmapolymers in the 21st century: Synthetic polymers in drug delivery applications. *Progress in Polymer Science*.
- Fabien, V., Minh-Quan, L., Michelle, S., Guillaume, B., Van-Thanh, T., & Marie-Claire, V. J. (2016). Development of prilling process for biodegradable microspheres through experimental designs. *International journal of pharmaceuticals*, 498(1-2), 96-109.
- Fang, Z., & Bhandari, B. (2010). Encapsulation of polyphenols—a review. *Trends in Food Science & Technology*, 21(10), 510-523.
- Fazli, M., Bjarnsholt, T., Kirketerp-Møller, K., Jørgensen, B., Andersen, A. S., Krogfelt, K. A., Givskov, M. & Tolker-Nielsen, T. (2009). Nonrandom distribution of *Pseudomonas aeruginosa* and *Staphylococcus aureus* in chronic wounds. *Journal of clinical microbiology*, 47(12), 4084-4089.
- Freiberg, S., & Zhu, X. X. (2004). Polymer microspheres for controlled drug release. *International journal of pharmaceuticals*, 282(1-2), 1-18.

- Frykberg, R. G., & Banks, J. (2015). Challenges in the treatment of chronic wounds. *Advances in wound care*, 4(9), 560-582.
- García-González, C. A., & Smirnova, I. (2013). Use of supercritical fluid technology for the production of tailor-made aerogel particles for delivery systems. *The Journal of Supercritical Fluids*, 79, 152-158.
- García-González, C. A., Alnaief, M., & Smirnova, I. (2011). Polysaccharide-based aerogels—Promising biodegradable carriers for drug delivery systems. *Carbohydrate Polymers*, 86(4), 1425-1438.
- García-González, C. A., Carenza, E., Zeng, M., Smirnova, I., & Roig, A. (2012). Design of biocompatible magnetic pectin aerogel monoliths and microspheres. *RSC Advances*, 2(26), 9816-9823.
- Goimil, L., Jaeger, P., Ardao, I., Gómez-Amoza, J. L., Concheiro, A., Alvarez-Lorenzo, C., & García-González, C. A. (2018). Preparation and stability of dexamethasone-loaded polymeric scaffolds for bone regeneration processed by compressed CO<sub>2</sub> foaming. *Journal of CO<sub>2</sub> Utilization*, 24, 89-98.
- González-Rodríguez, M. L., Holgado, M. A., Sanchez-Lafuente, C., Rabasco, A. M., & Fini, A. (2002). Alginate/chitosan particulate systems for sodium diclofenac release. *International Journal of Pharmaceutics*, 232(1-2), 225-234.
- Guo, S. A., & DiPietro, L. A. (2010). Factors affecting wound healing. *Journal of dental research*, 89(3), 219-229.
- Gutierrez, J., Barry-Ryan, C., & Bourke, P. (2008). The antimicrobial efficacy of plant essential oil combinations and interactions with food ingredients. *International journal of food microbiology*, 124(1), 91-97.
- Han, G., & Ceilley, R. (2017). Chronic wound healing: a review of current management and treatments. *Advances in therapy*, 34(3), 599-610.

- Heinzen, C., Marison, I., Berger, A., & von Stockar, U. (2002). Use of vibration technology for jet break-up for encapsulation of cells, microbes and liquids in monodisperse microcapsules. *Landbauforschung Völkenrode, SH241*, 19-25.
- Innerlohinger, J., Weber, H. K., & Kraft, G. (2006, December). Aerocellulose: aerogels and aerogel-like materials made from cellulose. In *Macromolecular Symposia* (Vol. 244, No. 1, pp. 126-135). Weinheim: WILEY-VCH Verlag.
- Järbrink, K., Ni, G., Sönnergren, H., Schmidtchen, A., Pang, C., Bajpai, R., & Car, J. (2017). The humanistic and economic burden of chronic wounds: a protocol for a systematic review. *Systematic reviews*, 6(1), 15.
- Jiménez-Saelices, C., Seantier, B., Cathala, B., & Grohens, Y. (2017). Effect of freeze-drying parameters on the microstructure and thermal insulating properties of nanofibrillated cellulose aerogels. *Journal of Sol-Gel Science and Technology*, 84(3), 475-485.
- Kim, H. J., Lee, H. C., Oh, J. S., Shin, B. A., Oh, C. S., Park, R. D., Yang, K. S., & Cho, C. S. (1999). Polyelectrolyte complex composed of chitosan and sodium alginate for wound dressing application. *Journal of Biomaterials Science, Polymer Edition*, 10(5), 543-556.
- Kogawa, A. C., & Salgado, H. R. N. (2012). Quantification of doxycycline hyclate in tablets by HPLC–UV method. *Journal of chromatographic science*, 51(10), 919-925.
- Kommanaboyina, B., & Rhodes, C. T. (1999). Trends in stability testing, with emphasis on stability during distribution and storage. *Drug development and industrial pharmacy*, 25(7), 857-868.
- Koyama, K., & Seki, M. (2004). Evaluation of mass-transfer characteristics in alginate-membrane liquid-core capsules prepared using

- polyethylene glycol. *Journal of bioscience and bioengineering*, 98(2), 114-121.
- Landin, M., & Rowe, R. C. (2013). Artificial neural networks technology to model, understand, and optimize drug formulations. In *Formulation Tools for Pharmaceutical Development* (pp. 7-37).
- Lazarus, G. S., Cooper, D. M., Knighton, D. R., Margolis, D. J., Percoraro, R. E., Rodeheaver, G., & Robson, M. C. (1994). Definitions and guidelines for assessment of wounds and evaluation of healing. *Wound Repair and Regeneration*, 2(3), 165-170.
- Leong, J. Y., Lam, W. H., Ho, K. W., Voo, W. P., Lee, M. F. X., Lim, H. P., Lim, S. L., Tey, B. T., Poncelet, D., & Chan, E. S. (2016). Advances in fabricating spherical alginate hydrogels with controlled particle designs by ionotropic gelation as encapsulation systems. *Particuology*, 24, 44-60.
- Li, J., Chen, J., & Kirsner, R. (2007). Pathophysiology of acute wound healing. *Clinics in dermatology*, 25(1), 9-18.
- Liebner, F., Haimer, E., Wendland, M., Neouze, M. A., Schlufter, K., Miethe, P., Heinze, T., Potthast, A., & Rosenau, T. (2010). Aerogels from Unaltered Bacterial Cellulose: Application of scCO<sub>2</sub> Drying for the Preparation of Shaped, Ultra-Lightweight Cellulosic Aerogels. *Macromolecular bioscience*, 10(4), 349-352.
- Llamas-Arriba, M. G., Puertas, A. I., Prieto, A., López, P., Cobos, M., Miranda, J. I., Marieta, C., Ruas-Madiedo, P., & Dueñas, M. T. (2019). Characterization of dextrans produced by *Lactobacillus mali* CUPV271 and *Leuconostoc carnosum* CUPV411. *Food Hydrocolloids*, 89, 613-622.
- López-Iglesias, C., Barros, J., Ardao, I., Monteiro, F. J., Alvarez-Lorenzo, C., Gomez-Amoza, J. L., & García-González, C. A. (2019). Vancomycin-

- loaded chitosan aerogel particles for chronic wound applications. *Carbohydrate polymers*, 204, 223-231.
- Madene, A., Jacquot, M., Scher, J., & Desobry, S. (2006). Flavour encapsulation and controlled release—a review. *International journal of food science & technology*, 41(1), 1-21.
- Maleki, H., Durães, L., García-González, C. A., del Gaudio, P., Portugal, A., & Mahmoudi, M. (2016). Synthesis and biomedical applications of aerogels: Possibilities and challenges. *Advances in colloid and interface science*, 236, 1-27.
- Mallepally, R. R., Bernard, I., Marin, M. A., Ward, K. R., & McHugh, M. A. (2013). Superabsorbent alginate aerogels. *The Journal of Supercritical Fluids*, 79, 202-208.
- Márquez, A. L., Medrano, A., Panizzolo, L. A., & Wagner, J. R. (2010). Effect of calcium salts and surfactant concentration on the stability of water-in-oil (w/o) emulsions prepared with polyglycerol polyricinoleate. *Journal of colloid and interface science*, 341(1), 101-108.
- Martins, E., Poncelet, D., Marquis, M., Davy, J., & Renard, D. (2017). Monodisperse core-shell alginate (micro)-capsules with oil core generated from droplets millifluidic. *Food Hydrocolloids*, 63, 447-456.
- Martins, E., Renard, D., Davy, J., Marquis, M., & Poncelet, D. (2015). Oil core microcapsules by inverse gelation technique. *Journal of microencapsulation*, 32(1), 86-95.
- Mehling, T., Smirnova, I., Guenther, U., & Neubert, R. H. H. (2009). Polysaccharide-based aerogels as drug carriers. *Journal of Non-Crystalline Solids*, 355(50-51), 2472-2479.

- Mikkonen, K. S., Parikka, K., Ghafar, A., & Tenkanen, M. (2013). Prospects of polysaccharide aerogels as modern advanced food materials. *Trends in food science & technology*, 34(2), 124-136.
- Mogoşanu, G. D., & Grumezescu, A. M. (2014). Natural and synthetic polymers for wounds and burns dressing. *International journal of pharmaceutics*, 463(2), 127-136.
- Morton, L. M., & Phillips, T. J. (2016). Wound healing and treating wounds: Differential diagnosis and evaluation of chronic wounds. *Journal of the American Academy of Dermatology*, 74(4), 589-605.
- Naseri-Nosar, M., & Ziora, Z. M. (2018). Wound dressings from naturally-occurring polymers: A review on homopolysaccharide-based composites. *Carbohydrate polymers*.
- Patrulea, V., Ostafe, V., Borchard, G., & Jordan, O. (2015). Chitosan as a starting material for wound healing applications. *European Journal of Pharmaceutics and Biopharmaceutics*, 97, 417-426.
- Pawar, S. N., & Edgar, K. J. (2012). Alginate derivatization: a review of chemistry, properties and applications. *Biomaterials*, 33(11), 3279-3305.
- Pays, K., Giermanska-Kahn, J., Pouligny, B., Bibette, J., & Leal-Calderon, F. (2001). Coalescence in surfactant-stabilized double emulsions. *Langmuir*, 17(25), 7758-7769.
- Pierre, A. C., & Pajonk, G. M. (2002). Chemistry of aerogels and their applications. *Chemical Reviews*, 102(11), 4243-4266.
- Pouton, C. W., & Porter, C. J. (2008). Formulation of lipid-based delivery systems for oral administration: materials, methods and strategies. *Advanced drug delivery reviews*, 60(6), 625-637.
- Quignard, F., Valentin, R., & Di Renzo, F. (2008). Aerogel materials from marine polysaccharides. *New journal of chemistry*, 32(8), 1300-1310.

- Reverchon, E. (2002). Supercritical-assisted atomization to produce micro- and/or nanoparticles of controlled size and distribution. *Industrial & engineering chemistry research*, 41(10), 2405-2411.
- Reverchon, E., & Marrone, C. (2001). Modeling and simulation of the supercritical CO<sub>2</sub> extraction of vegetable oils. *The Journal of Supercritical Fluids*, 19(2), 161-175.
- Robitzer, M., Di Renzo, F., & Quignard, F. (2011). Natural materials with high surface area. Physisorption methods for the characterization of the texture and surface of polysaccharide aerogels. *Microporous and Mesoporous Materials*, 140(1-3), 9-16.
- Robitzer, M., Tourrette, A., Horga, R., Valentin, R., Boissière, M., Devoisselle, J. M., Di Renzo, F., & Quignard, F. (2011). Nitrogen sorption as a tool for the characterisation of polysaccharide aerogels. *Carbohydrate polymers*, 85(1), 44-53.
- Rodríguez-Dorado, R., Landín, M., Altai, A., Russo, P., Aquino, R. P., & Del Gaudio, P. (2018). A novel method for the production of core-shell microparticles by inverse gelation optimized with artificial intelligent tools. *International journal of pharmaceutics*, 538(1-2), 97-104.
- Routh, A. F., & Russel, W. B. (1999). A process model for latex film formation: Limiting regimes for individual driving forces. *Langmuir*, 15(22), 7762-7773.
- Rowe, R. C., Sheskey, P. J., & Owen, S. C. (Eds.). (2006). *Handbook of pharmaceutical excipients* (Vol. 6). London: Pharmaceutical press.
- Sanz-Moral, L. M., Rueda, M., Mato, R., & Martín, Á. (2014). View cell investigation of silica aerogels during supercritical drying: Analysis of size variation and mass transfer mechanisms. *The Journal of Supercritical Fluids*, 92, 24-30.
- Schmidt, M., & Schwertfeger, F. (1998). Applications for silica aerogel products. *Journal of non-crystalline solids*, 225, 364-368.

- Sen, C. K., Gordillo, G. M., Roy, S., Kirsner, R., Lambert, L., Hunt, T. K., Gottrup, F., Gurtner, G. C., & Longaker, M. T. (2009). Human skin wounds: a major and snowballing threat to public health and the economy. *Wound repair and regeneration*, *17*(6), 763-771.
- Serp, D., Cantana, E., Heinzen, C., Von Stockar, U., & Marison, I. W. (2000). Characterization of an encapsulation device for the production of monodisperse alginate beads for cell immobilization. *Biotechnology and bioengineering*, *70*(1), 41-53.
- Sriamornsak, P. (2003). Chemistry of pectin and its pharmaceutical uses: A review. *Silpakorn University International Journal*, *3*(1-2), 206-228.
- Sriamornsak, P., Thirawong, N., & Puttipipatkachorn, S. (2004). Morphology and buoyancy of oil-entrapped calcium pectinate gel beads. *The AAPS journal*, *6*(3), 65-71.
- Stergar, J., & Maver, U. (2016). Review of aerogel-based materials in biomedical applications. *Journal of Sol-Gel Science and Technology*, *77*(3), 738-752.
- Suvarna, K., & Munira, M. (2013). Wound Healing Process and Wound Care Dressing: A Detailed Review. *J Pharm Res*, *2*(11), 6-12.
- Szekalska, M., Puciłowska, A., Szymańska, E., Ciosek, P., & Winnicka, K. (2016). Alginate: Current use and future perspectives in pharmaceutical and biomedical applications. *International Journal of Polymer Science*, 2016.
- Tabernerero, A., del Valle, E. M. M., & Galán, M. A. (2012). Supercritical fluids for pharmaceutical particle engineering: Methods, basic fundamentals and modelling. *Chemical Engineering and Processing: Process Intensification*, *60*, 9-25.
- Takeo, M., Lee, W., & Ito, M. (2015). Wound healing and skin regeneration. *Cold Spring Harbor perspectives in medicine*, *5*(1), a023267.

- Tkalec, G., Knez, Ž., & Novak, Z. (2015). Formation of polysaccharide aerogels in ethanol. *RSC Advances*, 5(94), 77362-77371.
- Tkalec, G., Kranvogel, R., Uzunalić, A. P., Knez, Ž., & Novak, Z. (2016). Optimisation of critical parameters during alginate aerogels' production. *Journal of Non-Crystalline Solids*, 443, 112-117.
- Tsai, F. H., Chiang, P. Y., Kitamura, Y., Kokawa, M., & Islam, M. Z. (2017). Producing liquid-core hydrogel beads by reverse spherification: Effect of secondary gelation on physical properties and release characteristics. *Food Hydrocolloids*, 62, 140-148.
- Tsiptsias, C., Michailof, C., Staurooulos, G., & Panayiotou, C. (2009). Chitin and carbon aerogels from chitin alcogels. *Carbohydrate Polymers*, 76(4), 535-540.
- Unnithan, A. R., Sasikala, A. R. K., Murugesan, P., Gurusamy, M., Wu, D., Park, C. H., & Kim, C. S. (2015). Electrospun polyurethane-dextran nanofiber mats loaded with Estradiol for post-menopausal wound dressing. *International journal of biological macromolecules*, 77, 1-8.
- Van Tomme, S. R., Storm, G., & Hennink, W. E. (2008). In situ gelling hydrogels for pharmaceutical and biomedical applications. *International journal of pharmaceutics*, 355(1-2), 1-18.
- Voragen, A. G., Coenen, G. J., Verhoef, R. P., & Schols, H. A. (2009). Pectin, a versatile polysaccharide present in plant cell walls. *Structural Chemistry*, 20(2), 263.
- Whelehan, M., & Marison, I. W. (2011). Microencapsulation using vibrating technology. *Journal of microencapsulation*, 28(8), 669-688.
- White, R. J., Antonio, C., Budarin, V. L., Bergström, E., Thomas-Oates, J., & Clark, J. H. (2010). Polysaccharide-Derived Carbons for Polar Analyte Separations. *Advanced Functional Materials*, 20(11), 1834-1841.

- White, R. J., Budarin, V. L., & Clark, J. H. (2010). Pectin-Derived Porous Materials. *Chemistry—A European Journal*, *16*(4), 1326-1335.
- Widgerow, A. D., King, K., Tocco-Tussardi, I., Banyard, D. A., Chiang, R., Awad, A., Afzel, H., Bhatnager, S., Melkumyan, S., Wirth, G., & Evans, G. R. (2015). The burn wound exudate—An under-utilized resource. *Burns*, *41*(1), 11-17.
- Wu, Q., Zhang, T., Xue, Y., Xue, C., & Wang, Y. (2017). Preparation of alginate core-shell beads with different M/G ratios to improve the stability of fish oil. *LWT-Food Science and Technology*, *80*, 304-310.
- Xiao, Q., Weng, H., Ni, H., Hong, Q., Lin, K., & Xiao, A. (2019). Physicochemical and gel properties of agar extracted by enzyme and enzyme-assisted methods. *Food Hydrocolloids*, *87*, 530-540.
- Xu, Y., Zhan, C., Fan, L., Wang, L., & Zheng, H. (2007). Preparation of dual crosslinked alginate-chitosan blend gel beads and in vitro controlled release in oral site-specific drug delivery system. *International Journal of Pharmaceutics*, *336*(2), 329-337.
- Yegappan, R., Selvaprithiviraj, V., Amirthalingam, S., & Jayakumar, R. (2018). Carrageenan based hydrogels for drug delivery, tissue engineering and wound healing. *Carbohydrate polymers*.
- Yu, Y., Shen, M., Song, Q., & Xie, J. (2018). Biological activities and pharmaceutical applications of polysaccharide from natural resources: A review. *Carbohydrate polymers*, *183*, 91-101.

**Webreference:** [www.accessdata.fda.gov/cdrh\\_docs/pdf17/K172324](http://www.accessdata.fda.gov/cdrh_docs/pdf17/K172324)

## **SUPPLEMENTARY MATERIAL**



Table S1. Skeletal density ( $\text{g}/\text{cm}^3$ ) of aerogel beads from SECTION B 3.2.1.

Aerogel Sample	$\rho$ Skeletal ( $\text{g}/\text{cm}^3$ )	
	Hydrogel	Alcogel
MMW125	$1.400 \pm 0.019$	$1.440 \pm 0.027$
MMW150	$1.330 \pm 0.014$	$1.407 \pm 0.029$
MMW200	$1.370 \pm 0.028$	$1.461 \pm 0.044$
MMW225	$1.378 \pm 0.056$	$1.490 \pm 0.047$
HMW125	$1.330 \pm 0.056$	$1.436 \pm 0.025$
HMW150	$1.484 \pm 0.031$	$1.491 \pm 0.029$
HMW200	$1.557 \pm 0.019$	$1.521 \pm 0.022$
HMW225	$1.515 \pm 0.021$	$1.518 \pm 0.021$

Figure S1: Aerogel (left) and cryogel (right) beads from SECTION B 3.2.1.



Table S2. Rules obtained by neurofuzzy logic regarding the shape of the microparticles from SECTION B 3.2.2.

Rules	for Shape Scores		
<i>SubModel 1</i>			
1	IF Q <sub>ALG</sub> is LOW AND [CaCl <sub>2</sub> ] is LOW AND Hz is LOW	THEN Shape Score is	HIGH (0.73)
2	IF Q <sub>ALG</sub> is LOW AND [CaCl <sub>2</sub> ] is LOW AND Hz is HIGH	THEN Shape Score is	HIGH (1.00)
3	IF Q <sub>ALG</sub> is LOW AND [CaCl <sub>2</sub> ] is HIGH AND Hz is LOW	THEN Shape Score is	LOW (0.95)
4	IF Q <sub>ALG</sub> is LOW AND [CaCl <sub>2</sub> ] is HIGH AND Hz is HIGH	THEN Shape Score is	LOW (1.00)
5	IF Q <sub>ALG</sub> is HIGH AND [CaCl <sub>2</sub> ] LOW AND Hz is LOW	THEN Shape Score is	HIGH (1.00)
6	IF Q <sub>ALG</sub> is HIGH AND [CaCl <sub>2</sub> ] is LOW AND Hz is HIGH	THEN Shape Score is	HIGH (1.00)
7	IF Q <sub>ALG</sub> is HIGH AND [CaCl <sub>2</sub> ] is HIGH AND Hz is LOW	THEN Shape Score is	LOW (1.00)
8	IF Q <sub>ALG</sub> is HIGH AND [CaCl <sub>2</sub> ] is HIGH AND Hz is HIGH	THEN Shape Score is	HIGH (0.98)
<i>SubModel 2</i>			
9	IF Q <sub>EM</sub> is LOW	THEN Shape Score is	LOW (0.88)
10	IF Q <sub>EM</sub> is HIGH	THEN Shape Score is	HIGH (1.00)
<i>SubModel 3</i>			
11	IF [ALG] is LOW AND [TW85] is LOW	THEN Shape Score is	LOW (1.00)
12	IF [ALG] is LOW AND [TW85] is MID	THEN Shape Score is	LOW (1.00)
13	IF [ALG] is LOW AND [TW85] is HIGH	THEN Shape Score is	HIGH (1.00)
14	IF [ALG] is HIGH AND [TW85] is LOW	THEN Shape Score is	HIGH (1.00)
15	IF [ALG] is HIGH AND [TW85] is MID	THEN Shape Score is	HIGH (1.00)
16	IF [ALG] is HIGH AND [TW85] is HIGH	THEN Shape Score is	LOW (1.00)

Table S3. Rules obtained by neurofuzzy logic regarding the oil content of the microparticles from SECTION 3.2.2.

<b>Rules</b>	<b>for Oil Content Score</b>		
<i>SubModel:1</i>			
1	IF [CaCl <sub>2</sub> ] is LOW AND [TW85] is LOW	THEN Oil Content Score is	LOW (0.61)
2	IF [CaCl <sub>2</sub> ] is LOW AND [TW85] is MID	THEN Oil Content Score is	HIGH (1.00)
3	IF [CaCl <sub>2</sub> ] is LOW AND [TW85] is HIGH	THEN Oil Content Score is	HIGH (0.51)
4	IF [CaCl <sub>2</sub> ] is HIGH AND [TW85] is LOW	THEN Oil Content Score is	LOW (1.00)
5	IF [CaCl <sub>2</sub> ] is HIGH AND [TW85] is MID	THEN Oil Content Score is	LOW (1.00)
6	IF [CaCl <sub>2</sub> ] is HIGH AND [TW85] is HIGH	THEN Oil Content Score is	HIGH (1.00)
<i>SubModel:2</i>			
7	IF Q <sub>EM</sub> is LOW	THEN Oil Content Score is	LOW (1.00)
8	IF Q <sub>EM</sub> is HIGH	THEN Oil Content Score is	HIGH (0.72)

Table S4. Rules obtained by neurofuzzy logic regarding the oil distribution of the microparticles from SECTION 3.2.2.

Rules	for Oil Distribution Score		
<i>SubModel:1</i>			
1	IF [CaCl <sub>2</sub> ] is LOW AND [TW85] is LOW AND Q <sub>EM</sub> is LOW	THEN Oil distribution is	LOW (1.00)
2	IF [CaCl <sub>2</sub> ] is LOW AND [TW85] is LOW AND Q <sub>EM</sub> is HIGH	THEN Oil distribution is	HIGH (1.00)
3	IF [CaCl <sub>2</sub> ] is LOW AND [TW85] is MID AND Q <sub>EM</sub> is LOW	THEN Oil distribution is	HIGH (1.00)
4	IF [CaCl <sub>2</sub> ] is LOW AND [TW85] is MID AND Q <sub>EM</sub> is HIGH	THEN Oil distribution is	HIGH (1.00)
5	IF [CaCl <sub>2</sub> ] is LOW AND [TW85] is HIGH AND Q <sub>EM</sub> is LOW	THEN Oil distribution is	LOW (0.99)
6	IF [CaCl <sub>2</sub> ] is LOW AND [TW85] is HIGH AND Q <sub>EM</sub> is HIGH	THEN Oil distribution is	HIGH (1.00)
7	IF [CaCl <sub>2</sub> ] is HIGH AND [TW85] is LOW AND Q <sub>EM</sub> is LOW	THEN Oil distribution is	LOW (1.00)
8	IF [CaCl <sub>2</sub> ] is HIGH AND [TW85] is LOW AND Q <sub>EM</sub> is HIGH	THEN Oil distribution is	LOW (1.00)
9	IF [CaCl <sub>2</sub> ] is HIGH AND [TW85] is MID AND Q <sub>EM</sub> is LOW	THEN Oil distribution is	LOW (1.00)
10	IF [CaCl <sub>2</sub> ] is HIGH AND [TW85] is MID AND Q <sub>EM</sub> is HIGH	THEN Oil distribution is	LOW (1.00)
11	IF [CaCl <sub>2</sub> ] is HIGH AND [TW85] is HIGH AND Q <sub>EM</sub> is LOW	THEN Oil distribution is	HIGH (0.51)
12	IF [CaCl <sub>2</sub> ] is HIGH AND [TW85] is HIGH AND Q <sub>EM</sub> is HIGH	THEN Oil distribution is	HIGH (1.00)

## **APPENDIX I**



## LIST OF PUBLICATIONS

### Papers

- Del Gaudio Pasquale, Russo Paola, **Rodríguez-Dorado Rosalía**, Sansone Francesca, Mencherini Teresa, Gasparri Franco, Aquino Rita Patrizia. Submicrometric hypromellose acetate succinate particles as carrier for soy isoflavones extract with improved skin penetration performance. *Carbohydrate Polymers*, 2017, 165, 22-29.
- **Rodríguez-Dorado Rosalía**, Landín Mariana, Altay Ayça, Russo Paola, Aquino Rita Patrizia, Del Gaudio Pasquale. “A novel method for the production of core-shell microparticles by inverse gelation optimized with artificial intelligent tools”. *International Journal of Pharmaceutics*, 2018, 538, 97-104.
- **Rodríguez-Dorado Rosalía**, López-Iglesias Clara, García-González Carlos Alberto, Auriemma Giulia, Aquino Rita Patrizia, Del Gaudio, Pasquale. Design of aerogels, cryogels and xerogels of alginate: effect of alginate molecular weight, gelation conditions and drying method on particles' micromeritics. *Molecules* 2019, 24(6), 1049.

### Presentation at conferences

- Del Gaudio Pasquale, **Rodríguez-Dorado Rosalía**, Russo Paola, Aquino Rita Patrizia. Poster presentation at the 2<sup>nd</sup> European Conference on Pharmaceutics, Krakow, Poland, April 3-4, 2017.
- Goimil Leticia, **Rodríguez-Dorado Rosalía**, Concheiro Angel, Alvarez-Lorenzo Carmen, Del Gaudio Pasquale, García-González Carlos Alberto. Poster presentation at the 16<sup>th</sup> European Meeting on Supercritical Fluids, Lisbon, Portugal, April 25-28, 2017.
- Del Gaudio Pasquale, **Rodríguez-Dorado Rosalía**, Russo Paola, Aquino Rita Patrizia. Poster presentation at the XXVI Congresso

Nazionale della Società Chimica Italiana. Paestum, Salerno, Italy, September 10-14, 2017.

- **Rodríguez-Dorado Rosalía**, Landín Mariana, Altai Ayça, Russo Paola, Aquino Rita Patrizia, Del Gaudio Pasquale. Oral presentation at the Advanced School of Nanomedicine, Pula, Cagliari, Italy, September 25-28, 2017.
- **Rodríguez-Dorado Rosalía**, Landín Mariana, Altai Ayça, Russo Paola, Aquino Rita Patrizia, Del Gaudio Pasquale. Poster presentation at the Controlled Release Society, Fisciano, Salerno, October 26-28, 2017.
- **Rodríguez-Dorado Rosalía**, Landín Mariana, Russo Paola, Aquino Rita Patrizia, Del Gaudio Pasquale. Poster presentation at the 11<sup>th</sup> World Meeting on Pharmaceutics, Biopharmaceutics and Pharmaceutical Technology, Granada, Spain, March 19-22, 2018.
- **Rodríguez-Dorado Rosalía**, García-González Carlos Alberto, Russo Paola, Aquino Rita Patrizia, Del Gaudio P. Poster presentation at the Innovation in Local Drug Delivery School for Doctorate in Pharmaceutical Technology, Lake Como, Italy, September 25-28, 2018.

## **Acknowledgments**

I want to specially thank to my parents, Fernando and Victoria, my brother Fernando, my grandparents, and all my entirely family for their efforts, their unconditional support and for being always there for me. This could not be possible without them.

I would like to thank Prof. Rita P. Aquino and Prof. Pasquale Del Gaudio for the opportunity they gave me and their scientific guidance that made possible the development of my PhD thesis. Furthermore, I want to thank Prof. Del Gaudio for his advices, help and availability in following my work every day during these years that allowed me to growth and improve my skills and knowledge.

I would like to gratefully thank Tiziana for her friendship, for all the enjoyable time that we spent together, for make me laugh until crying and for being my principal support every day in the laboratory during these years. I would not have done it without her.

I would like to thank Felicia for her friendship, for make me discovering Salerno and make me feel like at home. I am very grateful for all that she and her family have done it for me.

I would like to thank Giulia for her friendship, her advices and her availability to helping me, I will not forget all the good moments that we spent together both in Italy and in Spain.

I would like to thank Francesca, Teresa, Marilena, Chiara, Giulio, Paola and Patrizia for the enjoyable time spent together in the laboratory and for their welcome that made me feel like at home. I do really appreciate all the advices and the motivation that you gave me during those three years. Furthermore, I want also to thank all the graduate students that have worked with me

because this PhD thesis is also part of them: Angelo, Carmela, Roberta, Francesca, Anna and Donatella. I really do appreciate all that they have done for me and I will never forget it.

I want to thank my cousin Sara, for all the inspiration and motivation that she gives me and which makes me always strive to achieve my goals. She is always very supportive with me and I do really admire her. I want also to thank my best friends Cathy, Ana Diz, Olaya, Ana Marín and Ana Herrera for their friendship, for their unconditional support since we have known each other and for having the patience to listen to my very long messages. These years were not easy and they have been there for me all time. I am very grateful for that.

I want to thank Valerie for being like a sister for me despite the distance, for taking care of me and supporting me in everything. It means a lot for me.

I want to thank Pablo for being at my side at the beginning of this adventure making everything so much easier thus being my main support. I would not have been able to start this phase without him. Particularly, I want to thank him for supporting me in an unconditional manner even when times turned out difficult and for all the special moments that we lived in Italy, I will never forget Positano.

I want to thank Tito for his friendship, for being the best flatmate ever during my period in Santiago de Compostela, and for all the funny moments and the infinite laughs together. He made me feel happy every day even when the world was falling on me. I really do appreciate all the advices that he gave me and all the support that he transmitted to me even from thousands kilometers far away. I want also to thank all my friends Miguel, Berto, Julio, Litos, Lois, Alejo and Edo for makes me always smile and for their friendship and support.

I want to thank Luis for inspiring me to do a PhD, for being such a good friend despite the distance and for caring about me, being always very clear and supportive. I want to thank him for all the good moments that we shared in Santiago and all the things that I have learnt from him during those years.

I want to thank Ilenia, my Italian sister, for offering me her friendship and for being such a good flatmate during all those years in Salerno. I will not forget Casa Guerra and I do really appreciate how her and her family made me feel like at home.

I want to thank to my chemical friends Jennifer, Maru, Sabela, Marta, Marina, Adrián, Iván, Manu, Xoel and Cibrán for their understanding of what it means to do a PhD and for all the funny moments that we lived together during the five years in the university.

I want to thank María and Ángela, for being such a good flatmates and friends during my stays in Santiago. I will not forget all the special and funny moments that we lived together, talking all the night-long, making photo sessions and cooking for all the entirely city.

I want to thank Elena and Marta for being such a lovely friends and for all the support that they gave me during my PhD thesis.

I want to thank Carlota for all the funny moments that we spent together in the gym, in the university and in Salerno. I will not forget all the adventures that we lived together.

I want to thank to Anna Maria and Ilaria for all the moments that we shared and that have made easier the final of this difficult road.

I want to thank Dr. Renata Adami from the Department of Industrial Ingeneering for the research collaboration.

I want to thank Dr. Carlos A. García González from the University of Santiago de Compostela that as my supervisor during my research period in this university gave me many useful teachings and advices.

I want to specially thank Clara, Víctor, Mariano and Leticia for all the immense help that they gave me during the performance of my experiments at the University of Santiago de Compostela and I want also to thank Fernando, Sonia, Patricia, María, Ángela, Andrea, Xián and all people I met during my research period in there.

I want to thank Prof. Mariana Landín for the research collaboration and to Prof. Rosa Antonia Lorenzo Ferreira, Prof. Antonia María Carro Díaz, Prof. Carmen Álvarez Lorenzo, and Prof. Ángel Concheiro for showing me the research world and inspiring me to doing a PhD.

**Grazie / Thank you / Gracias**

